REMOVAL OF ELEMENTAL MERCURY FROM FLUE GAS USING NANOSTRUCTURED SILICA/TITANIA/VANADIA COMPOSITES

By

YING LI

A DISSERTATION PRESENTED TO THE GRADUATE SCHOOL
OF THE UNIVERSITY OF FLORIDA IN PARTIAL FULFILLMENT
OF THE REQUIREMENTS FOR THE DEGREE OF
DOCTOR OF PHILOSOPHY

UNIVERSITY OF FLORIDA

2007

To my wife and my parents for their constant love, understanding, and support.

ACKNOWLEDGMENTS

I sincerely thank Dr. Chang-Yu Wu (my supervisory committee chair) for his invaluable guidance, inspiration, and encouragement. I am truly grateful for his continuous and enthusiastic support of my graduate research and my career development. My supervisory committee members (Dr. Jean Andino, Dr. Kevin Powers, Dr. Jean-Claude Bonzongo, and Dr. Wolfgang Sigmund) have generously given their time and expertise to better my work. I thank them very much for their guidance and their good-natured support.

I would like to thank Patrick Murphy, who has been assisting me for one and a half years in my research project. He has given me a big hand in building the reaction system and conducting the experiments. I thank Sameer Matta for his assistance in doing the experiments and making the pellets in the past two semesters. My thanks also go to Jie Gao, who helped me analyze the amount of mercury captured on the catalysts. I greatly appreciate the help from Yu-Mei Hsu for miscellaneous lab items. I must acknowledge as well many other fellow students in our air resources group who kindly assisted my research.

I am grateful to the National Science Foundation for the financial support and VICI Metronics, Inc. for providing the mercury permeation tube. Finally, I am thankful to the scholarship and encouragement from the Air & Waste Management Association.

TABLE OF CONTENTS

page

LIST OF TABLES

LIST OF FIGURES

Abstract of Dissertation Presented to the Graduate School
of the University of Florida in Partial Fulfillment of the
Requirements for the Degree of Doctor of Philosophy

REMOVAL OF ELEMENTAL MERCURY FROM FLUE GAS USING NANOSTRUCTURED SILICA/TITANIA/VANADIA COMPOSITES

By

Ying Li

August 2007

Chair: Chang-Yu Wu
Major: Environmental Engineering Sciences

As a highly toxic pollutant, mercury (Hg) tends to bioaccumulate in the food chain and exerts adverse effects on human health. The U.S. EPA issued the Clean Air Mercury Rule in 2005 to permanently cap and reduce Hg emissions from coal-fired power plants. A low-cost methodology using a SiO_2-TiO_2 nanocomposite as a photocatalyst has been recently developed to effectively remove elemental Hg (Hg^0) under room conditions. In this research, a bench-scale fixed-bed reactor system has been established and Hg^0 removal on the SiO_2-TiO_2 nanocomposite was examined under both room and flue gas conditions. A kinetic study showed that Hg oxidation on the SiO_2-TiO_2 nanocomposite under UV irradiation followed the Langmuir-Hinshelwood rate expression. The flue gas components were found to have significant effects on Hg^0 removal using the SiO_2-TiO_2 nanocomposite. HCl and SO_2 promoted Hg^0 oxidation, while water vapor and NO significantly inhibited Hg removal. The mechanisms of these promotional and inhibitory effects were thoroughly explored in this research.

The active phase of the selective catalytic reduction (SCR) catalyst, V_2O_5, was added to the SiO_2 or SiO_2-TiO_2 composites in an effort to improve the catalytic activity for Hg removal. No UV light activation is needed for the V_2O_5 doped catalysts, which is a great advantage over the SiO_2-TiO_2 composites. The Hg^0 removal efficiency increased as the V_2O_5 loading increased from

2 to 8% but decreased as it further increased to 10%. The optimal V_2O_5 loading was found to be somewhere between 5 and 8%. The SiO_2-TiO_2-V_2O_5 exhibited a greater ability of oxidizing Hg compared to the SiO_2-V_2O_5. It was suggested that the Hg oxidation on the V_2O_5 doped catalysts follows an Eley-Rideal mechanism where HCl, NO, and NO_2 are first adsorbed on the catalyst surface and then react with gas-phase Hg^0.

This research also reported that atomic absorption spectrometry based continuous mercury monitors are subject to interferences by ozone due to its strong absorption bands near the Hg absorption line. On the other hand, Hg interferes with ozone measurement which is based UV adsorption. These mutual interferences can consequently affect the risk assessment of human exposure to both Hg and ozone.

CHAPTER 1
INTRODUCTION

Mercury and Its Health Effects

The 1990 Clean Air Act Amendments (CAAA) listed 189 hazardous air pollutants (HAPs). Among them, mercury (Hg) has attracted significant attention due to its increased levels in the environment and well-documented food chain transport and bioaccumulation (Brown et al., 1999). Human exposure by direct inhalation of Hg in the air is not a predominant public health concern because the Hg concentration in the air is typically very low. However, Hg in ambient air can eventually be re-deposited on land surfaces or directly into rivers, lakes, and oceans, and then biologically enter the food chain. In aquatic systems, Hg is often converted by bacteria to methylmercury (CH_3Hg^+), which is a neurotoxin and can be magnified through the aquatic food chain hundreds of thousands of times (Ravichandran, 2004). Hg and its compounds act as dangerous and insidious poisons and can be adsorbed through the gastrointestinal tract and also through the skin and lungs (Bidstrup, 1964). High-concentration of Hg can cause impairment of pulmonary and kidney function, chest pain and dyspnousea (Berglund and Bertin, 1969). An extreme example of the health effects of Hg is the high-dosage exposure from the consumption of methylmercury-contaminated fish by the residents living near Minamata Bay in Japan in the 1950s that resulted in fatalities and severe neurological damage (Mishima, 1992).

Mercury Emissions and Regulations

According to the *Mercury Study Report to Congress* prepared by the U.S. Environmental Protection Agency (USEPA) (USEPA, 1997a), the major anthropogenic Hg emission sources are coal-fired boilers (33%), municipal waste combustors (19%), industrial and commercial boilers (18%), and medical waste incinerators (10%). Hg emissions from manufacturing sources are generally lower compared to combustion sources with the exception of chlor-alkali plants using

the mercury cell process and portland cement manufacturing plants (USEPA, 1997a). Ever since the 1990 Clean Air Act, the U.S. EPA has issued a series of rules to regulate Hg emissions from solid waste combustors/incinerators (USEPA, 1997c, 2001b), and mercury cell chlor-alkali plants (USEPA, 2003). Since coal-fired utility boilers are currently the largest single-known source of anthropogenic Hg emissions (one-third of the 150 tons of Hg emitted annually) in the United States, the U.S. EPA issued the Clean Air Mercury Rule (CAMR) in 2005 to permanently cap and reduce Hg emissions from coal-fired power plants (USEPA, 2005a). CAMR will be implemented in two phases, with the first phase cap of 38 tons in 2010 followed by a final cap of 15 tons in 2018. The final cap requires an approximately 70% reduction from the 1999 emission levels.

Mercury Speciation and Control Technologies

There are three basic forms of Hg in the coal-derived flue gas: (1) elemental Hg (Hg^0), (2) oxidized Hg (Hg^{2+}), predominantly $HgCl_2$ due to the large excess of chlorine species in the flue gas, and (3) particle-bound Hg (Hg_p). During combustion, Hg is released from coal as Hg^0, and as the flue gas cools, some of the Hg^0 can be oxidized or bound on the fly ash. The Hg speciation in the flue gas is determined by various factors including coal properties, boiler operating conditions, flue gas composition, and the time-temperature profile (Romero et al., 2006). Hg^{2+} and Hg_p are relatively easy to remove from the flue gas using typical air pollution control devices (APCDs). Hg_p, bound on fly ash particles, is collected in electrostatic precipitators (ESPs) and/or baghouses. Hg^{2+} is soluble in water and is readily captured by wet flue gas desulfurization (FGD) equipment. Hg^0 is volatile and insoluble in water, and thus, it is difficult to be captured using these conventional control technologies. Unfortunately, Hg speciation studies showed that Hg^0 is the dominant species in flue gas when burning low rank (subbituminous or lignite) coals.

Therefore, the need exists for a low cost Hg oxidation/capturing process that can be applied for the flue gas treatment.

Many methodologies have been proposed for Hg emission control from flue gas. Among them, the technology of sorbent injection, particularly activated carbon injection (ACI), has been investigated most intensively (Pavlish et al., 2003). Both Hg^0 and Hg^{2+} can be captured by the sorbent and collected in ESPs and/or baghouses. This technology has been successfully implemented in the municipal waste incinerator industry, where 90% Hg removal can be achieved. However, the application of ACI in coal-fired utility boilers is far more challenging due to the shorter gas residence time, the lower equilibrium adsorption capacity and mass-transfer rate, and the compromise of fly ash properties by the injected sorbent. The high cost of ACI also limits its application (Pavlish et al., 2003).

Recently, selective catalyst reduction (SCR) catalysts are found to be capable of oxidizing Hg^0 in addition to its ability of removing nitrogen oxides (NOx) from the flue gas (Benson et al., 2005; Lee, Srivastava et al., 2004; Lee et al., 2006; Niksa and Fujiwara, 2005b; Senior, 2006). The extent of Hg^0 oxidation through SCR processes varies under different operating conditions burning different types of coal. However, the SCR process is treated as a "black box" and the mechanisms of Hg oxidation over SCR catalysts are yet to be understood.

A novel methodology using titanium dioxide (TiO_2) based nanostructured sorbents has been demonstrated to be very effective for capture of Hg^0 under ultraviolet (UV) irradiation (Lee et al., 2001; Pitoniak et al., 2003; Wu et al., 1998). Wu et al. (1998) and Lee et al. (2001) reported a high level of Hg^0 capture in simulated combustor exhaust using *in-situ* generated TiO_2 particles, while Pitoniak et al. (2003) used a highly porous silica (SiO_2) gel doped with TiO_2 nanoparticles and achieved synergistic adsorption and photocatalytic oxidation of Hg^0 in a fixed-

bed reactor. The high surface area and open structure of the SiO_2-TiO_2 nanocomposite allow effective irradiation by UV light and thus minimize the mass-transfer resistance for Hg^0 (Pitoniak et al., 2003; Wu et al., 1998). Using this material, Hg removal efficiency remained over 90% even after a 477-hr treatment (Pitoniak et al., 2005). Potential applications of the SiO_2-TiO_2 nanocomposite for Hg removal lie in two main areas. First, like ACI, a powdered form of the nanocomposite can be injected into combustion exhaust upstream of a particle control device (e.g. ESP). Second, a pellet form of the nanocomposite can be used in packed-bed columns to treat Hg emissions from flue gas. In this case, the device is preferably installed between an ESP and a wet scrubber.

Mercury Removal by SiO_2-TiO_2: Unknowns and Challenges

While the SiO_2-TiO_2 nanocomposites have demonstrated prominent effectiveness for Hg removal, the past studies were mainly conducted under room conditions and there is little knowledge so far about the performance of this novel material under real or simulated flue gas conditions. As is known, typical coal-derived flue gas consists of a high concentration of water vapor (normally 5~15 % v/v) and various minor gas components such as HCl, SO_2, and NOx. Among the factors that affect the efficiency of Hg^0 capture by the TiO_2 photocatalyst, moisture content in the Hg^0-laden gas was reported to be one of the most important (Pitoniak et al., 2003; Rodriguez et al., 2004). However, the understanding of the water vapor effects on Hg removal in literature is limited and some of the findings are controversial. It has also been reported that the minor acid gases are important to the heterogeneous adsorption and/or oxidation of Hg^0 on activated carbons or fly ash under flue gas conditions (Carey et al., 1998; Norton et al., 2003). In addition, the typical flue gas temperature at the cold-end of the boiler convective pass is in the range of 120 ~150 °C, much higher than the room temperature. Thus, it is expected that the

nature of Hg capture on the SiO_2–TiO_2 nanocomposite would be different under flue gas conditions from that reported under room conditions in the past studies.

Furthermore, the kinetics for catalytic oxidation of Hg is highly uncertain (Presto and Granite, 2006). The lack of understanding presents a severe limitation in predicting the extent of Hg oxidation in larger scale applications. In literature, kinetic modeling studies on Hg capture have mainly focused on activated carbon adsorption (Chen et al., 1996; Flora et al., 1998; Meserole et al., 2000; Rostam-Abadi et al., 1997), while modeling on photocatalytic oxidation using TiO_2 has mainly focused on degradation of volatile organic compounds (VOCs) (Kim and Hong, 2002; Raillard et al., 2004; Shang et al., 2002; Son et al., 2004). The kinetics for Hg oxidation using the SiO_2-TiO_2 nanocomposite is yet to be investigated.

While the performance of the SiO_2-TiO_2 nanocomposite under flue gas conditions is unknown at this point, it is reasonable to carry out a parallel study that focuses on the development of a modified or even new catalyst which would be more effective on Hg removal in flue gas. Considering the fact that industrial SCR catalysts, with an active phase of V_2O_5 supported on TiO_2, are capable of oxidizing Hg^0 in addition to its ability of removing NOx (Benson et al., 2005; Lee, Srivastava et al., 2004; Lee et al., 2006; Niksa and Fujiwara, 2005b; Senior, 2006), the addition of V_2O_5 to the existing SiO_2-TiO_2 nanocomposite would be expected to enhance the catalytic activity. Meanwhile, since the Hg oxidation across SCR catalysts is usually treated as a "black box" in pilot- or full-scale studies, a better understanding of the fundamental nature of the catalytic reactions is of great importance to the advancement of the catalysts.

Mercury Measurement Interference

Both Hg emission regulations and development of Hg control technologies require that reliable methods be used for accurate Hg measurement. Currently, the EPA accepted methods for

Hg measurement in the United States are manual procedures based on wet-chemistry such as EPA Methods 29 and 101A (for total mercury) and the Ontario Hydro Method (for speciated mercury) (Laudal et al., 2004). However, continuous mercury monitors (CMMs) have distinct advantages over these manual methods in that CMMs are able to provide a real-time or near-real-time response for Hg measurements and to perform long-term emission measurement. On the other hand, a significant disadvantage of CMMs lies in their measurement interferences.

Atomic absorption spectrometry (AAS) is one of the major techniques applied to current CMMs. In the case of AAS, the concentration of Hg^0 in a gas sample is determined by measuring the light that is absorbed by Hg atoms at their characteristic wavelengths (usually at the resonance line of 254 nm). Thus, interferences can occur when other components of the sample gas possess strong absorption bands near this wavelength (254 nm). Since the 254 nm Hg emission line also falls into the absorption spectra of ozone, which is capable of absorbing UV light below 290 nm, the presence of ozone in the sampling environment may impact the Hg measurement by AAS based CMMs. Granite and Pennline (2002) studied photochemical oxidation of Hg and speculated that photosensitized formation of ozone may interfere with Hg measurement by absorbing UV radiation. However, no quantitative data were reported in literature on the magnitude of ozone interference.

Research Objectives

To reveal the unknowns and to embrace the challenges mentioned above, five objectives are proposed in this doctoral research. The first objective is to study the kinetics of the Hg^0 photocatalytic oxidation on the SiO_2-TiO_2 nanocomposite. The competitive adsorption of water vapor in Hg^0 photocatalytic oxidation will be established in a kinetic expression as well. This modeling study is of importance in predicting Hg^0 removal efficiency and is useful for designing an effective reactor, under photocatalytically oxidizing conditions.

The second objective is to perform a mechanistic study probing the role of moisture on Hg^0 capture (adsorption and/or photocatalytic oxidation) using a SiO_2–TiO_2 nanocomposite. To provide an overall evaluation of the performance of the SiO_2–TiO_2 nanocomposite, possible reemission of captured Hg species will also be examined. The corresponding mechanisms of Hg^0 removal and reemission in the presence of water vapor will be investigated as well.

The third objective is to install a fixed-bed photocatalytic reactor and to investigate the performance of the SiO_2–TiO_2 nanocomposite under simulated flue gas conditions. The effects of the flue gas components on the removal of Hg^0 by the SiO_2–TiO_2 nanocomposite as well as the surface reaction mechanisms will be explored. An improved understanding of the role of the flue gas components can help evaluate the potential of applying this novel material for effective Hg control in coal-fired power plants.

The fourth objective is to develop a method to dope V_2O_5 on the SiO_2 or SiO_2-TiO_2 composites in an effort to improve the catalytic activity for Hg removal. The SiO_2-V_2O_5 and SiO_2-TiO_2-V_2O_5 composites will be synthesized and characterized. The catalytic abilities of those composites on Hg removal will be tested in a fix-bed reactor. The reaction mechanisms on the catalytic removal of Hg over the new catalysts will be investigated.

The last but not the least important objective of this research is to quantitatively investigate the mutual interferences of ozone and Hg on their measurements. This study may be of particular importance to the ambient and indoor measurements of ozone and Hg because these two air pollutants coexist in the environment.

CHAPTER 2
KINETIC STUDY FOR PHOTOCATALYTIC OXIDATION OF ELEMENTAL MERCURY ON A SILICA-TITANIA NANOCOMPOSITE*

Background

A solid understanding of the kinetics of photocatalytic oxidation of Hg^0 is of great importance to make an effective design of the photocatalytic reactor and to predict the reaction rate in larger scale applications. Lee et al. (2004) studied Hg^0 oxidation by TiO_2 nanoparticles with UV irradiation in a differential bed reactor (DBR) and an aerosol flow reactor (AFR), and correlated the overall reaction rate with the initial Hg^0 concentration and UV intensity. However, the kinetic parameters on water vapor dependence were not available in that study, while water vapor is an important component in the flue gas and plays a critical role in the chemistry of mercury in coal-fired boilers (Edwards et al., 2001; Niksa et al., 2001). Rodríguez et al. (2004) developed a mechanistic model to predict Hg^0 capture with in situ-generated TiO_2 nanoparticles by solving the equilibrium equations for electron-hole pair generation/consumption . They also compared their mechanistic model with the Langmuir-Hinshelwood (L-H) model used by Obee (1996) for characterizing photocatalytic oxidation of certain organic compounds. At low water vapor concentrations, the Hg capture rate predicted by the mechanistic model (Rodriguez et al., 2004) was proportional to the square root of the water vapor concentration, whereas the L-H model (Obee, 1996) indicated first-order dependence. At high water vapor concentrations, both models predicted a constant Hg capture rate that was independent of the water vapor concentration.

* Reprinted with permission from Li, Y., Wu, C.-Y., 2007. Kinetic Study for Photocatalytic Oxidation of Elemental Mercury on a SiO_2-TiO_2 Nanocomposite. Environ. Eng. Sci. 24, 3-12, published by Mary Ann Liebert, Inc., New Rochelle, NY

Some other modeling studies have been done on Hg capture using activated carbon. Rostam-Abadi et al. (1997) applied an empirical equation to the mass balance for Hg^0 sorption on carbon particles in a duct flow reactor and derived the minimum C/Hg ratio required to reduce Hg^0 at a certain inlet Hg^0 concentration. Chen et al. (1996) derived an equation to model mercury capture when it is limited by both mass transfer and capacity by assuming that adsorption at the surface obeys Henry's law. A conceptually similar approach was used by Flora et al. (1998) based on the Langmuir isotherm and by Meserole et al. (2000) based on the Freundlich equation. Several other studies (Kim and Hong, 2002; Raillard et al., 2004; Shang et al., 2002; Son et al., 2004) have been conducted on photocatalytic oxidation of various volatile organic compounds (VOCs) by TiO_2, and the experimental data matched well with the L-H kinetic model. This intriguing L-H nature of a wide range of VOCs warrants the investigation on the correlation between the kinetics of Hg^0 photocatalytic oxidation by TiO_2 and the L-H rate expression, whereas no relevant research has been done so far. In addition, the L-H model takes advantages over the other models previously described in incorporating the effect of competitive adsorption of water vapor. Therefore, the research goal of this chapter was to study the kinetics of the Hg^0 photocatalytic oxidation on a SiO_2-TiO_2 nanocomposite by using the L-H model to analyze the kinetic data. The role of water vapor in Hg^0 photocatalytic oxidation was established as well. This kinetic modeling study is of importance in predicting Hg^0 removal efficiency and is useful for designing an effective reactor, under photocatalyzed oxidizing conditions.

Materials and Methods

Synthesis of SiO_2-TiO_2 Nanocomposite

The SiO_2-TiO_2 nanocomposite was synthesized following a sol-gel method (Pitoniak et al., 2003) using deionized water, ethanol, tetraethyl orthosilicate (TEOS) with HNO_3 and HF added as catalysts to increase the hydrolysis and condensation rates. First, the chemicals were added to

a polymethylpentene container, and then TiO_2 nanoparticles (Deggusa, P25) were added to the batch with a magnetic stir plate providing sufficient mixing. After that, the solution suspended with TiO_2 nanoparticles was pipetted into polystyrene 96-well assay plates before the gelation occurred. The pellets were later aged at room temperature for 2 days and then at 65 °C for another 2 days. After aging, the pellets were removed from the plates, rinsed with deionized water to remove any residual acid or ethanol. Next, the pellets were placed in a programmable oven and heated at 103 °C for 18 h to remove any residues of liquid solution within the silica network and then at 180 °C for 6 h to harden the gel. Finally the temperature was slowly decreased back to room temperature over a 90 min period. The final size of an individual cylindrical pellet was approximately 5 mm in length and 3 mm in diameter. The loading of TiO_2 in the nanocomposite was 12 wt%, which corresponded to the optimum performance of Hg^0 removal using the SiO_2-TiO_2 nanocomposite (Pitoniak et al., 2003). The average BET (Brunauer, Emmett, and Teller equation) surface area of the nanocomposite was measured to be 280 m^2 g^{-1} using a Quantachrome NOVA 1200 Gas Sorption Analyzer (Boynton Beach, FL).

Apparatus and Procedure

Figure 2-1 shows the schematic diagram of the experimental system. An incoming cylinder air was divided into three streams, the flowrates of which were controlled by mass flow controllers (MFC, Model. FMA 5400/5500, Omega Engineering, Inc., Stamford, CT). The total flowrate remained constant at 2 L/min. One of the air streams was allowed to pass through a water bubbler for a humid flow or to bypass it for a dry flow. The second stream served as dilution to adjust the humidity level. The third stream passed through the surface of a liquid Hg^0 reservoir and introduced the saturated Hg^0 vapor into the system. The Hg^0 reservoir was placed in an ice-water bath to maintain a constant Hg^0 vapor pressure. Downstream of all the gases was the fixed-bed photocatalytic reactor, the lower part of which is a cylindrical tube of fused quartz

4.5 cm in diameter and 20 cm in length. The reactor was mounted with a fused quartz center with a diameter of 2 cm, which was used to house a UV lamp. The UV light has a peak wavelength of 365 nm with an intensity of 4 mW/cm^2 measured by a UVX radiometer (with a UVX-36 sensor probe). At the bottom of the reactor is a glass frit used to hold the SiO_2-TiO_2 pellets within the bed. A thermocouple (TC, Type K, Omega Engineering, Inc.) was used to monitor the temperature on the surface of the pellets. The Hg^0 concentration at the reactor outlet was measured by a RA-915+ Hg analyzer (OhioLumex Co., Cleveland, OH), which is based on Zeeman Atomic Absorption Spectrometry using High Frequency Modulated light polarization (ZAAS-HFM) (Sholupov et al., 2004). The inlet Hg^0 concentration was obtained when the Hg^0 laden air bypassed the reactor. Finally, the air stream passed through a carbon trap before it was exhausted into the fume hood.

Two sets of experiments were performed in this study. In the first set, no water vapor was introduced into the air stream but with variations in the inlet Hg^0 concentration (0.19 to 1.28 μ-mol m^{-3} or 38 to 256 μg m^{-3}). In the second set, the inlet Hg^0 concentration remained constant but with changes in water vapor concentration (0 to 0.95 mol m^{-3}). In each experiment, the Hg^0 laden air was allowed to pass through the reactor for one hour to ensure that the Hg^0 adsorption on the SiO_2-TiO_2 nanocomposite reached equilibrium, which was monitored by the online Hg analyzer. Then, the photocatalytic reaction was started by turning on the UV lamp and the Hg^0 concentrations were recorded for a certain period of time until no more reduction in Hg^0 concentration was observed. All the experiments were conducted under room conditions. In each test, 2.5 grams of fresh SiO_2-TiO_2 pellets were used, which corresponded to an average of 4 mm bed thickness (approximately one single layer of pellets).

Model Description

Photocatalytic oxidation of Hg^0 occurs when the SiO_2-TiO_2 nanocomposite is under UV irradiation as shown in Figure 2-2. The hole-electron pairs generated on the TiO_2 particle surfaces lead to the formation of highly reactive hydroxyl (OH) radicals, which are responsible for Hg^0 oxidation to form HgO (Pitoniak et al., 2003; Wu et al., 1998). The mechanism can be described as the following reactions:

$$TiO_2 + h\nu \rightarrow e^- + h^+ \quad (2\text{-}1)$$

$$H_2O \leftrightarrow H^+ + OH^- \quad (2\text{-}2)$$

$$h^+ + OH^- \rightarrow \cdot OH \quad (2\text{-}3)$$

$$h^+ + H_2O \rightarrow \cdot OH + H^+ \quad (2\text{-}4)$$

$$OH\cdot + Hg^0 \rightarrow HgO \quad (2\text{-}5)$$

Among the factors that affect the efficiency of Hg^0 capture by the SiO_2-TiO_2 nanocomposite, water vapor content in the Hg^0 laden air was reported to be one of the most important (Pitoniak et al., 2003). On one hand, surface moisture on TiO_2 nanoparticles is necessary for generating OH radicals (Reactions 2-4) which are responsible for photocatalytic Hg^0 oxidation. On the other hand, at high water vapor concentrations, competitive adsorption may reduce the number of sites available for Hg^0 (Pitoniak et al., 2003; Rodriguez et al., 2004).

Similar to the studies by other researchers (Canela et al., 1998; Obee, 1996; Obee and Hay, 1997), the rate of photocatalytic oxidation of Hg^0 is defined as

$$r = \frac{(C_{Hg}{}^{in} - C_{Hg}{}^{out}) \times Q}{A_e} \quad (2\text{-}6)$$

where $C_{Hg}{}^{in}$ is Hg^0 concentration at the inlet of the reactor, $C_{Hg}{}^{out}$ is Hg^0 concentration at the outlet of the reactor at steady state, Q is the volumetric flow rate of the Hg^0 laden air (2 L min^{-1}

or 0.12 m^3 h^{-1}), and A_e is the effective surface area of the pellets that is exposed to UV light. It should be noted that only a thickness of 0.1 mm from the surface of the pellets and only the areas facing the UV light can effectively contribute to Hg^0 oxidation (Pitoniak et al., 2005). Thus, A_e can be calculated as

$$A_e = SA \times m \times f_V \times f_P \quad (2\text{-}7)$$

where *SA* is the specific surface area of the pellets (280 m^2 g^{-1}), m is the mass of pellets used (2.5 g), f_V is the volume fraction of the 0.1 mm thickness layer that UV light can penetrate (estimated to be 0.15), and f_P is the packing factor that accounts for the fraction of the surface areas exposed to UV light (estimated to be 0.5).

To correlate the experimental data of photocatalytic oxidation rate of Hg^0, the L-H rate equation was used. If the concentration of water vapor is constant, the L-H expression can be simplified as

$$r = k \frac{K_{Hg} C_{Hg}}{1 + K_{Hg} C_{Hg}} \quad (2\text{-}8)$$

where *r* is the reaction rate (μ-mol m^{-2} h^{-1}), *k* is the L-H rate constant (μ-mol m^{-2} h^{-1}), K_{Hg} is the Langmuir adsorption constant of Hg^0 (m^3 μ-mol^{-1}), and C_{Hg} is the Hg^0 concentration (μ-mol m^{-3}). C_{Hg} is normally assigned to be the bulk or inlet concentration, C_{Hg}^{in} (Obee, 1996; Obee and Hay, 1997). The inverse of Equation 2-8 gives

$$\frac{1}{r} = \frac{1}{k K_{Hg}} \frac{1}{C_{Hg}} + \frac{1}{k} \quad (2\text{-}9)$$

If the assumed L-H expression is valid for Hg photocatalytic oxidation, a plot of r^{-1} vs. C_{Hg}^{-1} should be linear. Subsequently, the values of *k* and K_{Hg} can be derived from the combination of the intercept and the slope of the linear line. From these values, the photocatalytic Hg^0 oxidation rate can be predicted by the L-H model.

Similar to the modeling studies conducted by other researchers on photocatalytic oxidation of organic pollutants (Obee and Hay, 1997; Shang et al., 2002), when water vapor is present, the inhibitory effect of water vapor on Hg^0 photocatalytic oxidation can be assumed according to the following L-H form

$$r = k\frac{K_{Hg}C_{Hg}}{1 + K_{Hg}C_{Hg} + K_wC_w} \tag{2-10}$$

where K_w is the Langmuir adsorption constant of water and C_w is the water vapor concentration. The inverse of Equation 2-10 gives

$$\frac{1}{r} = \frac{K_w}{kK_{Hg}C_{Hg}}C_w + \frac{1}{k}\left(1 + \frac{1}{K_{Hg}C_{Hg}}\right) \tag{2-11}$$

The value of K_{Hg} can be obtained from previous analysis when water vapor is not present. When C_{Hg} remains at a constant level and only C_w varies, a plot of r^{-1} versus C_w should be linear if it follows the L-H model expression. Then the values of k and K_w can be derived from the plot.

Results and Discussion

Effect of Hg^0 Concentration

Figure 2-3 shows the outlet Hg^0 concentration as a function of UV illumination time at six different inlet levels ranging from 0.19 to 1.28 μ-mol m^{-3} (38 to 256 μg m^{-3}) when water vapor was not present. The outlet Hg^0 concentration dropped quickly when UV was first turned on for a few minutes and then gradually leveled off. From 20 to 30 min, no significant change in outlet Hg^0 concentration was observed and the pellet surface temperature remained almost constant (42.7 ± 0.3 °C). Therefore, 30 min was taken as the time the system reached steady state. Experiments were repeated three times at each inlet Hg^0 concentration level. The average Hg^0 removal efficiency ranged from 90 to 95% but was not an apparent function of the inlet Hg^0 concentration.

At each inlet Hg^0 concentration level, the photocatalytic oxidation rate r can be calculated from Equation 2-6 and the average value can be obtained. A plot of r^{-1} vs. C_{Hg}^{-1} is shown in Figure 2-4 and the observed linear relationship indicates that the kinetics of Hg^0 photocatalytic oxidation fits the L-H model very well. From Equation 2-9, values of the L-H rate constant k and the Langmuir adsorption constant K_{Hg} were calculated to be k = 0.024 μ-mol m^{-2} h^{-1} and K_{Hg}= 0.094 m^3 μ-mol^{-1}. Substituting the values of k and K_{Hg} back into Equation 2-8, the photocatalytic oxidation rates at different inlet Hg^0 concentrations can be predicted by the L-H model.

In the kinetic study of Hg^0 photocatalytic oxidation on TiO_2 particles by Lee et al. (2004), the reaction orders with respect to initial Hg^0 concentration (which ranged from 1-10 μg m^{-3} or 0.005-0.05 μ-mol m^{-3}) were reported to be 1.4 for the differential bed reactor (DBR) and 1.1 for the aerosol flow reactor (AFR). They also suggested that the higher value obtained for the DBR might be due to inherent experimental errors. In this work, the fix-bed reactor design is similar to the DBR used by Lee et al. (2004). With the inlet Hg^0 concentration ranging from 0.19 to 1.28 μ-mol m^{-3} in this study, the value of $K_{Hg}C_{Hg}$ is far less than 1. Thus, Equation 2-8 can be simplified as

$$r = kK_{Hg}C_{Hg} \qquad (2\text{-}12)$$

Equation 2-12 shows that the reaction order with respect to the initial Hg^0 concentration is 1, which is representative of a practical sorbent process (Lee, Biswas et al., 2004). Lee et al. (2004) also correlated the overall reaction order with respect to the UV intensity and reported an order of 0.35 for the DBR and 0.39 for the AFR. In this study, the effect of UV intensity was not investigated.

Useful prediction results can be obtained from the L-H model as shown in Figure 2-5, which is characterized by a steep rise of Hg^0 photocatalytic oxidation rate at inlet concentrations

approximately less than 20 μ-mol m^{-3} and subsequent mild increase at higher concentrations. Due to the limitations on the capability of the Hg generation unit and the measurement range of the Hg analyzer, experimental data greater than 20 μ-mol m^{-3} were not available in this study. Further research is needed on validating the L-H feature of Hg^0 photocatalytic oxidation in the high concentration range. On the other hand, it should be noted that typical Hg concentrations in coal-fired power plant flue gases are less than 0.05 μ-mol m^{-3} (10 μg m^{-3}) (Pavlish et al., 2003), which locates this process at the very lower end of the steep-rise range. This further demonstrates the great potential of the SiO_2-TiO_2 nanocomposite for Hg^0 removal from emission sources even with much higher Hg^0 concentrations.

Effect of Water Vapor

Water vapor experiments were conducted at a constant inlet Hg^0 concentration of 0.66 μ-mol m^{-3} with variations in the water vapor concentration, as shown in Figure 2-6. As the water vapor concentration increased from 0 to 0.95 mol m^{-3}, the steady-state Hg^0 removal efficiency (at 30 min) also decreased from 93% to 24%. This demonstrates a significant inhibitory effect of water vapor on photocatalytic Hg^0 oxidation. Experiments were repeated three times at each water vapor concentration level. The average values of r^{-1} versus C_w at a constant inlet Hg^0 concentration are plotted in Figure 2-7. The linear relationship between them shows a good match of the experimental data with the L-H model expression in humid air (Equation 2-11). The intercept and the slope of the linear plot give the L-H rate constant k = 0.031 μ-mol m^{-2} h^{-1} and the Langmuir adsorption constant of water K_w= 4.39 m^3 mol^{-1}. The previously obtained K_{Hg} (0.094 m^3 μ-mol^{-1} or 9.4×10^4 m^3 mol^{-1}) is four orders of magnitude larger than K_w, which indicates that the adsorption ability of the SiO_2-TiO_2 nanocomposite is much greater for Hg^0 than for water vapor. However, water vapor plays a very important role in Hg^0 removal because in the

flue gas Hg^0 concentration is at such trace levels (seven to eight orders of magnitude smaller) compared to that of water vapor.

Now that all the kinetic parameters have been estimated, the L-H model can be used to predict the rate of Hg^0 photocatalytic oxidation at any level of inlet Hg^0 concentration and water vapor concentration. Figure 2-8 compares the experimental data of the Hg^0 photocatalytic oxidation rate with L-H model predictions in humid air. For the six experimental conditions shown in Figure 2-8, the deviations of the experimental data from the L-H model predictions are less than 15%, which are within an allowable range of experimental error. This result once again verifies the L-H nature of Hg^0 photocatalytic oxidation by the SiO_2-TiO_2 nanocomposite, and suggests that it is appropriate to apply the L-H model to predict the photocatalytic reaction rate. Using the L-H model, the rate of Hg^0 oxidation by SiO_2-TiO_2 under coal combustion flue gas conditions can be predicted. At an inlet Hg^0 concentration of 0.05 μ-mol m^{-3} (10 μg m^{-3}) and a water vapor concentration of 10 vol%, the reaction rate is calculated to be 7.7×10^{-6} μ-mol m^{-2} h^{-1} and the Hg^0 removal efficiency is around 7% in the current system (Q = 0.12 m^3 h^{-1} and A_e = 52.5 m^2 or 2.5 g of pellets used). However, a 95% removal efficiency can be achieved by increasing A_e by 14 fold (using 35 g of pellets or 56 mm bed height) which is practically applicable in a bench-scale reactor like the one used in this work. In addition, increasing the UV power level can be another option to reduce the required amount of catalysts as the reaction rate is proportional to the UV intensity (Lee, Biswas et al., 2004).

It is generally believed (Kim and Hong, 2002; Pitoniak et al., 2003; Raillard et al., 2004; Rodriguez et al., 2004; Shang et al., 2002) that the inhibitory effect of water vapor on photocatalytic reactions at relatively high water vapor concentrations is due to the competition between water vapor and the pollutants at the TiO_2 surface, i.e., a high concentration of water

vapor blocks the adsorption sites from pollutants. Unlike the mechanistic model developed by Rodríguez et al. (2004) where water vapor promoted Hg^0 capture by in situ-generated TiO_2 particles at low water vapor concentrations (<2000 ppm_v or 0.0815 mol m^{-3} at 25°C), the Hg^0 capture rate by the SiO_2-TiO_2 nanocomposite in this study reached maximum in dry air and decreased as the water vapor concentration increased. An explanation for the highest photocatalytic oxidation rate without water vapor may be related to the silanol (Si-OH) groups on the surface of the SiO_2-TiO_2 nanocomposite. The sol–gel reactions are performed in water/alcohol systems that cannot avoid the reverse reactions during the sol–gel process, i.e. hydrolysis and alcoholysis for silanol formation (Yang and Chen, 2005). Yang and Chen (2005) reported that a SiO_2 nanolayer around TiO_2 nanocrystals can enhance the efficiency of photocatalysis because the transfer of electrons to the silica sites and the hole scavenging by the hydroxides at the TiO_2-SiO_2 interface prevent the electrons and holes from recombination. In the SiO_2-TiO_2 nanocomposite produced in this work, the hydroxyl groups from silanols may act as traps for the holes generated by TiO_2 under UV irradiation and thus, an adequate number of hydroxyl radicals may be produced resulting in photocatalytic oxidation of Hg^0 even in the absence of water vapor. Similar findings were reported by Kim and Hong (2002) that photodegradation of methanol by TiO_2 reached the highest rate at considerably low water concentrations, which was explained due to the production of hydroxyl radicals from hydroxyl groups of methanol itself. In this manner, hydroxyl radicals generated from water molecules might be insignificant, and addition of water vapor may only prohibit Hg^0 photocatalytic oxidation by blocking the Hg^0 adsorption sites on the surface of the SiO_2-TiO_2 nanocomposite. In the system of Rodríguez et al. (2004), Hg^0 photocatalytic oxidation rate increased with water vapor at low water vapor concentrations, which may be because water vapor was the only source

for hydroxyl radical production. Comparisons between this study and that by Rodríguez et al. (2004) suggest that hydrophilic adsorbents (such as SiO_2-TiO_2 nanocomposite) may have better performance in Hg^0 removal at dry or very low humidity environment, and on the other hand, hydrophobic materials (such as TiO_2 nanoparticles) may yield a larger Hg^0 removal rate as the humidity increases. However, the performance of both types of materials will be inhibited at very high water vapor concentrations.

Summary

The kinetics of Hg^0 photocatalytic oxidation on a SiO_2-TiO_2 nanocomposite under UV irradiation was studied through experiments in a fixed-bed reactor. A Langmuir-Hinshelwood model was used to analyze the kinetic data. Good agreement between the experimental data and the L-H model was demonstrated, indicating the validity of using the L-H model to describe the kinetics of Hg^0 photocatalytic oxidation. Model predictions demonstrate a great potential of the SiO_2-TiO_2 nanocomposite for Hg^0 removal even at very high Hg^0 concentrations. The rate of photocatalytic Hg^0 oxidation increased when the inlet Hg^0 concentration increased and it reached a maximum value in the absence of water vapor. The addition of water vapor was found to inhibit Hg^0 photocatalytic oxidation, which may be explained by the competitive adsorption of water vapor with Hg^0 on the TiO_2 surface.

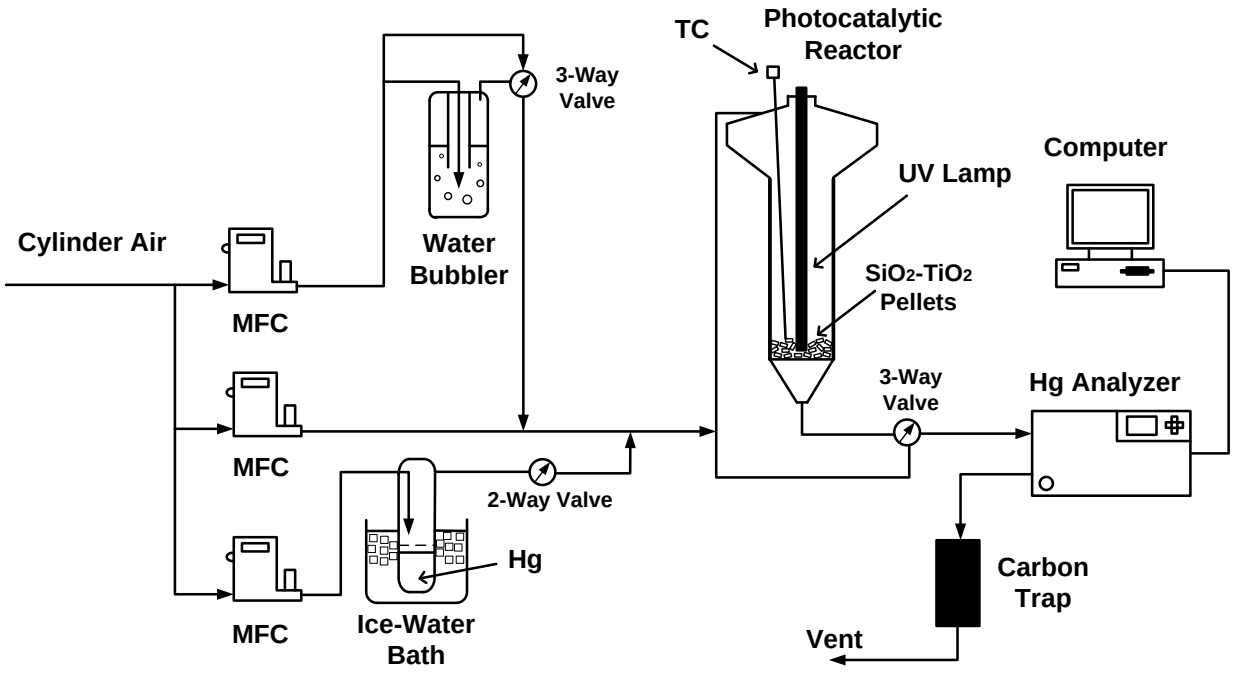

Figure 2-1. Experimental system for kinetic studies.

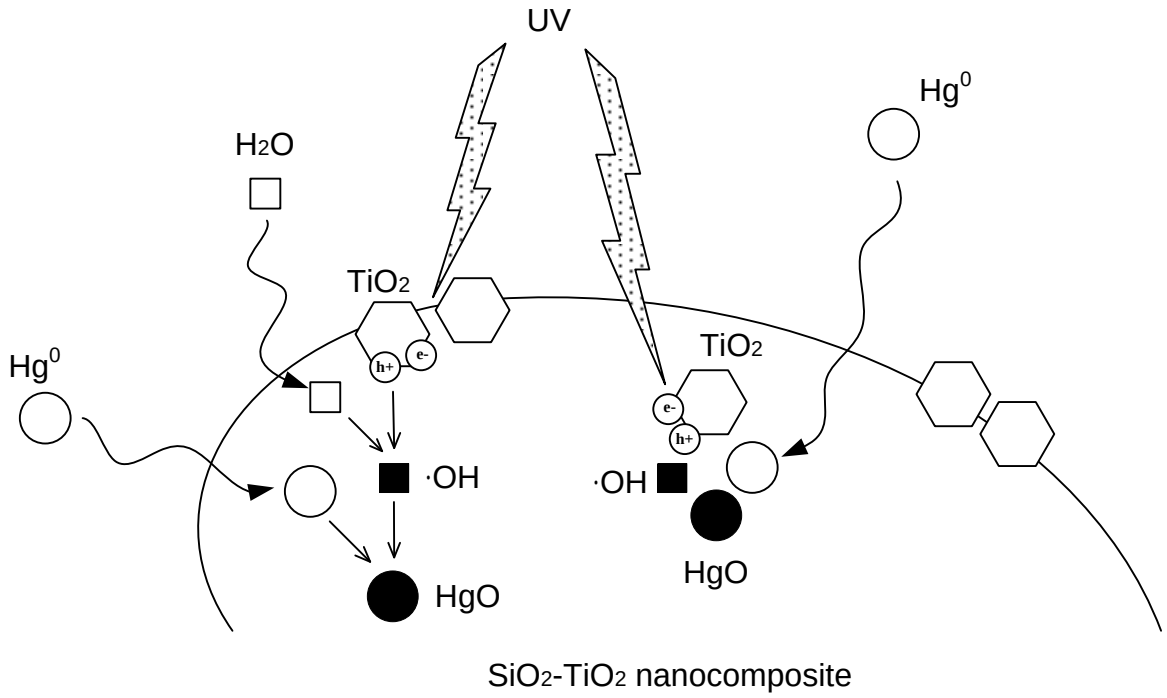

Figure 2-2. Description of Hg^0 photocatalytic oxidation on SiO_2-TiO_2 nanocomposites.

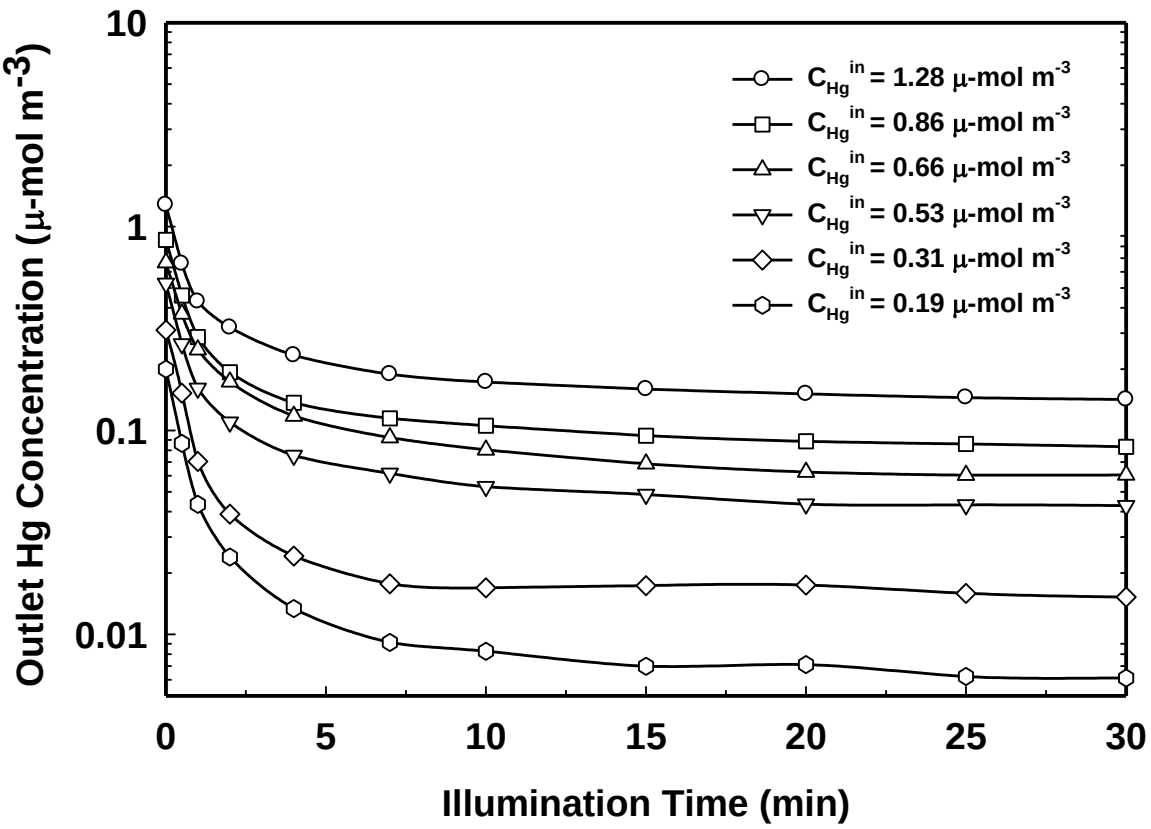

Figure 2-3. Photocatalytic oxidation of Hg^0 at different inlet Hg^0 concentrations without water vapor.

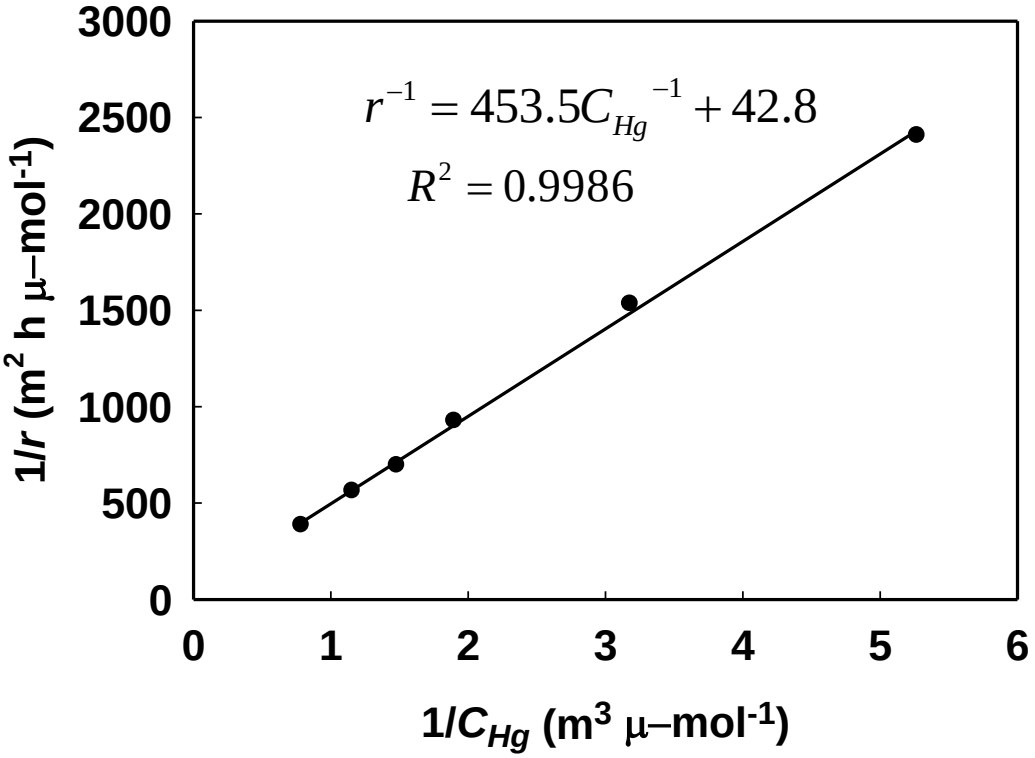

Figure 2-4. Inverse of Hg^0 photocatalytic oxidation rate versus the inverse of inlet Hg^0 concentration (without water vapor).

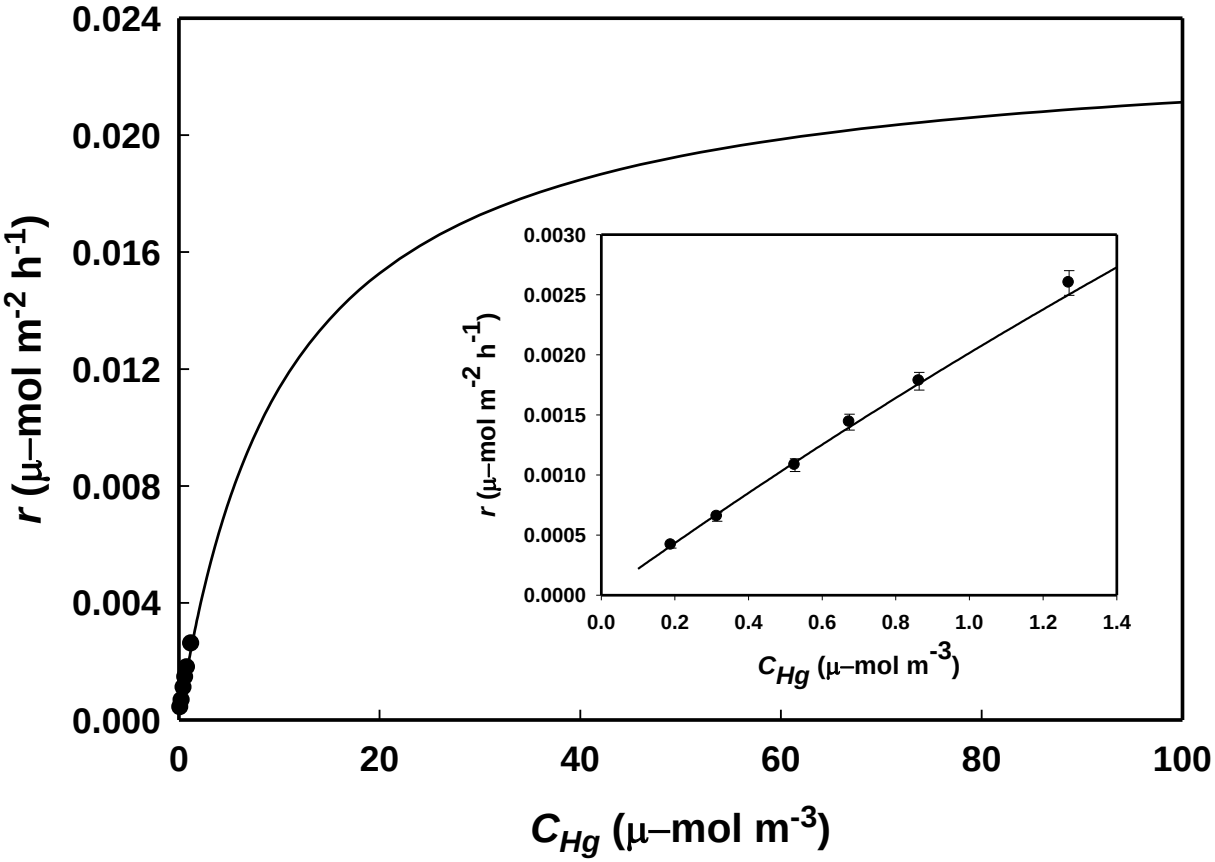

Figure 2-5. Rate of Hg^0 photocatalytic oxidation versus inlet Hg^0 concentration without water vapor (solid circles: experimental data; solid line: L-H model).

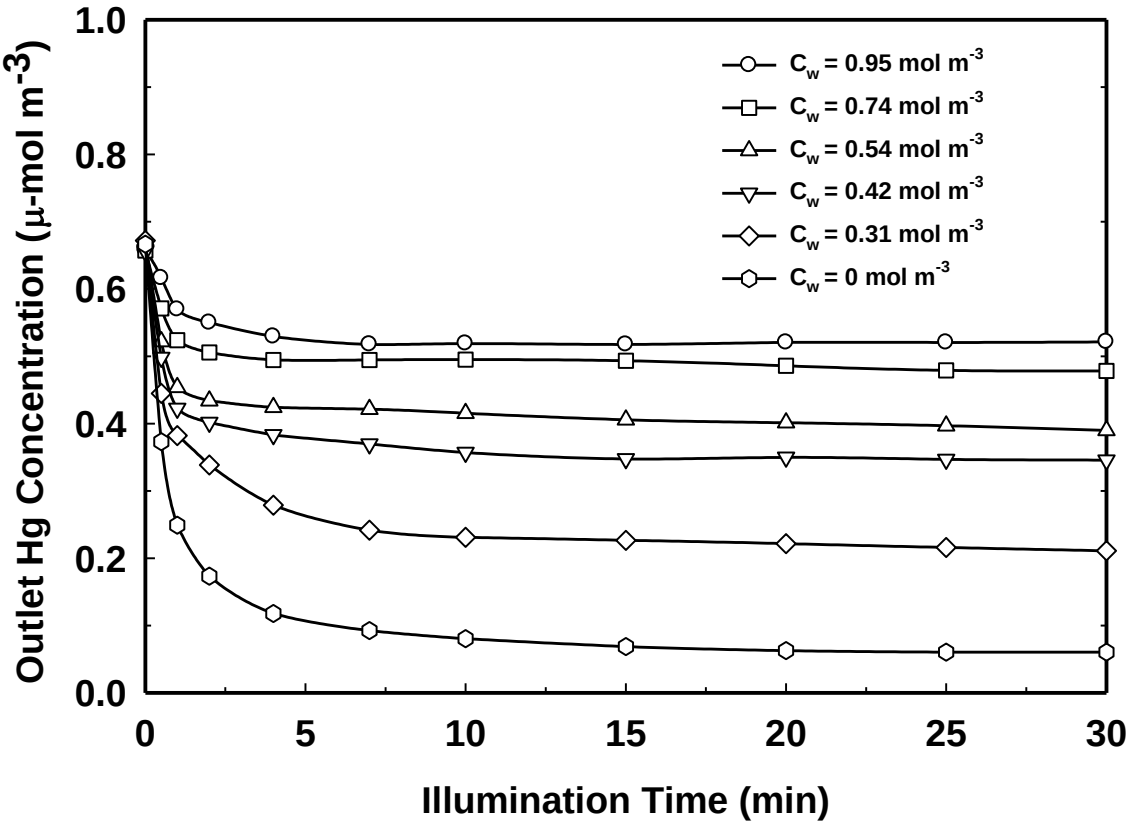

Figure 2-6. Photocatalytic oxidation of Hg^0 at a constant inlet Hg^0 concentration of 0.66 μ-mol m^{-3} with variation in water vapor concentration.

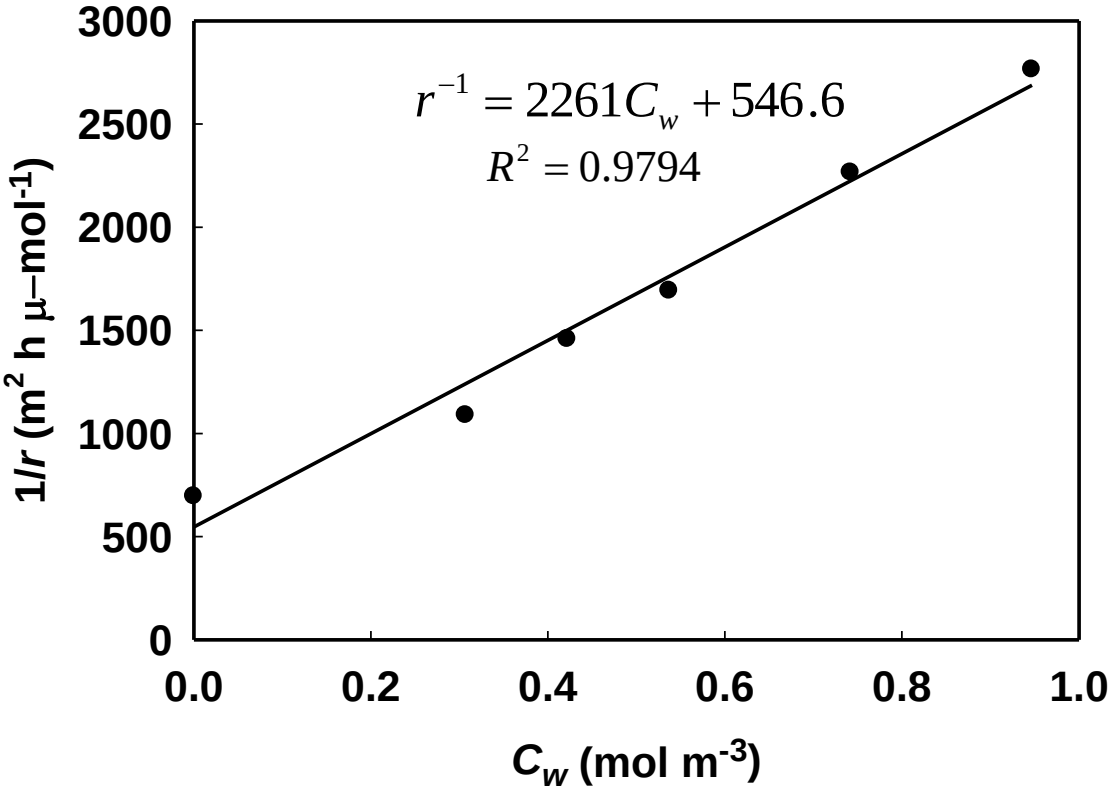

Figure 2-7. Inverse of Hg^0 photocatalytic oxidation rate versus water vapor concentration at a constant inlet Hg^0 concentration of 0.66 μ-mol m^{-3}.

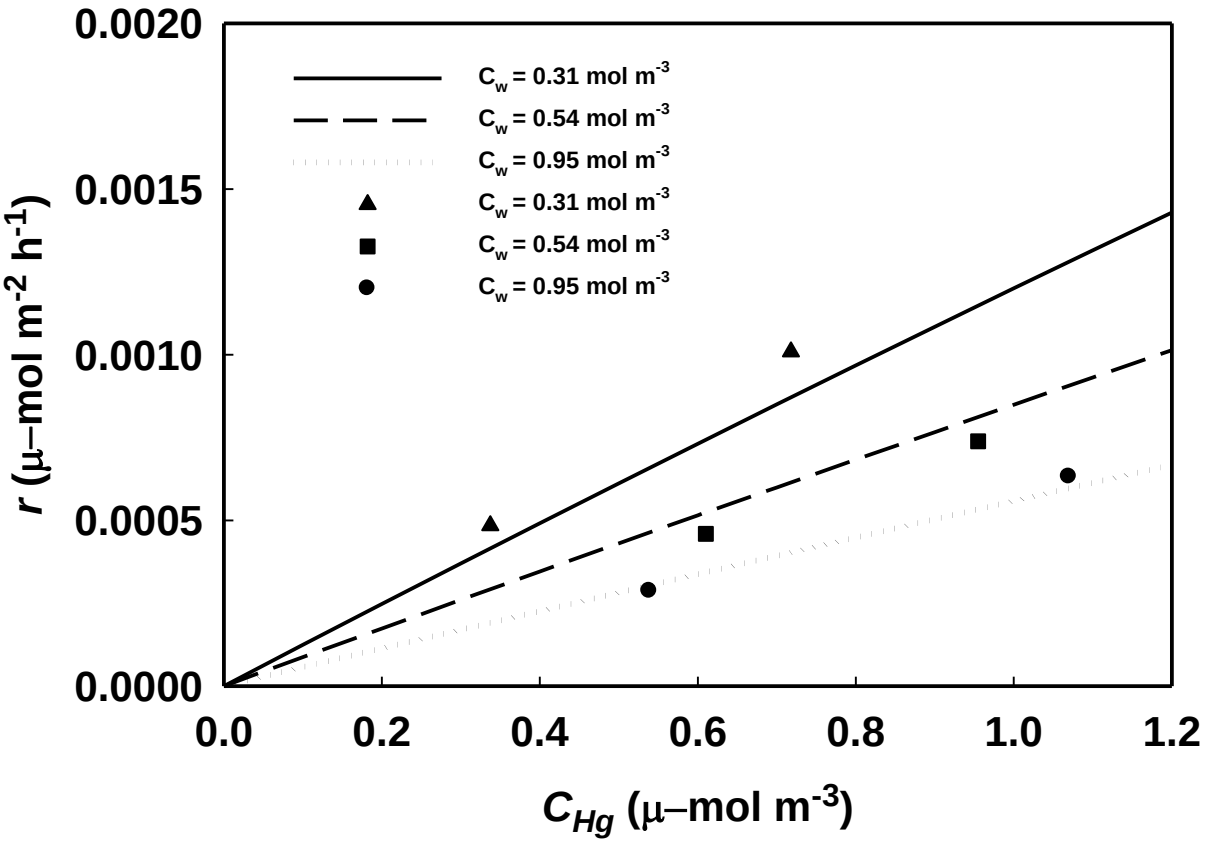

Figure 2-8. Rate of Hg^0 photocatalytic oxidation versus inlet Hg^0 concentration at different water vapor concentrations (markers: experimental data; lines: L-H model).

CHAPTER 3
ROLE OF MOISTURE IN ADSORPTION, PHOTOCATALYTIC OXIDATION, AND REEMISSION OF ELEMENTAL MERCURY ON A SILICA-TITANIA NANACOMPOSITE*

Background

Among the factors that affect the efficiency of Hg^0 capture by the TiO_2 photocatalyst, moisture content in the Hg^0-laden gas was reported to be one of the most important (Pitoniak et al., 2003; Rodriguez et al., 2004). Using *in-situ* generated TiO_2 nanoparticles in a flow reactor, Rodríguez et al. (2004) developed a mechanistic model and reported that Hg^0 capture was promoted by low water vapor concentrations (700 to 1800 ppm_v) but remained constant at higher water vapor concentrations. They also speculated that very high water vapor concentrations can inhibit Hg^0 oxidation by occupying available adsorption sites. Using a SiO_2–TiO_2 nanocomposite in a fixed-bed flow reactor, Pitoniak et al. (2003) reported that when the relative humidity increased from 15% to 90% at room temperature, the rate of Hg^0 adsorption decreased but that the rate of photocatalytic oxidation remained constant.

While there is limited understanding of the effect of water vapor on Hg^0 capture on TiO_2 surfaces, many research studies have investigated the effect of water vapor on photodegradation of organic pollutants in air streams using TiO_2 nanoparticles or thin films. Obee and Hay (1997) reported that moisture in the range of 0 to 25000 ppm_v inhibited photooxidation of ethylene by a TiO_2-coated glass plate. Shang et al. (2002) found that water vapor at concentrations of 3.7–22.4 g m^{-3} inhibited photocatalytic oxidation of heptane in a quartz reactor coated with TiO_2 particles. It was also reported that water vapor strongly inhibits the oxidation of trichloroethylene (TCE) and acetone (Kim and Hong, 2002) but enhances the oxidation of toluene (Augugliaro et al.,

* Reprinted with permission from Li, Y., Wu, C.-Y., 2006. Role of Moisture in Adsorption, Photocatalytic Oxidation, and Reemission of Elemental Mercury on a SiO_2-TiO_2 Nanocomposite. Environ. Sci. Technol. 40, 6444-6448. Copyright 2006 American Chemical Society.

1999; Kim and Hong, 2002). The results obtained using batch reactors coated with TiO_2 thin films were consistent with those using flow reactors packed with TiO_2 particles. These findings indicate that water vapor can either promote or inhibit photocatalyitc oxidation of different organic pollutants. This uncertainty about the effect of water vapor necessitates further investigation of the effect of moisture on Hg^0 oxidation by TiO_2-based photocatalysts.

The goal of this chapter was to probe the role of moisture on Hg^0 capture (adsorption and/or photocatalytic oxidation) using a SiO_2–TiO_2 nanocomposite. This study did not aim to explore the maximum Hg removal efficiency under certain emission conditions. Thus, the experimental conditions used in this study (65 °C gas temperature and up to 23,000 ppm_v H_2O) were designed to explore the range of emission conditions encountered in various combustion and manufacturing processes, and not to be representative of any specific process. In this study, possible reemission of captured Hg species was also examined, to provide an overall evaluation of the performance of the SiO_2–TiO_2 nanocomposite. The corresponding mechanisms of Hg^0 removal and reemission were investigated as well.

Experimental

Synthesis of SiO_2–TiO_2 Nanocomposite

The SiO_2–TiO_2 nanocomposite was made by a sol–gel method using deionized water, ethanol, and tetraethyl orthosilicate (TEOS). Nitric acid (HNO_3) and hydrogen fluoride (HF) were used as catalysts to increase the hydrolysis and condensation rates. A detailed synthetic procedure has been reported by Pitoniak et al. (2003). The nanocomposite was prepared in the form of cylindrical pellets approximately 5 mm in length and 3 mm in diameter. The weight fraction of TiO_2 in the prepared SiO_2–TiO_2 nanocomposite was approximately 13%.

Experimental Setup

A schematic diagram of the experimental system is shown in Figure 3-1. The incoming air flow was divided into three streams, the flowrates of which were controlled by mass flow controllers (FMA 5400/5500, Omega). The total flowrate remained constant at 2 L/min. One of the air streams was allowed to pass through a water bubbler (to provide a humid flow) or to bypass it for dry conditions. The second stream served as dilution to adjust the humidity level. The third stream passed through the surface of a liquid Hg^0 reservoir and introduced Hg^0–vapor-laden air into the system. The Hg^0 reservoir was placed in an ice–water bath to maintain a constant Hg^0 vapor pressure. After the three streams converged, a humidity sensor (HX94C, Omega) was used to measure the relative humidity, from which the partial pressure (volume fraction) of water can be calculated.

Downstream was the fixed-bed photocatalytic reactor, the lower part of which was a cylindrical tube of fused quartz 4.5 cm in diameter and 20 cm in length. The gas stream passed through the reactor from top to bottom. The reactor was mounted with a fused quartz center 2 cm in diameter, which was used to house a UV lamp. The UV light delivered 4 mW/cm^2 intensity measured by a UVX radiometer (with a UVX-36 sensor probe) at a peak wavelength of 365 nm. Aluminum foil was wrapped around the cylindrical tube to reflect UV energy. A heating mantle (regulated by a temperature controller) was used to heat the reactor to each selected temperature, which was monitored by a thermocouple (type K, Omega). At the bottom of the reactor a glass frit was used to hold the SiO_2–TiO_2 pellets within the bed. In this study, 2.5 g of fresh pellets was used in each test, which gave an average bed thickness of 4 mm (approximately one layer of pellets). Before each test, the pellets were heated at 130 °C for 3 h to remove any moisture that may have adsorbed from the storage environment.

A RA-915+ Hg analyzer (OhioLumex) was used to measure Hg^0 concentration at the outlet of the reactor. The Hg analyzer is based on Zeeman Atomic Absorption Spectrometry, which is selective only for Hg^0 and capable of providing a real-time response every 1 s. The calibration of the Hg analyzer was conducted by the manufacturer using a Dynacal® permeation device, which is certified traceable to NIST (National Institute of Standards and Technology) standards. In this study, the high-concentration mode of the analyzer was used (with a detection limit of 0.5 μg m^{-3} and an upper measurable concentration of 200 μg m^{-3}). A condenser was installed upstream of the Hg analyzer to remove excess moisture in the gas stream to minimize possible interference from water vapor. Although a Hg speciation converting unit could be used to analyze both Hg(II) and Hg^0 in the gas phase, it was not installed in this study. This is because HgO is the only product for the reaction between Hg^0 and hydroxyl radicals (Pal and Ariya, 2004; Sommar et al., 2001) and its extremely low saturation vapor pressure, 9.2×10^{-12} Pa at 25 °C (Schroeder and Munthe, 1998), causes HgO to deposit on the catalyst in the reactor. Baseline Hg^0 concentration was obtained when the Hg^0-laden air bypassed the reactor. The Hg^0 removal efficiency was obtained by comparing the outlet Hg^0 concentration with the baseline level. Finally, the air stream was passed through a carbon trap before it was exhausted into the fume hood.

Results and Discussion

Role of Moisture in Hg^0 Capture

To investigate the effect of moisture on Hg^0 capture by the SiO_2–TiO_2 nanocomposite, experiments were conducted at different water vapor concentrations (0, 13000, and 23000 ppm_v). Blank runs without the nanocomposite were performed at concentrations of around 65 μg m^{-3} Hg^0 and 0 and 23000 ppm_v water vapor. Less than 0.5% reduction in Hg^0 concentration was observed when the Hg^0-laden air passed through the reactor with or without UV light. Tests were also conducted to examine any possible interference of water vapor on measurements by the Hg

analyzer. While exactly the same experimental parameters were maintained, variations in the Hg readings were less than 1% when switching from a dry to a humid (23000 ppm_v H_2O) condition, indicating negligible interference from water vapor in this range.

In each experiment, the baseline Hg^0 concentration (Hg^0_{BL}, ~65 µg m^{-3}) was measured first. Then the Hg^0-laden air was passed through the reactor for 10 min and concentrations defining the initial adsorption (IA) of Hg^0 were recorded. Next, the UV light was turned on for 10 min—allowing photocatalytic oxidation of Hg^0 to take place—and then turned off for 5 min. Another two such UV on/off cycles were repeated, and concentrations defining the final removal (FR) efficiency were recorded. After that, Hg^0_{BL} was checked again, and the Hg^0-laden air was passed through the reactor without UV for 15 min. Finally concentrations to compute the adsorption at the end of the test (EA) were recorded.

The temperature at the pellet surface was maintained near 65 °C throughout the experiment. Measured 5 mm above the pellets, the temperature of the gas passing through the pellets was approximately 1.5 °C lower than that of the pellets. To maintain a relatively constant temperature, the heating mantle around the reactor was turned off when the UV lamp was switched on in each cycle and back on when UV was switched off. The fluctuations in temperature of both pellets and gas were measured to be ±2 °C. A preliminary test showed that the change in the final removal efficiency was less than 5% when the average temperature of the pellets increased from 65 to 70 °C. This indicated that the fluctuations within this range of temperature had negligible effects on the reaction rate.

Figure 3-2 shows the dimensionless Hg^0 concentration [Hg^0/Hg^0_{BL}] at the outlet of the reactor in dry and humid conditions. Under dry conditions (Figure 3-2A), Hg^0 removal efficiency increased with successive cycles and FR reached 95% during the fourth irradiation. Adsorption

was initially insignificant (IA = 5%), but it was enhanced at the end of the test (EA = 22%). In contrast, when the water vapor concentration was increased to 13000 ppm_v (Figure 3-2B), Hg^0 removal increased only slightly with successive cycles and FR ended at only 51%. When the water vapor concentration was further increased to 23000 ppm_v (Figure 3-2C), FR decreased to 28%.

In addition, Hg^0 adsorption was found to be insignificant throughout the test under these two humid conditions. A separate test was conducted extending the adsorption time to 2 h (without UV), and no adsorption was observed. This verified that the recorded values of IA and EA were measured at adsorption equilibrium. Experiments under the three humidity conditions were repeated and similar results were recorded. The results indicated that increased humidity can significantly suppress both Hg^0 adsorption and photocatalytic oxidation on the nanocomposite.

Role of Moisture in Hg^0 Reemission

Potential reemission of Hg species from the SiO_2–TiO_2 nanocomposite after their capture is an important factor in evaluating the overall performance of the nanocomposite. The experiment to examine Hg reemission began by exposing 2.5 g of fresh pellets for 3 h to UV light in a stream containing approximately 300 $\mu g/m^3$ Hg^0 vapor in dry air at room temperature. During the 3-h pretreatment, Hg^0 capture efficiency by the nanocomposite reached about 90% after 30 min and remained relatively steady between 90 and 95% for the rest of the time (as shown in the insert in Figure 3-3). The Hg species retained on the nanocomposite are predicted to be a mixture of HgO (due to photocatalytic oxidation) and Hg^0 (due to adsorption enhanced by HgO) (Pitoniak et al., 2005).

After the pretreatment, Hg^0 release from the nanocomposite at room temperature was examined by feeding Hg^0-free air into the reactor (see Figure 3-3). During the first 5 min, dry air

(condition I) was allowed to pass through the pretreated pellets and only traces of reemitted Hg^0 were found. However, immediately after the air stream was switched from dry to humid ([H_2O] = 23000 ppm_v, condition II), a significant release of Hg^0 was observed, peaking briefly at 68 $\mu g/m^3$, about 23% of the Hg^0 feeding level during pretreatment. Even though the Hg^0 reemission level decreased over time, it remained relatively high (43 $\mu g/m^3$) after 20 min. Hg^0 reemitted during this 20-min period was calculated to be approximately 2.1% of the total Hg species (Hg^0 and HgO) retained on the pellets during the 3-h pretreatment.

At 25 min, UV light was turned on while the air stream remained humid (condition III), and the Hg^0 concentration quickly dropped to approximately 10 $\mu g/m^3$. This suggests that a large portion of the Hg^0 reemitted was photooxidized during irradiation. At 35 min, the UV light was turned off (return to condition II), and the rate of Hg^0 reemission did not recover to the previous high level, but further decreased to approximately 6.5 $\mu g/m^3$. Turning the UV on again (return to condition III) at 45 min caused the Hg^0 concentration to return to an extrapolation of the line observed during the first period at condition III. When the condition was switched at 55 min to dry air with UV on (condition IV), the Hg^0 concentration decayed to approximately zero in 5 min. The results of the reemission test were repeatable using another batch of pellets undergoing the same pretreatment procedure.

One may draw three conclusions about Hg^0 reemission under the conditions tested: (1) Hg^0 reemission does not occur in dry air, with or without UV light. (2) Introducing water vapor causes significant Hg^0 reemission, which slowly decreases over time. (3) Exposure to UV light in humid air can either inhibit or promote Hg^0 reemission.

Mechanisms of Hg^0 Capture and Reemission

To explain these intriguing findings, a comprehensive model is developed in this work elucidating the fate of Hg species on the surface of this SiO_2–TiO_2 nanocomposite. In this model,

as illustrated in Figure 3-4, Hg^0 capture is accomplished by photocatalytic oxidation and adsorption, while Hg^0 reemission results from desorption and photocatalytic reduction.

Photocatalytic oxidation of Hg^0 occurs during UV irradiation of the SiO_2–TiO_2 nanocomposite, as shown in Figure 3-4a. Hg^0 is oxidized by OH radicals generated on the TiO_2 surface, and HgO has been reported to be the final oxidation product in literature (Lee et al., 2001; Pal and Ariya, 2004; Pitoniak et al., 2003; Pitoniak et al., 2005; Rodriguez et al., 2004; Sommar et al., 2001). Pal and Ariya (2004) experimentally identified HgO as the only product for gas-phase reaction of Hg^0 with OH radicals, while HgOH was suggested to be an intermediate reaction product (Pal and Ariya, 2004; Rodriguez et al., 2004; Sommar et al., 2001) that has a very short lifetime (Goodsite et al., 2004). The fast removal of Hg^0 in this study (see Figure 3-2) was consistent with rates reported by researchers (Pitoniak et al., 2003; Pitoniak et al., 2005) using similar experimental systems. It was faster than OH–Hg reactions reported under simulated atmospheric conditions (Calvert and Lindberg, 2005; Pal and Ariya, 2004; Sommar et al., 2001), most likely due to the much higher concentration of OH radicals produced on the high-surface-area, open-structured SiO_2–TiO_2 nanocomposite. The overall mechanism of photocatalytic oxidation can be described by the following reactions:

$$TiO_2 + h\nu \rightarrow e^- + h^+ \quad (3\text{-}1)$$

$$H_2O \leftrightarrow H^+ + OH^- \quad (3\text{-}2)$$

$$h^+ + OH^- \rightarrow \cdot OH \quad (3\text{-}3)$$

$$h^+ + H_2O \rightarrow \cdot OH + H^+ \quad (3\text{-}4)$$

$$OH\cdot + Hg^0 \xrightarrow{overall} HgO \quad (3\text{-}5)$$

It should be noted that the specifications of the cylinder air indicated a water vapor concentration of less than 24 ppm_v. This low concentration of water vapor could not be detected

by the humidity sensor, and thus, the air was considered "dry." However, this water vapor concentration is 3 orders of magnitude higher than that of Hg^0 used in this study. Further, the SiO_2–TiO_2 pellets have a great capacity to adsorb water vapor. Tests demonstrated that 2.5 g of SiO_2–TiO_2 pellets can adsorb an average of 0.16 g of water vapor in 30 min when exposed to an air flow containing 23000 ppm_v water vapor. Therefore, even though the pellets were pretreated at 130 °C for 3 h before each experiment to remove any interior moisture, they adsorbed enough moisture (compared to the trace amount of Hg^0) from the cylinder air to support the generation of OH radicals and subsequent photocatalytic oxidation.

Physisorption of Hg^0 is minor if the SiO_2–TiO_2 nanocomposite is not exposed to UV light, but it can be enhanced by HgO that is deposited on the composite's surface after photocatalytic oxidation takes place (Figure 3-4b). This is likely due to the high affinity between Hg^0 and HgO, which was characterized by a decrease in the contact angle of Hg on the HgO-enriched sorbent surface (Pitoniak et al., 2005). However, this enhanced adsorption ability was not observed in humid conditions due to the inhibitory effect of water vapor.

It is generally believed that water vapor inhibits photocatalytic reactions by blocking the available adsorption sites on the surface of TiO_2 catalysts (Kim and Hong, 2002; Pitoniak et al., 2003; Shang et al., 2002). The results of this study suggest that desorption of bound Hg^0 by a high concentration of water vapor (Figure 3-4c) also contributes to the reduced Hg^0 capture rate. The reason is likely related to the photoinduced superhydrophilicity of TiO_2 surfaces (Fujishima et al., 2000; Wang et al., 1997). During the process of photocatalysis, the electrons tend to reduce the Ti(IV) cations to the Ti(III) state, and the holes oxidize the O^{2-} anions. In the process, oxygen atoms are ejected, creating oxygen vacancies. Water molecules can then occupy these oxygen vacancies and create adsorbed OH groups, which tend to make the surface hydrophilic.

Hence, in our experiments, when humid air passed through the reactor, the superhydrophilic surface of TiO_2 may attract excessive amount of water and result in ejection of adsorbed Hg^0 (which is superhydrophobic) from the surface (Figure 3-4c). This mechanism is similar to the self-cleaning (stain proofing) quality of TiO_2-coated glass (Fujishima et al., 2000; Guan, 2005), from which organic stains are washed away by rainfall (or water) on the superhydrophilic surface.

A sharp decrease in Hg^0 concentration was detected when switching from the initial condition II to III (Figure 3-3). A very possible reason is that the desorbed Hg^0 was reoxidized upon UV irradiation and re-captured onto the pellets. However, the increase in Hg^0 concentration when switching from the second condition II to III indicated that UV irradiation contributed to the reemission of Hg^0 from the pellets. This can be explained by the photocatalytic reduction of HgO to Hg^0 by the free electrons generated on TiO_2 surface under UV light (Figure 3-4d). The mechanism is expressed in Reaction 3-6, which has a reduction potential of 0.098V vs. normal hydrogen electrode (NHE) (Meites, 1963):

$$HgO + H_2O + 2e^- \rightarrow Hg + 2OH^- \qquad (3\text{-}6)$$

To validate the occurrence of Reaction 3-6 in this study, its redox potential was compared with those in other photocatalytic reactions on TiO_2 reported in the literature. Fujishima et al. (2000) reported reduction of O_2 to H_2O_2 on a TiO_2 photocatalyst. Zhang et al. (2004) used TiO_2-modified sewage sludge carbon for photocatalytic removal and recovery of Hg^{2+} in the form of Hg^0 from water. The redox potentials of O_2/H_2O_2 and Hg^{2+}/ Hg are 0.28V (Fujishima et al., 2000) and 0.85V (Meites, 1963), respectively. Thus, it is reasonable to infer that Reaction 3-6, which has a much lower redox potential (0.098V), can occur in our system. The necessity of H_2O

in Reaction 3-6 is also consistent with the finding that no Hg^0 reemission occurred in dry air with UV irradiation.

Separate experiments were conducted in pure O_2 and N_2, respectively, and the results further supported the hypothesis that photocatalytic reduction caused the reemission of Hg^0. Under humid conditions and UV irradiation, a higher Hg^0 reemission level was observed in N_2 than in O_2. Because the redox potential of O_2/O_2^- (-0.28 V) is lower than that of HgO/Hg, O_2 is a stronger electron trap than HgO. The absence of O_2 increased the chance for HgO to trap electrons, and thus more HgO was reduced to Hg in pure N_2.

The intriguing finding that UV irradiation can result in either inhibition or promotion of Hg^0 reemission (as shown in Figure 3-3) can then be explained by the competition between photocatalytic oxidation of reemitted Hg^0 to form HgO (Reaction 3-5) and photocatalytic reduction of HgO to form Hg^0 (Reaction 3-6), accompanied by the physical desorption of Hg^0 caused by water vapor at the same time. At the moment when the condition was first changed from II to III, the concentration of desorbed Hg^0 was very high, and thus photocatalytic oxidation prevailed over reduction, which resulted in a sharp decrease in Hg^0 concentration. Over time, the rate of photocatalytic oxidation decreased as the Hg^0 desorption rate decreased. When the condition was switched from II to III for the second time, the rate of photocatalytic oxidation dropped to a lower level than that of photocatalytic reduction, so the level of Hg^0 reemission increased.

The above discussion boils down to a conclusion that Hg^0 capture on the SiO_2–TiO_2 nanocomposite in a humid environment under UV irradiation is controlled by four mechanisms: adsorption; photocatalytic oxidation; desorption; photocatalytic reduction. Water vapor concentration is a significant parameter affecting the Hg^0 capture efficiency. The inhibitory

effect of water vapor is due to its competitive occupancy of the available adsorption sites, displacement of adsorbed Hg^0, and participation in the photocatalytic reduction of HgO to Hg^0.

Hg^0 reemission seems to be inevitable since humidity exists in most environmental conditions. However, the mechanisms discussed above imply that appropriate application of UV irradiation can be utilized to mitigate this Hg^0 reemission. The difference between the first and second condition II in Figure 3-3 shows that UV treatment caused a significant drop of the Hg^0 reemission level. However, further exposure to UV light caused an increase in the Hg^0 reemission due to the dominant photocatalytic reduction later on. Therefore, determining the optimal time of UV treatment and avoiding further exposure to UV sources (including sunlight) are critical to achieving minimal Hg^0 reemission.

Summary

A novel silica–titania (SiO_2–TiO_2) nanocomposite has been developed to effectively capture elemental mercury (Hg^0) under UV irradiation. Moisture has been reported to have an important impact on this nanocomposite's performance. In this work, the role of moisture on Hg^0 removal and reemission as well as the corresponding mechanisms was investigated. Hg^0 removal experiments were carried out in a fixed-bed reactor at 65 °C using air as the carrier gas. Without UV irradiation, Hg^0 adsorption was found to be insignificant, but it could be enhanced by the photocatalytic oxidation product, mercuric oxide (HgO), possibly due to the high affinity between HgO and Hg^0. Under dry conditions 95% of Hg^0 can be removed; however, increased humidity levels remarkably suppress both Hg^0 adsorption and photocatalytic oxidation. Introducing water vapor can also result in significant reemission of captured Hg^0 from the nanocomposite, which may be ascribed to the repellant effect of water vapor adsorbed on the superhydrophilic TiO_2 surface. Exposure to UV light was found either to prohibit Hg^0 reemission when photocatalytic oxidation of reemitted Hg^0 prevailed or to promote Hg^0 reemission when

photocatalytic reduction of HgO to Hg^0 dominated later on. The results indicate that minimization of Hg^0 reemission can be achieved by appropriate application of UV irradiation.

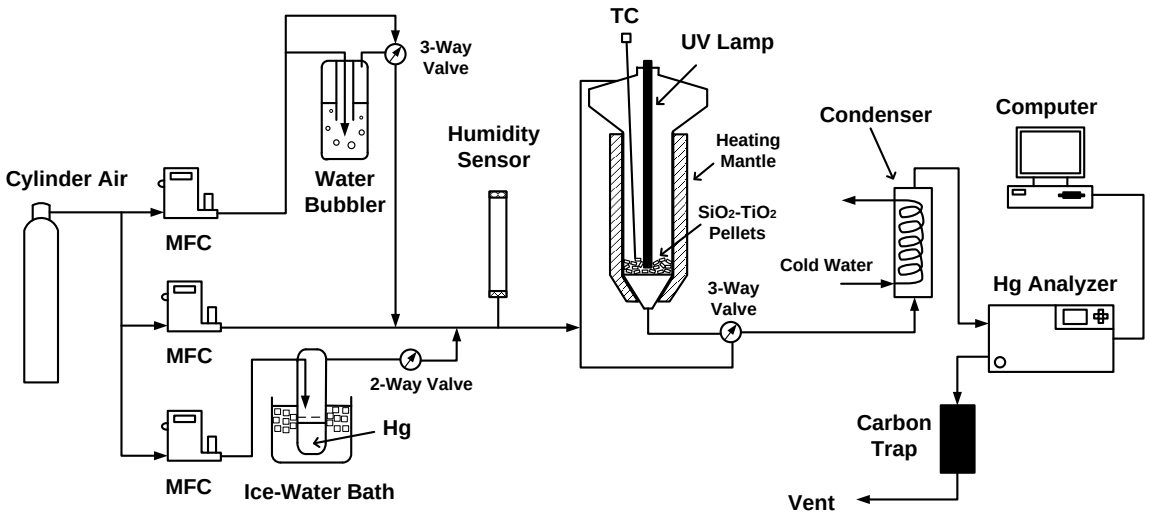

Figure 3-1. Experimental system for studies on the role of water vapor.

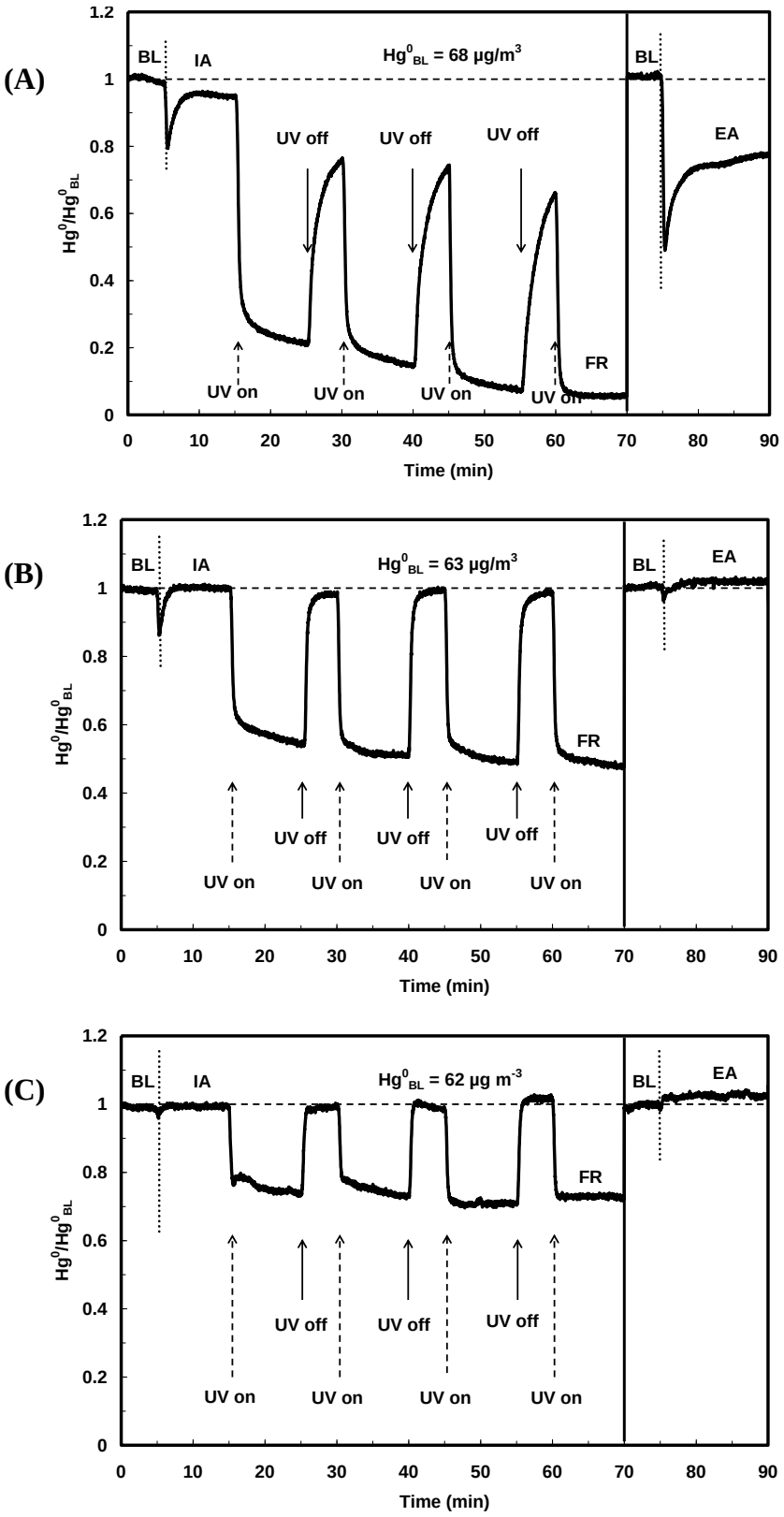

Figure 3-2. Dimensionless Hg^0 concentration at the reactor outlet (A, $[H_2O]$ = 0 ppm_v; B, $[H_2O]$ = 13000 ppm_v; C, $[H_2O]$ = 23000 ppm_v)

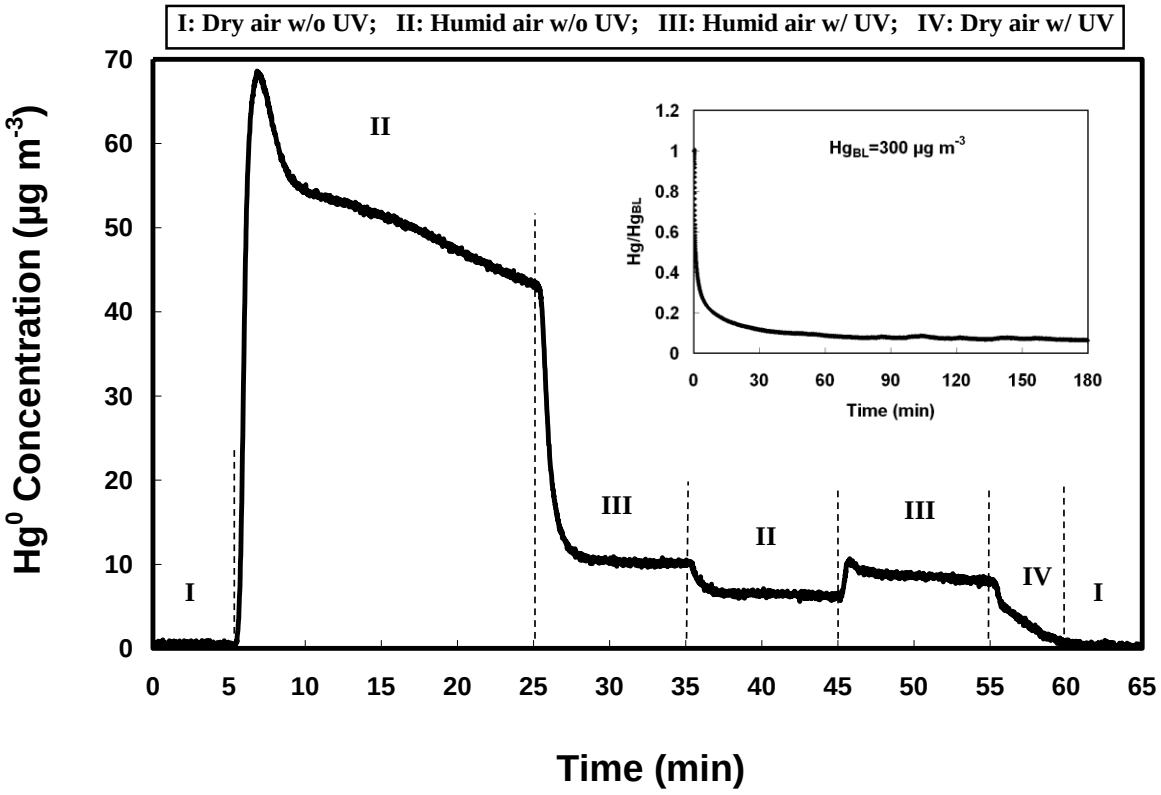

Figure 3-3. Hg^0 reemission from SiO_2–TiO_2 nanocomposite after 3-h pretreatment (The inset shows the dimensionless Hg concentration during the pretreatment).

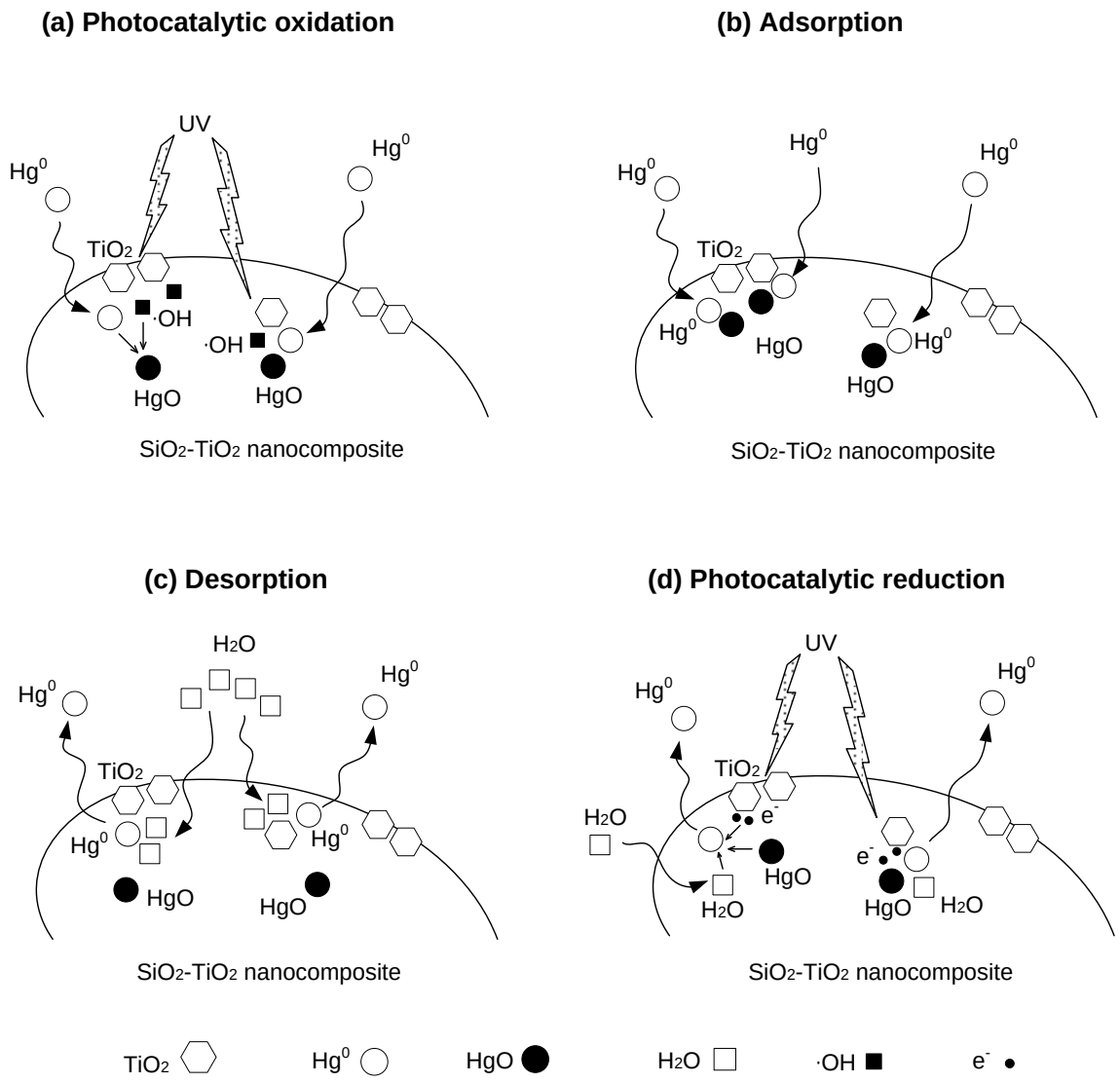

Figure 3-4. Mechanisms of Hg capture and reemission on the surface of SiO_2–TiO_2 nanocomposite.

CHAPTER 4
REMOVAL OF ELEMENTAL MERCURY FROM FLUE GAS USING A SILICA-TITANIA NANOCOMPOSITE*

Background

The SiO_2-TiO_2 nanocomposite has exhibited very high efficiency of Hg^0 removal (up to 99%) under room conditions with low relative humidity (Pitoniak et al., 2003). However, as reported in Chapters 2 and 3, at room temperature but higher water vapor concentrations (up to 23,000 ppm_v), Hg^0 capturing on the nanocomposite was hindered due to the competitive adsorption of water vapor on the active sites, and the extent of prohibition in Hg^0 removal was proportional to the water vapor concentration (Li and Wu, 2006, 2007). It should be noted that in coal-fired boiler flue gas, the concentration of water vapor typically accounts for several percent in volume, much higher than that in the room conditions. Thus, it is expect that water vapor may have a greater inhibitory effect on Hg^0 removal in flue gas. One the other hand, the catalyst developed in this work was designed for application in the cold-end of the boiler convective pass (e.g. between the electrostatic precipitator and the wet scrubber), where the typical flue gas temperature (120 to 150°C) is higher than room temperature. In this aspect, the competitive adsorption of water vapor on the catalyst would be smaller at higher temperatures. These two counteracting effects warrant further investigation on the performance of the SiO_2–TiO_2 nanocomposite for Hg^0 removal in flue gas.

Typical coal-derived flue gas consists of various minor gas components such as HCl, SO_2, and NOx, concentrations of which vary when burning different types of coal. It has been reported that these minor gases are important to the heterogeneous adsorption and/or oxidation of Hg^0 on activated carbons or fly ash in flue gas conditions (Carey et al., 1998; Norton et al.,

* Reprinted with permission from Li, Y., Murphy, P.D., Wu, C.Y. Removal of Elemental Mercury from Flue Gas Using A Silica-Titania Nanocomposite. Submitted to Fuel Process. Technol.

2003). Carey et al. (1998) reported that the adsorption capacity for both Hg^0 and $HgCl_2$ by Darco FGD carbon dramatically increased as HCl concentration increased from 0 to 50 ppm but decreased as the SO_2 concentration increased from 0 to 500 ppm. Norton et al. (2003) reported that in the presence of fly ash, NO_2, HCl, and SO_2 resulted in greater levels of Hg oxidation while NO inhibited Hg oxidation. It is expected that the nature of Hg capture on the SiO_2–TiO_2 nanocomposite would be different in flue gas conditions from that reported in room conditions in our previous studies.

In this work, a photocatalytic reactor packed with SiO_2–TiO_2 nanocomposite was installed. The goal of this research was to identify the effects of the flue gas components on the removal of Hg^0 by SiO_2–TiO_2 nanocomposite and to explore possible surface interaction mechanisms. An improved understanding of the role of the flue gas components can help evaluate the potential of applying this novel material as an effective Hg control strategy for coal-fired power plants.

Experimental Methods

Synthesis of the SiO_2–TiO_2 Nanocomposite

The SiO_2–TiO_2 nanocomposite was made by a sol–gel method using deionized water, ethanol and tetraethyl orthosilicate (TEOS). Nitric acid (HNO_3) and hydrogen fluoride (HF) were used as catalysts to increase the hydrolysis and condensation rates. A detailed procedure was described in our previous study (Li and Wu, 2007). The nanocomposite was prepared in the form of cylindrical pellets approximately 5 mm in length and 3 mm in diameter. The weight fraction of TiO_2 in the prepared SiO_2–TiO_2 pellets was approximately 12%, which corresponded to the optimum performance of Hg^0 removal in room conditions (Pitoniak et al., 2003). The average BET (Brunauer, Emmett, and Teller equation) surface area of the nanocomposite was measured to be 280 $m^2\ g^{-1}$ using a Quantachrome NOVA 1200 Gas Sorption Analyzer (Boynton Beach, FL).

Experimental Setup and Procedure

A schematic diagram of the experimental setup is shown in Figure 4-1. The simulated flue gas consisted of three major gases: O_2, CO_2, and N_2. The N_2 flow was divided into three branches. One of the N_2 streams converged with the O_2 and CO_2 to form the main gas flow, which was allowed to pass through a heated water bubbler to introduce water vapor into the system. The second stream of N_2 served to dilute the main flow so as to adjust the humidity of the total gas stream. The third stream of N_2 passed through a Dynacal® Hg^0 permeation tube (VICI Metronics) and introduced the saturated Hg^0 vapor into the system. The permeation tube was placed in a U-shape glass tube which was immersed in a constant-temperature (90 ± 0.2 °C) water bath to ensure a constant Hg^0 permeation rate. Hg^0 concentration in the system was controlled in the range of 75~80 μg m^{-3}. Minor gases including HCl, SO_2, NO, and NO_2 were introduced into the main flow individually or in combination. A mass flow controller (MFC) was used to control each of the gas flow with a total gas flow rate controlled to be 2.0 L/min. The gas concentrations were designated to be within the range of typical flue gas composition (Senior et al., 2000): 4% O_2, 12% CO_2, 4~16% H_2O, 10~50 ppm HCl, 400~1200 ppm SO_2, 50~300 ppm NO, 10~30 ppm NO_2, and balanced with N_2. The experimental conditions for investigation of the flue gas effects are listed in Table 4-1.

Downstream of all the gas flows was the packed-bed photocatalytic reactor placed horizontally. The SiO_2–TiO_2 pellets were packed in a U-shape quartz tube with an inner diameter of 13 cm. A heating cord was wrapped around the U-tube so that the flue gas temperature can be controlled at around 135 °C, which was monitored by a Teflon thermocouple (Type K, Omega). A UV lamp was placed in a separate quartz tube centered in the reactor and 5 cm above the centerline of the U-tube. The UV light had a peak wavelength of 365 nm with an intensity of 4 mW/cm^2 measured by a UVX radiometer (with a UVX-36 sensor probe). A stream of cooling air

was continuously purged through the UV lamp to lower the lamp temperature to around 60 °C. The entire reactor was placed inside an aluminum cylinder so that the UV light could be reflected back to the pellets and a maximum utilization of the UV energy could be achieved.

A wet-chemistry conversion system (Laudal et al., 2004; McLarnon et al., 2005) and a RA-915+ Hg analyzer (OhioLumex) were used to measure gas-phase Hg speciation (Hg^0 and Hg(II)) downstream the reactor. The Hg analyzer is based on Zeeman Atomic Absorption Spectrometry (ZAAS), which is selective only for Hg^0. In the conversion system, the sampling gas was divided into two streams, one for measuring Hg^0 and the other for total Hg (Hg^T). The solution used for Hg^0 measurement consisted of 10% potassium chloride (KCl), which captures Hg(II) and allows only Hg^0 to pass through. Hg^T measurement was accomplished using an acidic 10% stannous chloride ($SnCl_2$) solution, which reduces Hg(II) to Hg^0, thus producing Hg^T. The concentration of Hg(II) can then be calculated by the difference between Hg^T and Hg^0. The two streams converged to a 10% sodium hydroxide (NaOH) before entering the Hg analyzer. The NaOH solution captured acid gases, such as HCl and SO_2, to prevent corrosion of the detecting cell of the Hg analyzer. In addition, as part of the conversion process, a NaOH solution was used to remove SO_2 before the sampling gas entered the $SnCl_2$ solution, as SO_2 can interfere with the reduction of Hg(II) by $SnCl_2$ (Laudal et al., 2004). A condenser was installed upstream of the Hg analyzer to remove excess moisture in the gas stream. This aimed to avoid condensation of water vapor inside the Hg detection cell and thus to minimize possible interference from water vapor. The Hg analyzer was capable of providing a real-time response every 1 s. The calibration of the Hg analyzer was conducted by the manufacturer using a Dynacal® permeation device. In this study, the high-concentration mode of the Hg analyzer was used (with a detection limit of 0.5 μg m^{-3} and an upper measurable concentration of 200 μg m^{-3}). Finally, the gas stream was passed

through a carbon trap before it was exhausted into the fume hood. The entire system was Teflon lined. To avoid condensation of the water vapor along the pathway, all the lines before the condenser were heated by heating tapes to above 90°C.

Results and Discussion

Baseline Test

Tests were first conducted to examine any possible interference caused by the flue gas components on the measurement of the Hg analyzer. Balanced with pure N_2, 8% H_2O, 50 ppm HCl, 1200 ppm SO_2, 300 ppm NO, and 30 ppm NO_2 were individually introduced to the system without the presence of Hg. In all cases, no significant Hg readings were observed (i.e. the interference was less than the detection limit, 0.5 μg m^{-3}) with or without the UV irradiation. This indicated negligible interference by the flue gas components in the concentration ranges studied in this paper. In addition, tests were performed by introducing 80 μg m^{-3} Hg^0 to an empty reactor (i.e. no catalyst) with or without UV irradiation. Less than 0.5% reduction in Hg^0 concentration was observed, which indicated that the loss of Hg^0 on the reactor wall was negligible.

To examine the effect of individual flue gas components, a baseline test without the minor gases (Set 1) was first conducted. While a larger amount of SiO_2–TiO_2 pellets could be used to achieve a Hg removal efficiency greater than 90%, only 8 g of pellets (~1 g TiO_2) were used to better manifest possible enhancement by the minor gases in subsequent tests. As shown in Figure 4-2, the inlet Hg concentration was measured within the first 10 min when the gas stream bypassed the reactor (Period A). Next, the gas stream was passed through the reactor without UV light for another 10 min (Period B) and then the UV light was turned on to activate the photocatalytic reaction (Period C). The concentrations of Hg^T and Hg^0 at the outlet of the reactor

were recorded in alternation and were averaged every 2 min for Periods A and B and every 10 min for Period C.

In Period A, the concentration of Hg^T was equal to that of Hg^0, confirming that the Hg source in this study was only Hg^0. In Period B when the gas passed through the reactor, the outlet Hg concentration first dropped by approximately 10%, probably due to the physical adsorption by the porous SiO_2–TiO_2 pellets. However, it quickly recovered to the same level of the inlet concentration indicating the adsorption was saturated. A significant decrease in Hg concentration was detected only when the UV light was turned on in Period C. The concentration of Hg^T dropped to 59% of the inlet level during the first 10 min of UV irradiation and slowly decreased to 53% in the next 80 min. At 100 min, the rate of the decrease of Hg^T was approaching zero, and thus it was assumed that the performance of the catalyst reached a relatively stable level at this point. At 100 min, the outlet concentration of Hg^0 decreased to 34% of the inlet Hg^0 level while Hg(II) slowly increased to 19%. The amount of Hg captured on the pellets can be expressed as

$$Hg_{cap} = Hg^T_{in} - Hg^T_{out} \quad (4\text{-}6)$$

where Hg_{cap} represents captured Hg, and Hg^T_{in} and Hg^T_{out} represent Hg^T at the inlet and outlet of the reactor, respectively. Since the inlet Hg source is 100% Hg^0 and negligible Hg^0 capture was observed without UV, it is reasonable to assume that the captured Hg species under UV irradiation was only Hg(II) due to the photocatalytic oxidation. Hence, the total amount of Hg^0 oxidized can be expressed as

$$Hg_{oxi} = Hg^0_{in} - Hg^0_{out} \quad (4\text{-}7)$$

where Hg_{oxi} represents oxidized Hg, and Hg^0_{in} and Hg^0_{out} represent Hg^0 at the inlet and outlet of the reactor, respectively. It should be noted that Hg^T_{in} was equal to Hg^0_{in} in this study. In the

baseline test, the percentage of oxidized Hg was calculated to be 66%, while 47% was captured by the pellets and 19% penetrated through the reactor. In other word, the inlet Hg^0 partial pressure was around 9.5 ppb and approximately 6.3 ppb (66%) of Hg^0 was oxidized to form HgO over the SiO_2-TiO_2 nanocomposite. The saturated vapor pressure of HgO at 135 °C, calculated according to Borderieux et al. (2004), is 6.0 ppb. The measured partial pressure of HgO (6.3 ppb) is very close to the saturated vapor pressure, indicating that most of the HgO formed would stay in the gas-phase at 135 °C. Then a fraction of the gaseous HgO (47%) was captured by the nanocomposite, and the rest (19%) penetrated through the reactor.

Effects of Individual Flue Gas Components

The effects of individual flue gas components were examined and the results were compared with the baseline. At least two runs were performed at each of the experimental condition listed in Table 1. The average values of Hg capture and oxidation efficiencies are shown in Figure 4-3, where the error bars represent the envelope of minimum and maximum values.

An inhibitory effect of water vapor on Hg removal was observed as shown in Figure 4-3a. Experiments were first conducted in a relatively dry condition (<0.1%) by bypassing the water bubbler and then in humid conditions with an increasing water vapor concentration. In the dry condition, the efficiencies of both Hg capture and oxidation reached over 99%. As the water vapor concentration increased from 4% to 16% (baseline was 8%), the Hg capture efficiency decreased from 73% to 18%, and the Hg oxidation efficiency decreased from 88% to 32%. The inhibitory effect of water vapor is very likely due to its competitive adsorption with Hg^0 on the active sites, and as shown in Figure 4-3a, the extent of inhibition on Hg removal is proportional to the concentration of water vapor. This trend agrees with the results obtained at room temperature and low water vapor concentrations (< 2.3 %) (Li and Wu, 2006), which indicates

that even at a higher temperature (135 °C in this work) the competitive adsorption of water vapor is still significant. It has been reported that Hg^0 is not adsorbed (or is only weakly adsorbed) on the surface of sorbents including unburned carbon and selective catalytic reduction (SCR) catalysts (Niksa and Fujiwara, 2005a, 2005b). The weakly bonded Hg^0 can even be desorbed from the surface of SiO_2-TiO_2 composite by water vapor at high concentrations (Li and Wu, 2006). The desorption process would also lead to a lower efficiency of Hg^0 removal. Since the concentration of water vapor in this study was seven to eight orders of magnitude higher than that of Hg^0, the inhibitory effect of water vapor could be very significant even at higher temperatures.

It should also be noted that penetration of oxidized Hg from the reactor (i.e. the difference between Hg oxidized and captured) occurred in humid conditions (4 – 16% H_2O) but not in the dry condition. This can be explained by the competitive adsorption of water vapor with the gas-phase oxidized Hg. Since Hg^0 is not adsorbed (or is only weakly adsorbed) on the sorbent surface (Niksa and Fujiwara, 2005a, 2005b), it is very possible that a portion of the oxidized Hg, which is the product of the reaction between Hg^0 and OH radicals, existed in the gas phase in the vicinities of the reaction sites. In the dry condition, the oxidized Hg in the gas phase was adsorbed and thus there was no penetration. However, in humid conditions, water vapor competes with the oxidized Hg and consequently not all oxidized Hg in the gas phase can be adsorbed. The superhydrophilic surface of TiO_2 after exposure to UV irradiation can further enhance the adsorption of water vapor (Li and Wu, 2006) but reduce the capture of oxidized Hg. As a result, penetration of oxidized Hg was usually observed in humid conditions in this work.

The effect of HCl on Hg removal was found to be promotional (Figure 4-3b). In the range of 10 to 50 ppm HCl, Hg capture efficiency increased to approximately 75% and Hg oxidation

efficiency increased to over 90%. However, the extent of promotion was not apparently related to the HCl concentration in the range studied. The promotional effect of HCl is consistent with the literature that HCl promotes heterogeneous Hg oxidation (Presto and Granite, 2006). It has been reported that in the presence of an appropriate catalyst (e.g. metal oxides), a Deacon process (Pan et al., 1994) could convert HCl in flue gas to Cl_2 at high temperatures (300-400 °C), thereby enhancing Hg^0 oxidation (or chlorination). Niksa et al. proposed that Hg oxidation occurs via an Eley-Rideal mechanism, where adsorbed HCl reacts with gas-phase (or weakly adsorbed) Hg^0 (Niksa and Fujiwara, 2005a, 2005b). The mechanism was also consistent with the observation of enhanced Hg^0 sorption to halogen-promoted sorbents and fly ashes in literature (Granite et al., 2000; Maroto-Valer et al., 2005). In this work, the Deacon process was less likely to occur because of the relatively low flue gas temperature (135 °C). Instead, it is more likely to follow the Eley-Rideal mechanism. In the Eley-Rideal mechanism, HCl may first be adsorbed on the surface of SiO_2-TiO_2 nanocomposite, and then react with gas-phase Hg^0. This, together with the Hg^0 oxidation by OH radicals, can result in a higher Hg removal efficiency. Further investigation is needed to confirm the reaction mechanism.

As shown in Figure 4-3c, SO_2 was found to have a promotional effect on Hg capture and oxidation and the promotion was proportional to the concentration of SO_2 in the range of 0~1200 ppm. The Hg capture and oxidation efficiencies reached 73% and 91% respectively at 1200 ppm SO_2. The effect of SO_2 on heterogeneous Hg oxidation was not conclusive in literature. It has been reported that SO_2 competes with HCl for sites on activated carbon and fly ash sorbents and thus inhibits mercury oxidation and adsorption in flue gas (Laudal et al., 2000; Laumb et al., 2004). Carey et al. reported that the adsorption capability of a Darco FGD carbon for both Hg^0 and $HgCl_2$ decreased as the SO_2 concentration increased from 0 to 500 ppm but neither capacity

changed significantly above 500 ppm SO_2 (Carey et al., 1998). However, in some cases, SO_2 appears to enhance Hg^0 oxidation (Eswaran and Stenger, 2005; Norton et al., 2003). Eswaran and Stenger reported a promotional effect of SO_2 on Hg^0 oxidation over a selective catalytic reduction (SCR) catalyst (Eswaran and Stenger, 2005). The mechanism was proposed as:

$$SO_2 + \tfrac{1}{2} O_2 \rightarrow SO_3 \quad (4\text{-}8)$$

$$Hg + SO_3 + \tfrac{1}{2} O_2 \rightarrow HgSO_4 \quad (4\text{-}9)$$

Similar mechanism can be used to explain the promotional effect of SO_2 in this work, where SO_3 was formed through the oxidation of SO_2 by OH radicals (Bai et al., 2006), which were generated on the SiO_2–TiO_2 pellets under UV irradiation.

The effect of NO on Hg removal was found to be inhibitory at a significant but relatively constant level in the concentration range of 50~300 ppm NO (Figure 4-3d). The Hg capture and oxidation efficiencies both decreased to around 10% in the presence of NO. NO has been reported as an inhibitor for heterogeneous Hg^0 oxidation on fly ash (Norton et al., 2003), but the mechanism was not clear. In this study, it is very likely that the scavenging of OH radicals by NO hindered the photocatalytic oxidation of Hg^0. The inhibition occurred via (Niksa et al., 2001)

$$OH + NO + M \rightarrow HONO + M \quad (4\text{-}10)$$

In the presence of 10~30 ppm NO_2, the efficiencies of Hg capture and oxidation were slightly lower than those in the baseline (Figure 4-3e). However, the effect of NO_2 in this range can be considered as insignificant compared to other flue gas components. It has been reported in literature that NO_2 can enhance heterogeneous oxidation of Hg^0 in the presence of fly ash (Norton et al., 2003) or iron oxides (Borderieux et al., 2004; Galbreath et al., 2005), though this effect is often considered of minor importance compared to chlorination.

Hg Removal in Simulated Flue Gases

The performance of the SiO_2–TiO_2 nanocomposite was finally tested in two simulated flue gases, the compositions of which were in line with those reported in literature (Pavlish et al., 2003). Flue gas 1 (FG1, Set 7) represents burning of high rank (bituminous) coals that contain higher chlorine and sulfur contents. Flue gas 2 (FG2, Set 8) represents burning of low rank (subbituminous and lignite) coals, which contain less chlorine and sulfur but more moisture. As shown in Figure 4-3f, Hg removal in Flue Gas 1 was close to that in baseline, indicating that the prohibitory effect of 300 ppm NO counteracted the promotional effects of 30 ppm HCl and 1200 ppm SO_2. Hg removal in Flue Gas 2 was less than in Flue Gas 1, very likely due to the higher concentration of H_2O and lower concentrations of HCl and SO_2. Hence, high rank coals are preferable to low rank coals for the application of the SiO_2–TiO_2 nanocomposite. Minimizing the adverse effect of NO so as to improve the overall performance of the catalyst would be an important task for future research.

Summary

A novel SiO_2–TiO_2 nanocomposite has been synthesized to removal Hg^0 from simulated coal-fired power plant flue gas. The flue gas components were found to have significant effects on Hg removal efficiency in a fixed bed study. HCl and SO_2 promoted Hg oxidation and capture, while H_2O and NO inhibited Hg removal and the effect of NO_2 was not significant. Experiments of Hg removal in simulated flue gases showed that high rank coals are preferable to low rank coals because of the lower moisture and higher HCl and SO_2 concentrations in the flue gas. It is essential, however, to minimize the adverse effect of NO to improve the catalytic performance of the SiO_2–TiO_2 nanocomposite.

Table 4-1. Experimental conditions for investigation of the flue gas effects

	H_2O (%)	HCl (ppm)	SO_2 (ppm)	NO (ppm)	NO_2 (ppm)
Set 1 (baseline)	8	–	–	–	–
Set 2	0, 4, 12, 16				
Set 3	8	10, 30, 50	–	–	–
Set 4	8	–	400, 800, 1200	–	–
Set 5	8	–	–	50, 100, 300	–
Set 6	8	–	–	–	10, 20, 30
Set 7 (FG1)	8	30	1200	300	10
Set 8 (FG2)	12	10	400	300	10

Note: All the conditions contained 4% O_2, 12% CO_2, 75~80 μg m^{-3} Hg^0 (inlet), and balanced with N_2; the temperature was controlled at approximately 135 °C.

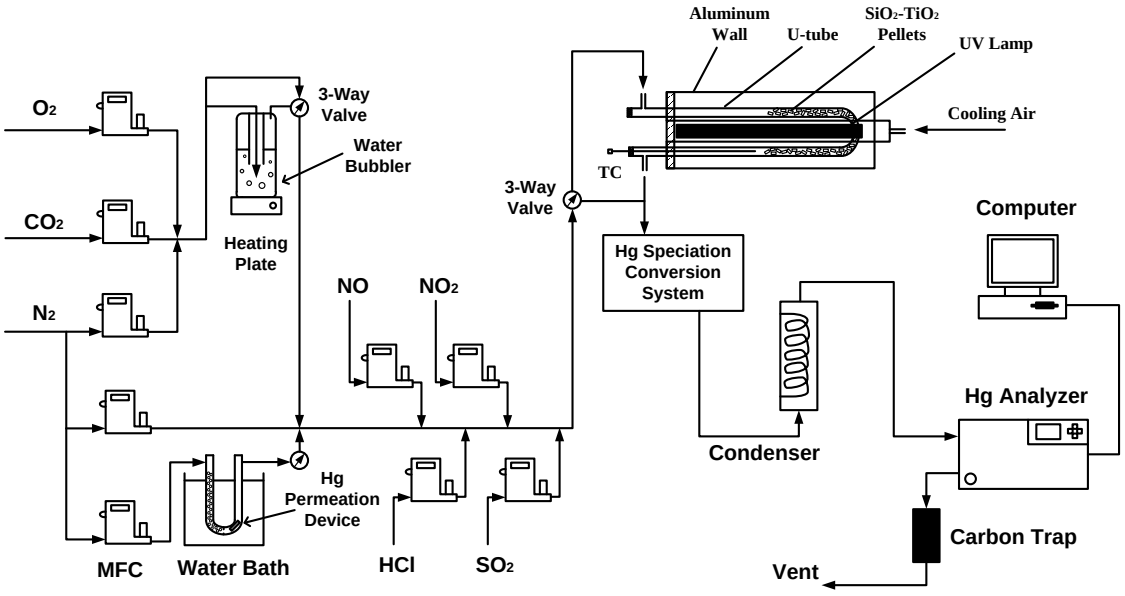

Figure 4-1. Photocatalytic reaction system under flue gas conditions.

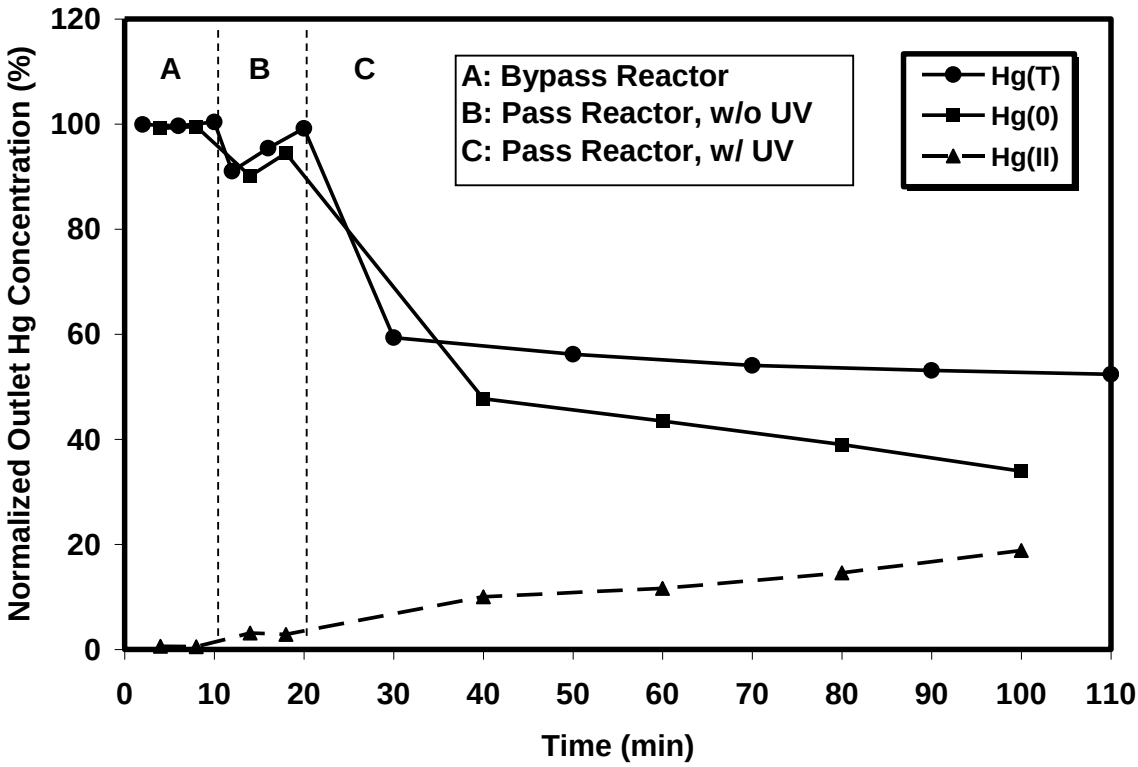

Figure 4-2. Hg speciation at the outlet of the reactor in the baseline test

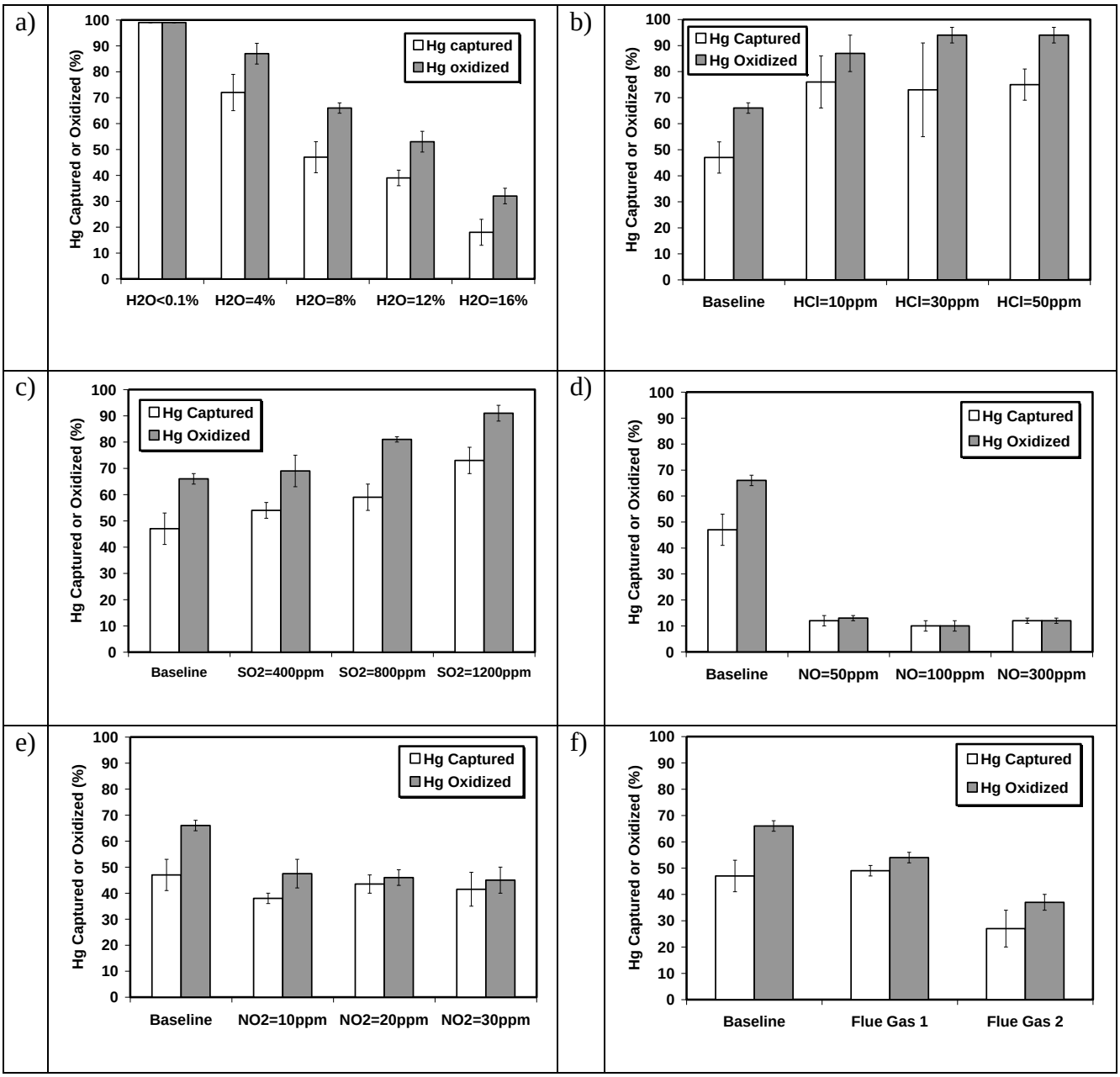

Figure 4-3. Effects of flue gas components on Hg capture and oxidation under various conditions of a) H_2O, b) HCl, c) SO_2, d) NO, e) NO_2, and f) simulated flue gases

CHAPTER 5
DEVELOPMENT OF SILICA/VANADIA/TITANIA COMPOSITES FOR REMOVAL OF ELEMENTAL MERCURY FROM FLUE GAS

Background

As indicated in Chapter 4, the performance of the SiO_2-TiO_2 nanocomposite is significantly affected by the flue gas composition. NO, particularly, has a dramatically inhibitory effect on Hg oxidation. To minimize the adverse effect of NO, there are two feasible ways. One way is to remove NO from the flue gas before passing the gas through the photocatalytic bed. Actually, in industrial practices, NO removal from the flue gas is usually achieved by selective catalytic reduction (SCR) of NO with ammonia (NH_3) (Parvulescu et al., 1998). However, the results in Chapter 4 show that even at a relatively low concentration (i.e. 50 ppm), NO still greatly inhibits Hg oxidation and capture by the SiO_2-TiO_2 nanocomposite. This undesired impact implies that unless NO can be completely or nearly completely removed from the flue gas, the adverse effect of NO is inevitable and a larger amount of the catalyst must be used to compensate the effect. Apparently, this is not a cost-effective method.

The other way to enhance the catalytic performance in Hg oxidation is to modify the composition of the catalyst or even develop a new catalyst that is more effective under the flue gas conditions. Recently, it has been reported that the SCR catalyst is capable of oxidizing Hg^0 in addition to its ability of removing NO (Benson et al., 2005; Lee, Srivastava et al., 2004; Lee et al., 2006; Niksa and Fujiwara, 2005b; Senior, 2006). The extent of Hg^0 oxidation through SCR processes varies under different operating conditions burning different types of coal. It was reported that Cl species in the flue gas promote the Hg^0 oxidation across SCR (Lee et al., 2006; Senior, 2006), although the exact mechanism is still poorly understood. In contrast, the mechanisms of the reduction of NO with NH_3 by various SCR catalysts have been extensively investigated (Parvulescu et al., 1998; Weckhuysen and Keller, 2003). Bosch and Janssen (1988)

reported a broad survey of metal oxide catalysts active for the reduction of NOx with NH_3, and they indicated vanadium oxide (V_2O_5) to be the most active and selective catalyst. The active sites on industrial SCR catalysts are V_2O_5 species supported on TiO_2 (Busca et al., 1998). The nature of the support, on the other hand, is also an important factor for the catalytic activity (Weckhuysen and Keller, 2003). TiO_2 as a support normally has drawbacks such as low surface area and low resistance to sintering, and thus, a common practice is to use a silica support coated with TiO_2 (Kobayashi et al., 2005; Martra et al., 2000; Tesser et al., 2004). In addition, Shikada et al. (1981) reported that the order of activity of NO reduction for supported V_2O_5 is SiO_2-TiO_2 > γ-Al_2O_3 > SiO_2. The SiO_2-TiO_2 composite used in this research for Hg removal has a high surface area and is in line with the composition of the high-activity support reported by Shikada et al. (1981). Hence, it is speculated that an addition of V_2O_5 to the SiO_2-TiO_2 composite could further enhance the capability of oxidizing Hg.

In this chapter, V_2O_5 was doped onto the SiO_2-TiO_2 matrix to form a SiO_2-TiO_2-V_2O_5 composite. The catalytic ability of the new material in Hg removal was compared to that of the SiO_2-TiO_2 composite. In addition, in order to investigate whether V_2O_5 is the active species for Hg oxidation, SiO_2-V_2O_5 composite was also synthesized and tested for its catalytic performance. Since SiO_2 is generally considered as an inert support, the hypothesis is that the activity of the SiO_2-V_2O_5 composite would represent the nature of the doped V_2O_5 species. Therefore, the objectives of this chapter are: (1) to synthesize and characterize the SiO_2-V_2O_5 and SiO_2-TiO_2-V_2O_5 composites; (2) to test the catalytic abilities of those composites in Hg removal in a fix-bed reactor; and (3) to investigate the reaction mechanisms of the catalytic removal of Hg.

Materials and Methods

Catalyst Preparation

The details of the procedure of synthesizing the SiO_2-TiO_2 composite are described in Chapter 2. When synthesizing the SiO_2-TiO_2-V_2O_5 composite, the same procedure was used but with one more step of adding V_2O_5. Vanadium triisopropoxide oxide (VTPO) (Alfa Aesar) was used as the precursor of V_2O_5. A known amount of VTPO was first dissolved in well stirred ethanol to form an orange-brown solution. It was then added dropwise to the prepared silica sol under vigorous stirring. TiO_2 nanoparticles (P25 Degussa) were finally added to the mixture before it started to gel. When synthesizing the SiO_2-V_2O_5 composite, the step of adding TiO_2 nanoparticles was skipped. In this study, the synthesized SiO_2-V_2O_5 composite had a weight fraction of V_2O_5 ranging from 2% to 10%. The synthesized SiO_2-TiO_2-V_2O_5 composite had 12 wt.% of TiO_2 and varied contents of V_2O_5. The composites were originally made in the pellet form (3 mm in diameter and 5 mm in length). Powder form of the composites was also obtained by grinding the pellets and sieving through meshes. Both the pellets and powders of the composites were tested in a fix-bed study. The powders used have a mesh size of 40×100 (425 ×150 μm). The names of the catalysts were abbreviated by way of STxVy, where S represents SiO_2, T represents TiO_2, V represents V_2O_5, and x and y represent the weight percentages of the TiO_2 and V_2O_5, respectively.

Catalyst Characterization Techniques

The BET (Brunauer, Emmett, and Teller equation) surface areas of the catalysts were measured using a Quantachrome NOVA 1200 Gas Sorption Analyzer (Boynton Beach, FL). The powder samples were outgassed at 180 °C for 3 hours before the analysis. X-ray diffraction (XRD) patterns of the powders were recorded with a Philips APD 3720 diffractometer using Cu-Kα radiation ($\lambda = 0.1542$ nm) in the range of 15 to 40° (2θ) with a step size of 0.02°.

Catalyst Activity Measurement

As reported in Chapter 4, the SiO_2-TiO_2 composite needs activation by UV light for catalytic oxidation of Hg. Thus, the necessity of UV light activation for V_2O_5 based composites was first investigated. Pellet form of the catalysts was then used because the space between the pellets allows penetration of UV light so that a maximum exposure of the catalyst to the light can be achieved. In contrast, for a catalyst bed densely packed with powders, it is difficult for the UV light to reach the central part of the bed. However, if tests indicate that the UV light is unnecessary, powders are preferable to pellets because of better contact of the gas with the inner pore surfaces of the catalyst.

Table 5-1 lists the experimental parameters for measuring the photocatalytic activities using pellet catalysts. The three catalysts (SiO_2-TiO_2, SiO_2-V_2O_5, and SiO_2-TiO_2-V_2O_5) were tested following the same procedure as described in Chapter 4 using the reactor system previously illustrated in Figure 4-1. Experiments were conducted under two flue gas conditions, FG1 and FG2, as listed in Table 4-1 in Chapter 4. FG1 has relatively higher concentrations of HCl and SO_2 and lower concentration of water vapor, which represents flue gas burning high rank coals. In contrast, FG2 represents flue gas burning low rank coals.

Next, the powder catalysts were tested with a modified reactor as shown in Figure 5-1. The experimental parameters are listed in Table 5-2. No UV irradiation was supplied in this modified system. The U-tube quartz reactor (13 mm ID) was immersed in an oil bath heated by a hotplate to a constant temperature at 135 °C (± 0.5 °C). The catalyst powders were packed in between glass wools in the reactor. The flue gas (FG3) in this series of experiments contained 4% O_2, 12% CO_2, 8% H_2O, 10 ppm HCl, 400 ppm SO_2, 300 ppm NO, 10 ppm NO_2, and balanced with N_2. The inlet Hg concentration was maintained in a relatively constant range of 15.0~16.5 ppb. The total flow rate was controlled at 1.5 L/min. Finally, to explore the reaction mechanisms and

the roles of the flue gas components in the catalytic reactions, the catalytic activity of a fixed amount of catalyst (SV5) was examined with introduction of individual flue gas components.

Results and Discussion

Characterization of the Catalysts

The BET specific surface areas of the catalysts are listed in Table 5-3. All the catalysts exhibit high surface areas (> 250 m^2/g). Without any doping, the pure silica gel had the highest surface area, 341.8 m^2/g. The inclusion of 12% TiO_2 to the silica gel (ST12) slightly reduced the surface area to 319.4 m^2/g. The doping of V_2O_5 (2 – 10%) to the silica gel moderately reduced the surface area, but all the SiO_2-V_2O_5 catalysts had the similar level of surface areas and did not exhibit any clear dependence on the V_2O_5 loading. The surface areas of the SiO_2-TiO_2-V_2O_5 catalysts were close to those of the SiO_2-V_2O_5 catalysts.

The XRD patterns of the catalysts are shown in Figure 5-2. No visible crystal phase of V_2O_5 (peak at $2\theta = 26.1°$) was detected for SV2 and SV5, which indicated that the vanadium contents were highly dispersed on these catalysts (Kobayashi et al., 2006). A very small peak of crystalline V_2O_5 was detected for SV8, and SV10 showed a relatively broader and more prominent peak of crystalline V_2O_5. The molecular structures of the vanadium oxides at different surface loadings have been widely reported in literature (Parvulescu et al., 1998; Rodella et al., 2001; Weckhuysen and Keller, 2003). At low surface vanadia concentrations mainly monomeric vanadyl (V^{4+}) species are formed containing one terminal V=O bond and three bridging V–O–support bonds. As the vanadia loading increases, the monomeric species react to form polymeric vanadates (V^{5+}) which consist of a terminal V=O bond with one V–O–support and two bridging V–O–V bonds. The presence of these monomeric and polymeric vanadium oxide species has been identified by Raman and/or Infrared (IR) spectroscopy. As the vanadia loading further increases, a fraction of the vanadia aggregates to form amorphous and crystalline V_2O_5 clusters.

The XRD results in this study indicated that crystalline V_2O_5 begins to grow as the vanadia loading increases to somewhere between 5 and 8%.

The XRD pattern of ST12 showed a strong anatase phase (peaks at $2\theta = 25.3°$ and 38.0°) and a weak rutile phase (peak at $2\theta = 27.6°$) of TiO_2. This agrees with the composition of the TiO_2 nanoparticles (P25 Degussa AG) which is an 80/20 mixture of anatase/rutile phases. For the catalyst of ST12V5, no crystal phase of V_2O_5 was detected because of the relatively low vanadia loading. It has been reported that TiO_2-anatase is metastable and tends to convert to the thermodynamically stable form rutile and that V_2O_5 favors this anantase-to-rutile phase transformation (Busca et al., 1998). This may explain the finding that the peak of anatase TiO_2 in ST12V5 was lower than in ST12. However, no increase in the rutile phase in ST12V5 was observed.

Mercury Removal Using Pellet Catalysts

Mercury removal tests were first conducted using pellet catalysts to investigate their photocatalytic activities. The results are summarized in Figure 5-3. It was found that the catalytic abilities of SV2 and ST12V2 on Hg removal were almost the same with or without UV irradiation. Thus, only the results without UV are demonstrated in Figure 5-3 for SV2 and ST12V2. In contrast, ST12 had to be activated under UV irradiation and without UV there was negligible removal of Hg. Apparently, the addition of V_2O_5 is advantageous. It simplifies the system by eliminating the UV devices and reduces the cost by saving the energy of UV irradiation.

Figure 5-3 also compares the behavior of the catalysts under different flue gas conditions and mass loadings. As described in Chapter 4, the oxidized Hg is calculated as the difference between inlet and outlet Hg^0 concentrations, and the captured Hg is calculated as the difference

between the inlet and outlet Hg^T concentrations. In flue gas 1 (FG1), 8 g of ST12V2 demonstrated a very high efficiency of Hg capture/oxidation (~ 92%), compared to only about 50% capture/oxidation of Hg by 8g of ST12. This increase in Hg removal is obviously caused by the addition of the 2% V_2O_5. When reducing the mass loading of the ST12V2 from 8 g to 4 g, the efficiency of Hg oxidation decreased a little to 73% but that of Hg capture dramatically decreased to 27%. The reduction in Hg capturing ability might result from the decrease in total available surface area due to lower mass loading. It is interesting to find that compared to 4 g of SV2, 4 g of ST12V2 had a higher Hg oxidation efficiency but a lower Hg capturing efficiency. The enhanced oxidizing ability of ST12V2 is in line with the literature where the SiO_2-TiO_2 supported V_2O_5 has a higher activity than SiO_2 supported V_2O_5 for reduction of NO (Shikada et al., 1981). It has also been reported that the V–O–support bonds are the most critical structures for the catalytic oxidation of methanol to formaldehyde (Weckhuysen and Keller, 2003). Thus, it is possible that the V–O–Ti bonds have superior activities than the V–O–Si bonds, which resulted in a higher oxidation of Hg on the SiO_2-TiO_2-V_2O_5 composite than on the SiO_2-V_2O_5 composite. The reason for the penetration of oxidized Hg from ST12V2 may be related to the selectivity of the reactions, i.e. ST12V2 may have a higher capacity of converting Hg^0 to volatile oxidized Hg species such as $Hg(NO_3)_2$. This agrees with the suggestions by other researchers that the V–O–support bonds are determinant for activity and selectivity of different reactions (Tesser et al., 2004; Weckhuysen and Keller, 2003). More discussion relevant to the formation of $Hg(NO_3)_2$ is provided later in this chapter.

In flue gas 2 (FG2), the behavior of the catalysts followed a similar pattern as in FG1. For 4 g of ST12V2 and 4g of SV2, no obvious change in the Hg removal efficiency was observed in FG2 compared to in FG1. For the case of 8 g ST12V2, the oxidized Hg was at the same level as

in FG1 but the captured Hg was much lower than that in FG1. The difference may be due to the higher water vapor concentration in FG2 which competes with oxidized Hg for the adsorption sites. It is also possible that a larger fraction of certain volatile Hg compounds (such as $Hg(NO_3)_2$) were produced in FG2. However, identification of the oxidized Hg species in the current system is technically difficult due to their trace amounts.

Mercury Removal Using Powder Catalysts

The previous experiments using pellet catalysts showed no necessity of UV light activation for the SiO_2-V_2O_5 and SiO_2-TiO_2-V_2O_5 catalysts. Hence, no UV light was used for the study of powder catalysts. Tests were first performed to verify that the glass wools (used as the support of powders) and pure silica powders were inert to Hg removal. Then, with a feed of approximately 16 ppb Hg, each flue gas component (4% O_2, 8% H_2O, 50 ppm HCl, 1200 ppm SO_2, 300 ppm NO, or 30 ppm NO_2) balanced with N_2 was individually introduced to the system. In all cases, the change of the Hg concentration was observed to be within ±5%. Since the Hg permeation tube has an error of ±2%, the result indicates that homogeneous oxidation of Hg in the gas-phase was negligible.

The first set of experiments was carried out using 500 mg of SiO_2-V_2O_5 catalysts (corresponding to a bed height of 17 mm in average) but with different V_2O_5 loadings (2 – 10 wt.%). The results are shown in Figure 5-4. In the beginning, the flue gas bypassed the reactor to obtain the inlet Hg concentration. It then passed through the reactor and the extent of the catalytic oxidation was recorded. After a 6-hr period, the flue gas bypassed the reactor again and the inlet Hg concentration was checked. It was observed that the Hg removal efficiency increased as the V_2O_5 loading increased from 2 to 8%. For SV2 (Figure 5-4a) and SV5 (Figure 5-4b), the outlet concentration of Hg^T and Hg^0 were at the same level, indicating that all the oxidized Hg has been captured. For SV2, the Hg removal efficiency was initially around 22%

and slowly decreased to 12% in 6 hours. For SV5, the Hg removal efficiency was initially around 65% and slowly decreased to 45% in 6 hours. For SV8, as shown in Figure 5-4c, the outlet Hg^T concentration was initially dropped to a very low level (corresponding to 93% capture), and then it increased and was relatively stabilized at around 32% of the inlet Hg concentration (i.e. 68% capture). The outlet Hg^0 concentration was found to be always lower than the Hg^T concentration, indicating that a portion of the oxidized Hg penetrated the reactor. The Hg oxidation efficiency at the end of the 6-hr test was around 77%, higher than that of SV2 and SV5. For SV10, as shown in Figure 5-4d, a different pattern of Hg removal was observed. The outlet Hg^T concentration slowly dropped to 40% of the inlet level in the 6-hr period, unlike the previous cases where the outlet Hg^T concentrations dropped to their minimum levels immediately after the flue gas passed through the reactor. The outlet Hg^0 concentration was relatively stable at 30% of the inlet level during the last 3 hours. Both the Hg capturing and oxidation efficiencies of SV10 were lower than those of SV8.

Next, 500 mg of ST12V5 was tested for its catalytic activity and the result is shown in Figure 5-4e. The outlet Hg^0 concentration remained almost constantly low at 15% of the inlet level (i.e. 85% oxidation). The outlet Hg^T concentration initially dropped to 11% of the inlet level but quickly increased and stabilized around 65% (i.e. 35% capture). Similar to the findings observed in the study of pellet catalysts (Figure 5-3), ST12V5 powder has a higher oxidation but lower capturing efficiency compared to SV5.

The amounts of Hg captured/oxidized on the various catalysts in the 6-hr test are summarized in Table 5-4. To better compare the effectiveness of the catalysts, the capabilities of the catalysts were normalized to unit mass of catalyst and unit mass of V_2O_5 (the active phase), respectively. Table 5-4 showed that the amount of Hg captured per gram of the SiO_2-V_2O_5

catalyst increased as the V_2O_5 loading increased from 2 to 8% but decreased as the V_2O_5 loading further increased to 10%. When normalized to per gram of V_2O_5, the capacity of SV5 was the highest; either lower (2%) or higher (8% and 10%) V_2O_5 loadings reduced the capacity. These results suggested that the optimal V_2O_5 loading for an optimal catalytic activity is somewhere between 5 and 8%. This is coincident with the XRD result that the maximum loading of V_2O_5 without the formation of crystalline V_2O_5 is somewhere between 5 and 8%. It should be noted that ST12V5 exhibited an even greater ability of oxidizing Hg than SV5, although its Hg capturing ability was lower than SV5. Applications of ST12V5 can be beneficial to coal-fired power plants equipped with wet-scrubbers where oxidized Hg can be easily captured. Therefore, ST12V5 surpasses SV5 in terms of the total potential for Hg removal.

As shown in Figure 5-4, the Hg removal efficiencies slowly decreased in the 6-hr test for SV2, SV5, and SV8. To investigate whether a 100% breakthrough would happen, a smaller amount (250 mg) of SV5 was subject to a test with a longer period of time, as shown in Figure 5-5. The outlet Hg^T (or Hg^0) concentration initially dropped to 65% of the inlet level when the flue gas passed the bed. Then the Hg concentration slowly increased to 80% in a 9-hr period. Thereafter, the Hg removal efficiency remained relatively stable at approximately 20% for another 3 hr (in Day 1). With the same batch of catalyst under the same flue gas conditions, the experiment was continued in Day 2 after a pause of 40 hours. Only the Hg^T concentration was recorded in Day 2 since Hg^0 was found to be at the same level of Hg^T in Day 1. This time when the flue gas passed through the bed, the Hg^T concentration first dropped to 68%, very close to the lowest level of Hg^T concentration (65%) in Day 1. Then the Hg^T concentration increased to 81% in 2 hr and remained at this level for another 4 hr. This 20-hr test suggested that a steady-state catalytic activity was reached (approximately 20% Hg removal) using either fresh (Day 1) or

used (Day 2) catalyst. This transition to a steady-state activity is in agreement with the reported kinetics of oxidative dehydrogenation of propane over V_2O_5/TiO_2 in literature (Grabowski et al., 2002; Sloczynski, 1996). Those researchers observed that the rate of reduction is limited by the adsorption of reductant at the surface of the vanadium phase and that reoxidation of the reduced catalysts proceeds via two stages: (i) a quick surface reaction, and (ii) a slow process limited by bulk diffusion through the growing coat of the oxidation product. They also indicated that the surface reoxidation rate is considerably higher than that of the reduction. According to these theories and findings, the rate of Hg oxidation in this work should quickly reach a maximum point at the beginning and then gradually decrease due to the reduced number of available vanadium sites and/or the increasing difficulty of O_2 diffusing through the coat of oxidized Hg. However, this decrease in the catalytic activity proceeded so slowly that the catalyst behaved like reaching a steady-state activity for a relatively long time (Grabowski et al., 2002). This agrees with the result that the captured Hg on the 250 mg SV5 during the 20-hr test was calculated to account for only 0.2 mol % of the total vanadium sites. Future study is needed to investigate the long-term performance of the catalyst.

Mercury Removal Mechanisms

To explore the Hg removal mechanisms on the SiO_2-V_2O_5 catalyst, it is important to understand the role of the flue gas components in the catalytic reactions. Hence, experiments were conducted by mixing Hg with individual flue gas components (e.g. HCl, SO_2, and NOx) and/or in combination with O_2. The role of water vapor was also examined. 250 mg of fresh SV5 was used in each test since 5% V_2O_5 was previously found to be close to the optimal loading.

Role of O_2

The role of O_2 on Hg removal was first investigated because O_2 is an important oxidant in flue gas. A background test was conducted using high purity N_2 (>99.995%, Airgas) as the

carrier gas and around 5% of Hg removal was detected, as shown in Figure 5-6. Considering that the carrier gas contained a maximum of 50 ppm impurity very likely consisting of O_2, the 5% Hg removal might be contributed by the trace amount of O_2. When 4% O_2 was introduced, the Hg removal increased to about 15%. Hg removal further increased to 26% as O_2 increased to 20%. Granite et al. (2000) studied various metal oxides for catalytic Hg removal from flue gas and they proposed that lattice oxygen of the metal oxides can serve as the oxidant of Hg, forming mercuric oxide (HgO). It has also been reported in literature that lattice oxygen is the most abundant reactive intermediates that are responsible for oxidative dehydrogenation of alkanes over V_2O_5 based catalysts (Argyle et al., 2004; Grabowski et al., 2002). Gas-phase O_2, on the other hand, reoxidizes the reduced metal oxides, replenishing the lattice oxygen (Grabowski et al., 2002; Granite et al., 2000). In this work, a similar redox cycle is proposed for the catalytic oxidation of Hg on SiO_2-V_2O_5 in the presence of O_2:

$$V_2O_5 + Hg \rightarrow V_2O_4 + HgO \qquad (5\text{-}1)$$

$$V_2O_4 + \tfrac{1}{2}O_2 \rightarrow V_2O_5 \qquad (5\text{-}2)$$

The overall reaction can be written as:

$$Hg + \tfrac{1}{2}O_2 \rightarrow HgO \qquad (5\text{-}3)$$

O_2 plays an important role in the redox mechanism, which is supported by finding that Hg oxidation on the catalyst is proportional to the concentration of O_2.

Role of HCl

HCl was found to enhance Hg oxidation over the SiO_2-V_2O_5 catalyst (Figure 5-6). 10 ppm HCl (balanced with N_2) resulted in 15% Hg removal, and as HCl increased to 50 ppm, the Hg removal increased to 25%. The combination of 50 ppm HCl with 20% O_2 further improved the Hg removal to 39%. It has been reported in literature that Hg^0 is not adsorbed (or is only weakly

adsorbed) on the surface of unburned carbon and SCR catalysts (Niksa and Fujiwara, 2005a, 2005b). The researchers also proposed that Hg oxidation occurs via an Eley-Rideal mechanism, where adsorbed HCl reacts with gas-phase (or weakly adsorbed) Hg; however, the specific reaction pathway was not given. In this work, it was also found that Hg is not (or only weakly) adsorbed on the SiO_2-V_2O_5 catalyst, which is verified by the result that there was only 5% removal of Hg in the environment of pure N_2. The Eley-Rideal mechanism can be used as well to explain the reaction on the SiO_2-V_2O_5 catalyst in the presence of HCl. The pathway of HCl adsorption can be inferred from literature about HCl adsorption on other types of metal oxide surfaces. Parfitt et al. (1971) conducted an infra-red study of HCl adsorption on rutile surface and found an increase in surface hydroxyl (OH) groups due to the introduction of HCl. The OH groups further react with excess HCl to form Cl and water. Tseng et al. (2003) reported the adsorption of HCl on the CuO surface forming a hydroxychloride (Cu(OH)Cl) intermediate. Similar to the mechanisms reported in those studies, it is proposed that the formation of adsorbed Cl on the V_2O_5 surface occurs via:

$$V-O-V+HCl \leftrightarrow V-OH-V-Cl \qquad (5\text{-}4)$$

$$V-OH+HCl \leftrightarrow V-Cl+H_2O \qquad (5\text{-}5)$$

Actually, the V–OH structures are one type of the active sites readily present on the surface of the vanadia based catalysts (Busca et al., 1998; Kantcheva et al., 1994; Parvulescu et al., 1998). Thus, the reaction with HCl can directly start from Reaction 5-5. The adsorbed Cl species then react with gas-phase Hg through the Eley-Rideal mechanism to generate an intermediate HgCl species, which then further reacts with HCl or Cl to form a more stable mercuric chloride, $HgCl_2$. The overall reaction can be written as:

$$\tfrac{1}{2}O_2+2HCl+Hg \xrightarrow{V_2O_5} HgCl_2+H_2O \qquad (5\text{-}6)$$

It should be noted that chlorination of Hg may take place without the presence of O_2, as shown in Figure 5-6. In this case, V_2O_5 is consumed to form V_2O_4. The addition of 20% O_2 to 50 ppm HCl enhanced the total oxidation of Hg, very likely due to the oxidation of V_2O_4 to V_2O_5, i.e. the regeneration of the catalyst.

Role of NO_2

The effect of NOx was also found to be promotional in Hg oxidation over the SiO_2-V_2O_5 catalyst (Figure 5-6). In the presence of 10 ppm NO_2, 57% of Hg was oxidized while 50% was captured. It should be noted that the cylinder gas of NO_2 was balanced with both N_2 and O_2 with O_2 concentration three times as much as NO_2. Thus, 30 ppm O_2 was present in the gas together with 10 ppm NO_2. When 20% O_2 was added, the Hg oxidation remained at a similar level. Increasing the concentration of NO_2 to 30 ppm (with 20% O_2) increased the Hg oxidation to 68% and Hg capture to 57%. The results indicated that NO_2 greatly promoted Hg oxidation with or without O_2. It has been reported in literature that NO_2 significantly improves heterogeneous oxidation of Hg on fly ash (Norton et al., 2003) and on activated carbon based sorbents (Miller et al., 2000). Mercuric nitrate ($Hg(NO_3)_2$) was suggested to be the reaction product initiated by NO_2 (Laumb et al., 2004; Miller et al., 2000). Other researchers have reported that adsorption of NO_2 on TiO_2 supported V_2O_5 catalysts was the first step in the process of selective catalytic reduction of NOx (Kantcheva et al., 1994; Parvulescu et al., 1998). Kantcheva et al. (1994) indicated two pathways for the NO_2 adsorption on V_2O_5 involving V=O and V–OH sites:

$$V^{5+}{=}O + N^{4+}O_2 \rightarrow V^{4+}{-}N^{5+}O_3 \qquad (5\text{-}7)$$

$$2V^{5+}{-}OH + 3NO_2 \rightarrow 2V^{5+}{-}NO_3 + H_2O + NO \qquad (5\text{-}8)$$

In this work, similar mechanism can be applied to explain the oxidation of Hg in the presence of NO_2. NO_2 is first adsorbed on V_2O_5 via Reactions 5-7 and 5-8 and then transformed

to adsorbed nitrate species, which react with gaseous Hg to form $Hg(NO_3)_2$ via the Eley-Rideal mechanism. The overall reaction can be written as:

$$O_2 + 2NO_2 + Hg \rightarrow Hg(NO_3)_2 \qquad (5\text{-}9)$$

Considering the low melting point of $Hg(NO_3)_2$, 79 °C (Weast et al., 1983), it is likely that the formed $Hg(NO_3)_2$ is volatile at the reactor temperature (135 °C) and thus part of it may be released from the reactor in the gas-phase, as shown in Figure 5-6. This formation of volatile $Hg(NO_3)_2$ initiated by NO_2 is in agreement with the findings by other researchers. Using a carbon-based sorbent to remove Hg^0, Miller et al. (2000) observed nearly 100% breakthrough of a volatile oxidized Hg species in a gas mixture of SO_2 and NO_2. In a follow-up study conducted by Olson et al. (2002) using both MnO_2 and carbon sorbents, they identified this volatile Hg species to be $Hg(NO_3)_2$ by trapping the effluent in cold acetonitrile followed by analysis using gas chromatography – mass spectroscopy (GC–MS). Considering the much higher melting/decomposing point of $HgCl_2$ (277 °C) and HgO (500 °C) (Weast et al., 1983), the penetration of these two less volatile Hg species is less likely or occurs to a very small extent, as shown in Figure 5-6.

Role of NO

As also shown in Figure 5-6, in the presence of 300 ppm NO, there was 29% removal of Hg and an addition of 20% O_2 further increased the removal to 48%. The oxidation and capture of Hg increased with the increase of NO concentration. Decreasing the NO concentration to 100 ppm moderately decreased the Hg removal efficiency. The Hg removal may be ascribed to the adsorbed NO species on the V_2O_5 surface. It is generally agreed that NO adsorbs as nitrosyl and dinitrosyl surface species on reduced vanadia surfaces, whereas it does not adsorb over fully oxidized surfaces (Busca et al., 1998). The adsorbed NO can be oxidized on the surface, giving

rise to species like NO^+, NO_2, and NO_3^-, or it can be reduced by reduced catalyst centers (Busca et al., 1998). It is likely that these adsorbed species derived from NO are responsible for the observed Hg oxidation, but the exact reaction pathways and products are unknown. It has been reported that gas-phase NO can first be oxidized by O_2 and then is adsorbed as NO_2 on the SCR catalyst (Parvulescu et al., 1998). This route is less likely to occur on the SiO_2-V_2O_5 catalyst in this work, because there was no penetration of the oxidized Hg through the reactor in the presence of NO, unlike that observed in the presence of NO_2.

Role of SO_2

Figure 5-6 shows that the effect of SO_2 on Hg removal was insignificant in the concentration range of 400~1200 ppm. When combining 20% O_2 with 400 ppm SO_2, the Hg oxidation/capture efficiency was very close to or slightly lower than that without SO_2. It has been reported that SO_2 competes with HCl for sites on activated carbon and fly ash sorbents and thus inhibits Hg oxidation and adsorption in flue gas (Laudal et al., 2000; Laumb et al., 2004). Other studies, however, reported that SO_2 can promote heterogeneous oxidation of Hg over fly ash sorbents (Norton et al., 2003) or SCR catalysts (Eswaran and Stenger, 2005). Hence, further investigations involving the combination of SO_2 with other flue gas components (e.g. HCl and NOx) would warrant a more comprehensive understanding of the role of SO_2 for Hg removal on the SiO_2-V_2O_5 catalyst.

Role of H_2O

It has been well discussed in Chapters 2 to 4 that a high concentration of water vapor can inhibit Hg oxidation or capture on SiO_2-TiO_2 in room or flue gas conditions. In this work, H_2O was also found to have a dramatic inhibitory effect on Hg removal over SiO_2-V_2O_5 (Figure 5-7). Under flue gas conditions (FG3) using 250 mg SV5, when the gas was switched from humid (8% H_2O) to dry, the Hg removal efficiency increased from 20% to 66%. A H_2O concentration as low

as 0.6% (6000 ppm) also exhibited inhibitory effects. In a test with 10 ppm HCl and 20% O_2, switching the gas from dry to a 0.6% H_2O caused a decrease in Hg capture from 30% to 19%. Similarly, in another test with 10 ppm NO_2 and 20% O_2, the introduction of 0.6% H_2O caused a decrease in Hg capture from 43% to 24%. The competitive adsorption of water vapor on the active sites may have prohibited the adsorption of reactive species such as HCl and NOx. The findings agree with the literature where Laumb et al. (2004) reported that the absence of water vapor increased the adsorption of Cl compounds on activated carbon in flue gas condition.

Summary

In this chapter, the active phase of SCR catalysts, V_2O_5, was doped on the SiO_2 and SiO_2-TiO_2 supports. Compared to SiO_2-TiO_2 composites, improvements in Hg removal from flue gas were observed in fixed-bed studies using both pellet and powder forms of the SiO_2-V_2O_5 and SiO_2-TiO_2-V_2O_5 catalysts. No UV light activation is needed for the vanadia based catalysts, which simplifies the system and reduces the operating cost. For SiO_2-V_2O_5 catalysts, the Hg removal efficiency increased as the V_2O_5 loading increased from 2 to 8% but decreased as the V_2O_5 loading further increased to 10%. The results suggested that the optimal V_2O_5 loading for an optimal catalytic activity is somewhere between 5 and 8%. The SV5 catalyst reached a steady-state activity during a 20-hr test and no deactivation of the catalyst was observed. The SiO_2-TiO_2-V_2O_5 catalysts have an even greater ability of oxidizing Hg compared to SiO_2-V_2O_5, which can be advantageous to power plants equipped with wet-scrubbers where oxidized Hg can be easily captured. The different supports of V_2O_5 may account for the difference in their catalytic activity. The mechanisms of Hg oxidation on the SiO_2-V_2O_5 catalyst have also been investigated. It was found that the Hg oxidation may follow an Eley-Rideal mechanism where HCl, NO, and NO_2 are first adsorbed on the catalyst and then react with gas-phase Hg. While HCl, NO, and NO_2 promote Hg oxidation, SO_2 has an insignificant effect and water vapor

dramatically inhibits Hg oxidation. Penetration of oxidized Hg was observed in the presence of NO_2, which is probably due to the formation of volatile $Hg(NO_3)_2$. It was verified in this work that V_2O_5 is the active center for the Hg oxidation, but further studies are needed to better understand the enhancement of Hg oxidation by the SiO_2-TiO_2-V_2O_5 catalysts.

Table 5-1. Experimental parameters for activity measurement of the catalysts in pellet form

Catalyst	Composition	Mass (g)	Carrier gas	UV light
ST12	12% TiO_2 + 88% SiO_2	8.0	FG1, FG2	On/Off
ST12V2	12% TiO_2 + 2% V_2O_5 + 86% SiO_2	4.0, 8.0	FG1, FG2	On/Off
SV2	2% V_2O_5 + 98% SiO_2	4.0	FG1, FG2	On/Off

Table 5-2. Experimental parameters for activity measurement of the catalysts in powder form

Catalyst	Composition	Mass (mg)	Carrier gas
SV2	2% V_2O_5 + 98% SiO_2	500	FG3
SV5	5% V_2O_5 + 95% SiO_2	500	FG3; individual gases
SV8	8% V_2O_5 + 92% SiO_2	500	FG3
SV10	10% V_2O_5 + 90% SiO_2	500	FG3
ST12V5	12% TiO_2 + 5% V_2O_5 + 83% SiO_2	500	FG3

Table 5-3. BET surface areas of the catalysts

Sample	BET specific surface area (m^2/g)
Silica gel	341.8
SV2	263.4
SV5	283.2
SV8	273.8
SV10	262.9
ST12	319.4
ST12V2	258.0
ST12V5	262.5

Table 5-4. Amounts of Hg captured and oxidized on the catalysts in a 6-hr test

Catalyst	Hg Captured (μg/g-catalyst)	Hg Captured (μg/g-V_2O_5)	Hg Oxidized (μg/g-catalyst)	Hg Oxidized (μg/g-V_2O_5)
SV2 (500 mg)	22.5	1130	22.5	1130
SV5 (500 mg)	75.1	1500	75.1	1500
SV8 (500 mg)	83.7	1050	106.3	1320
SV10 (500 mg)	63.1	630	86.6	870
ST12V5 (500mg)	52.2	1040	117.4	2350

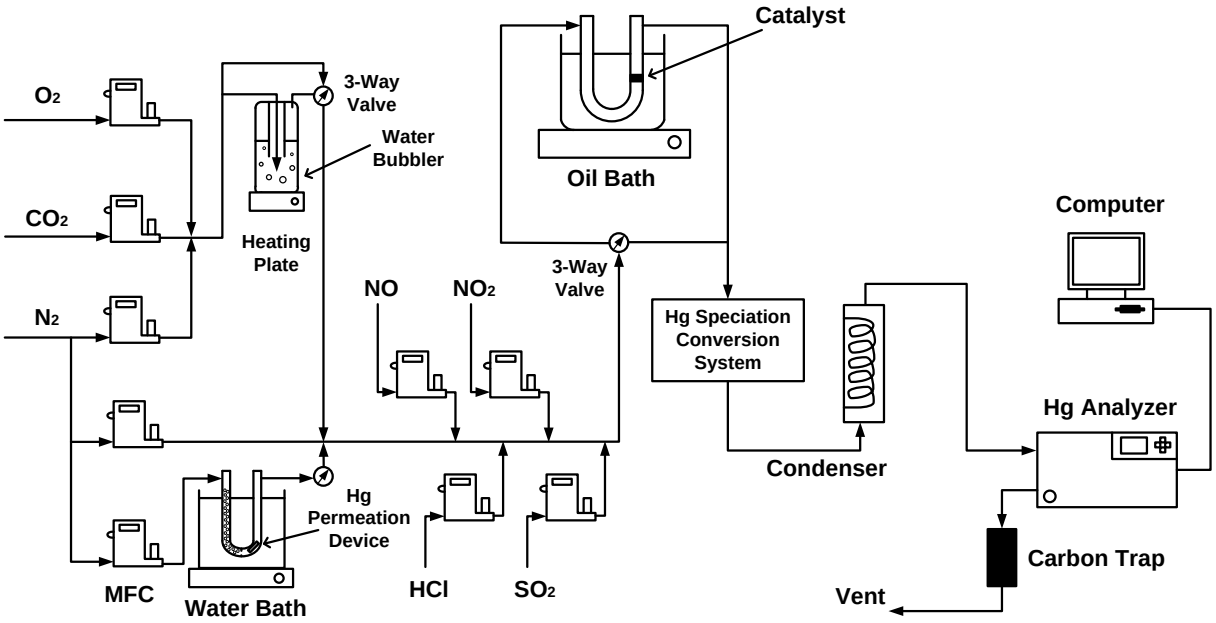

Figure 5-1. Experimental system for the fixed-bed study using powder catalysts

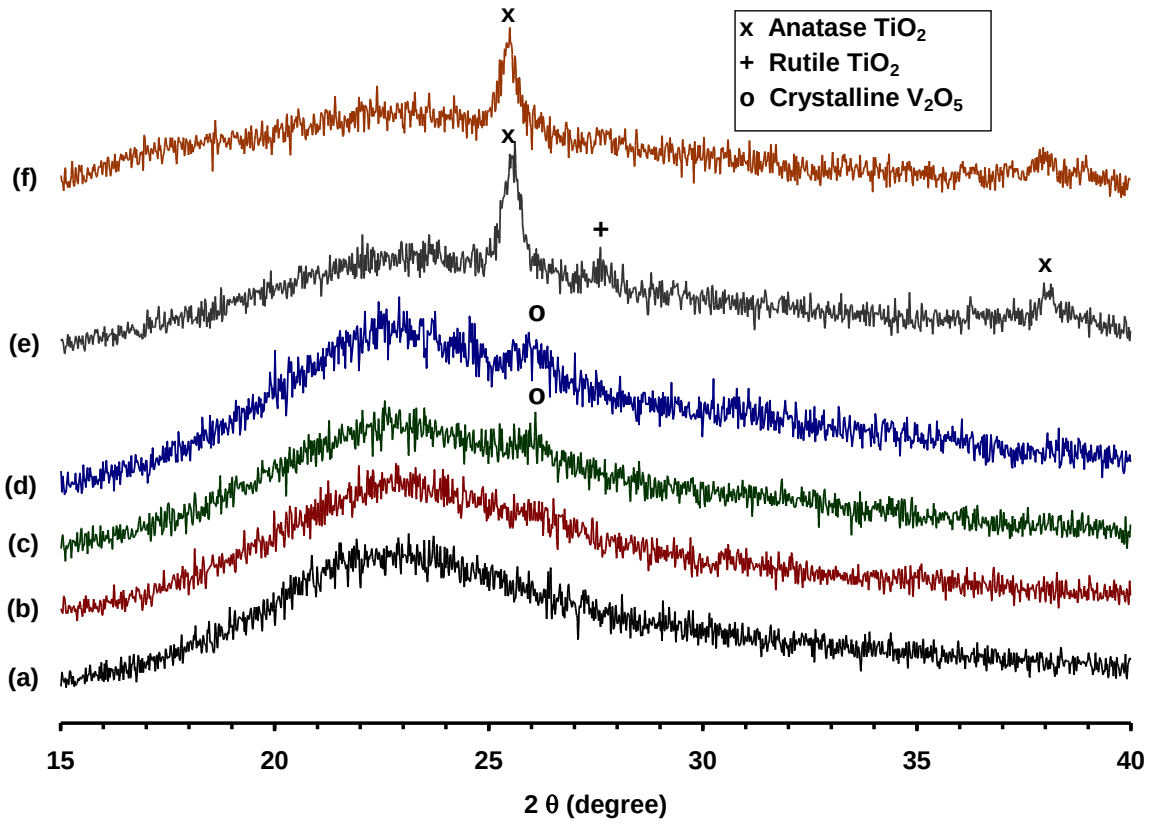

Figure 5-2. XRD patterns of (a) SV2, (b) SV5, (c) SV8, (d) SV10, (e) ST12, and (f) ST12V5.

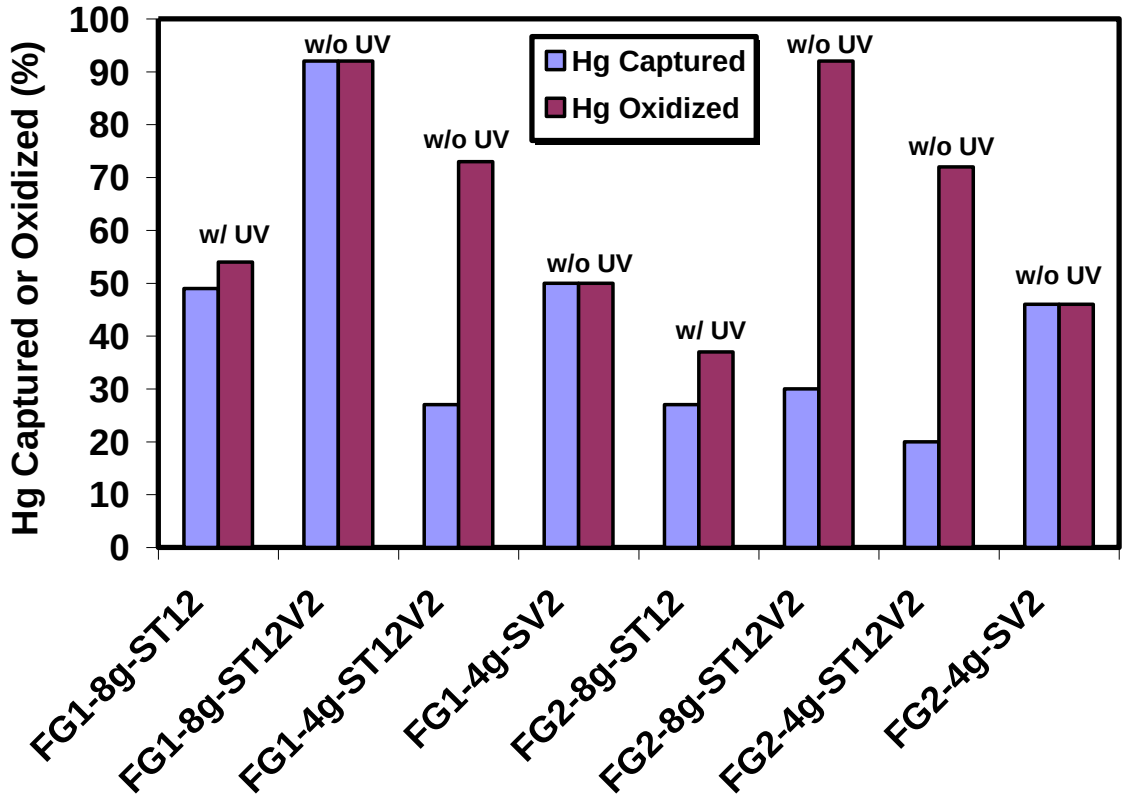

Figure 5-3. Catalytic removal of Hg using the pellet catalysts under various conditions

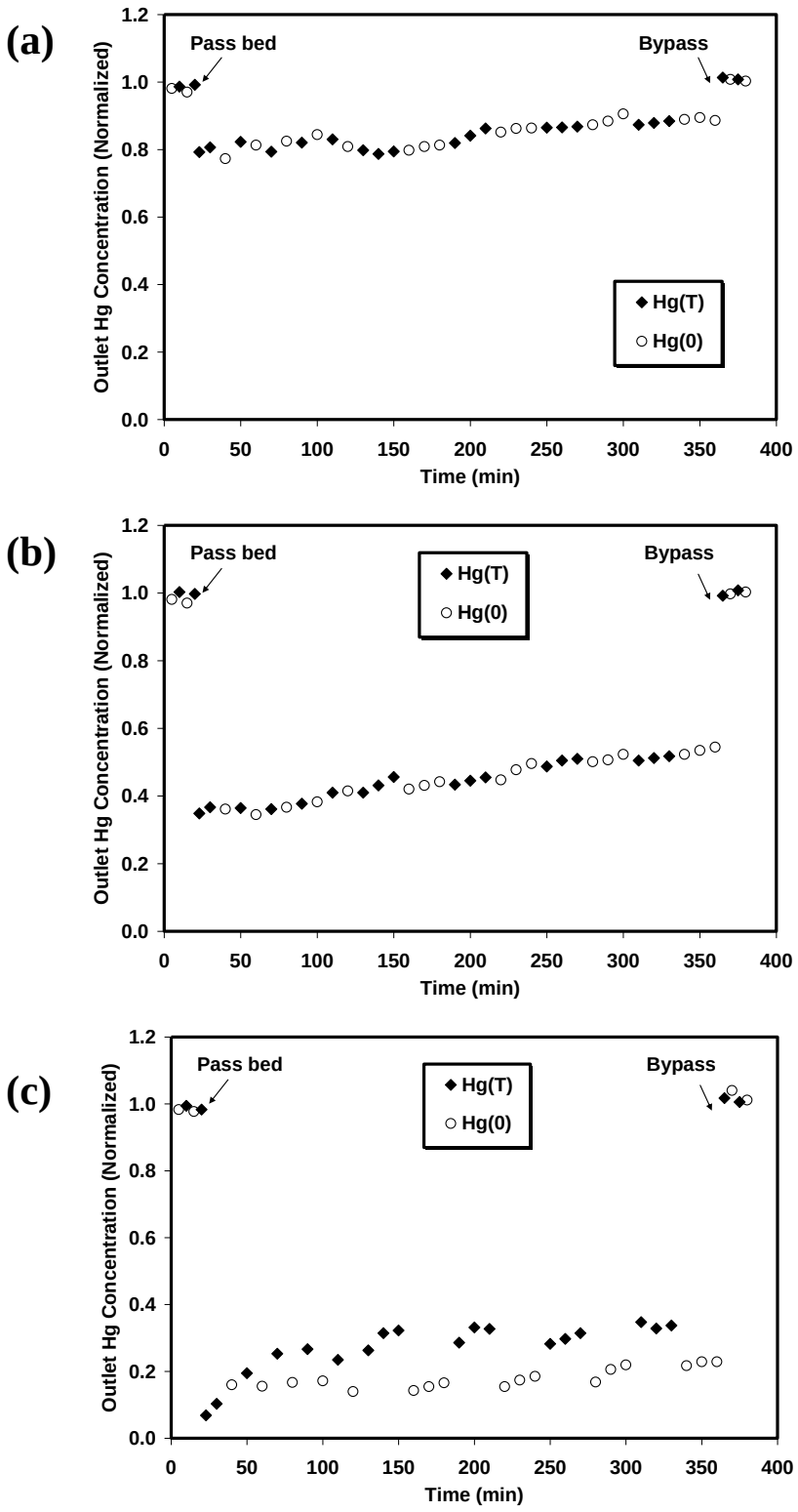

Figure 5-4. Outlet Hg concentration as a function of time using 500 mg powder of (a) SV2, (b) SV5, (c) SV8, (d) SV10, and (e) ST12V5.

(d)

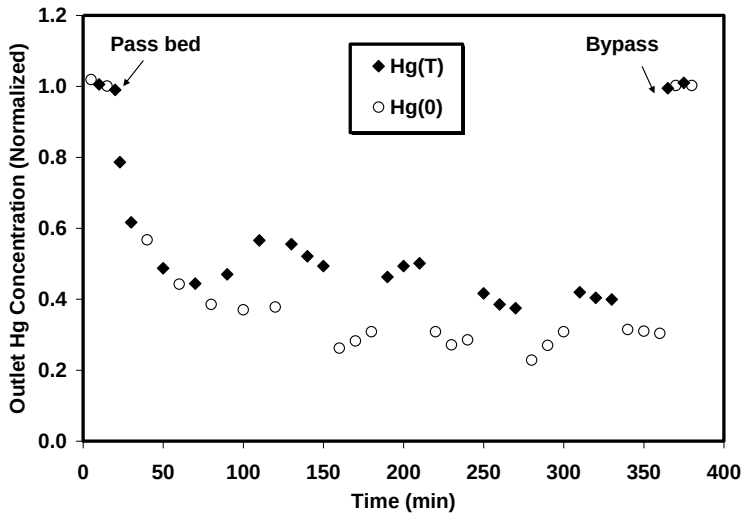

(e)

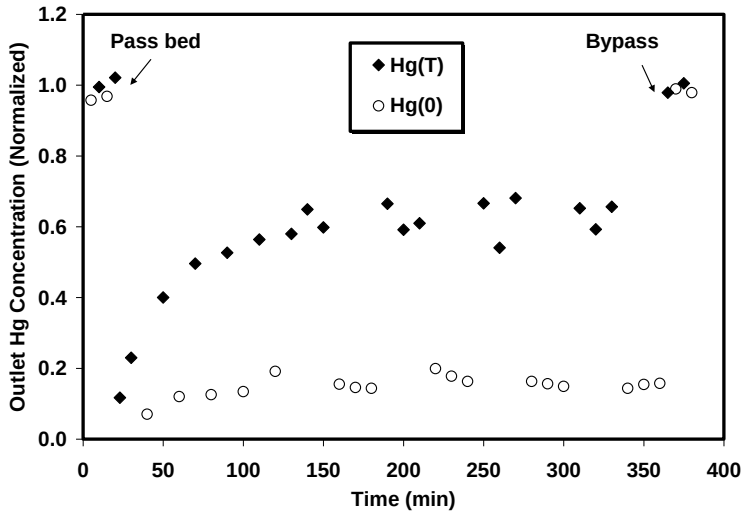

Figure 5-4. Continued.

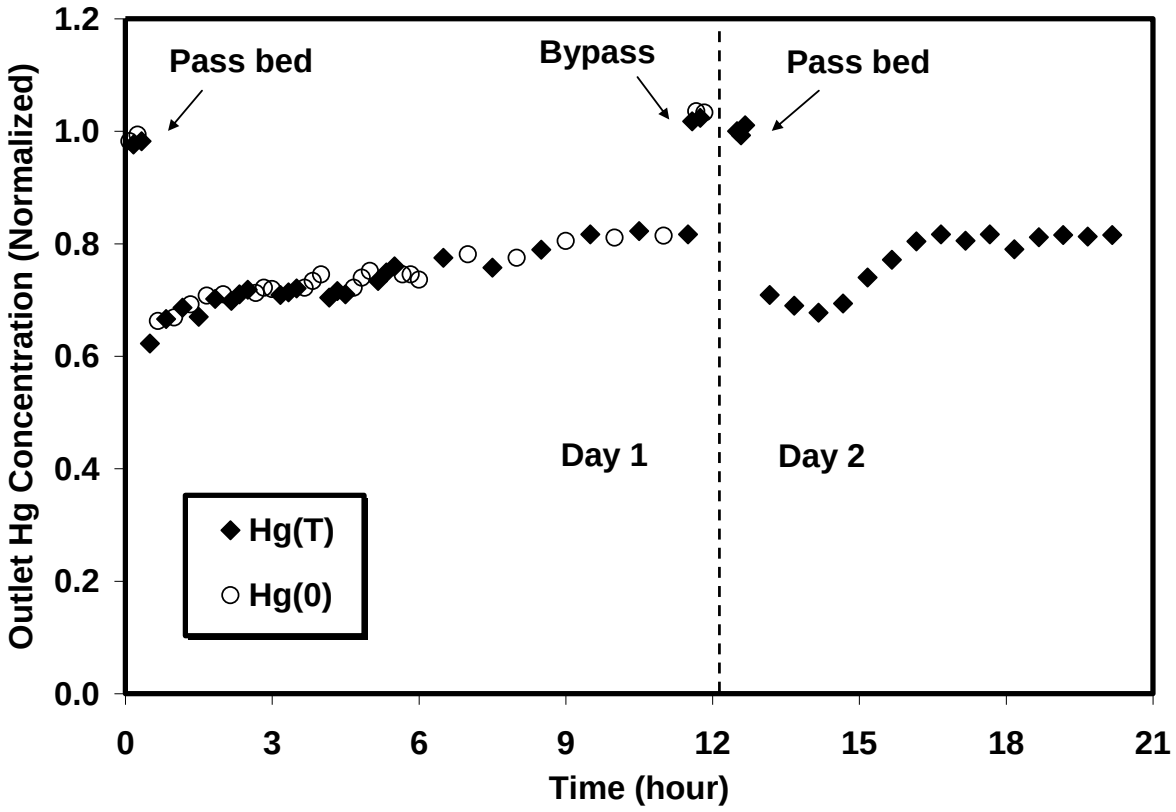

Figure 5-5. Outlet Hg concentration as a function of time using 250 mg powder of SV5 (20-hr test).

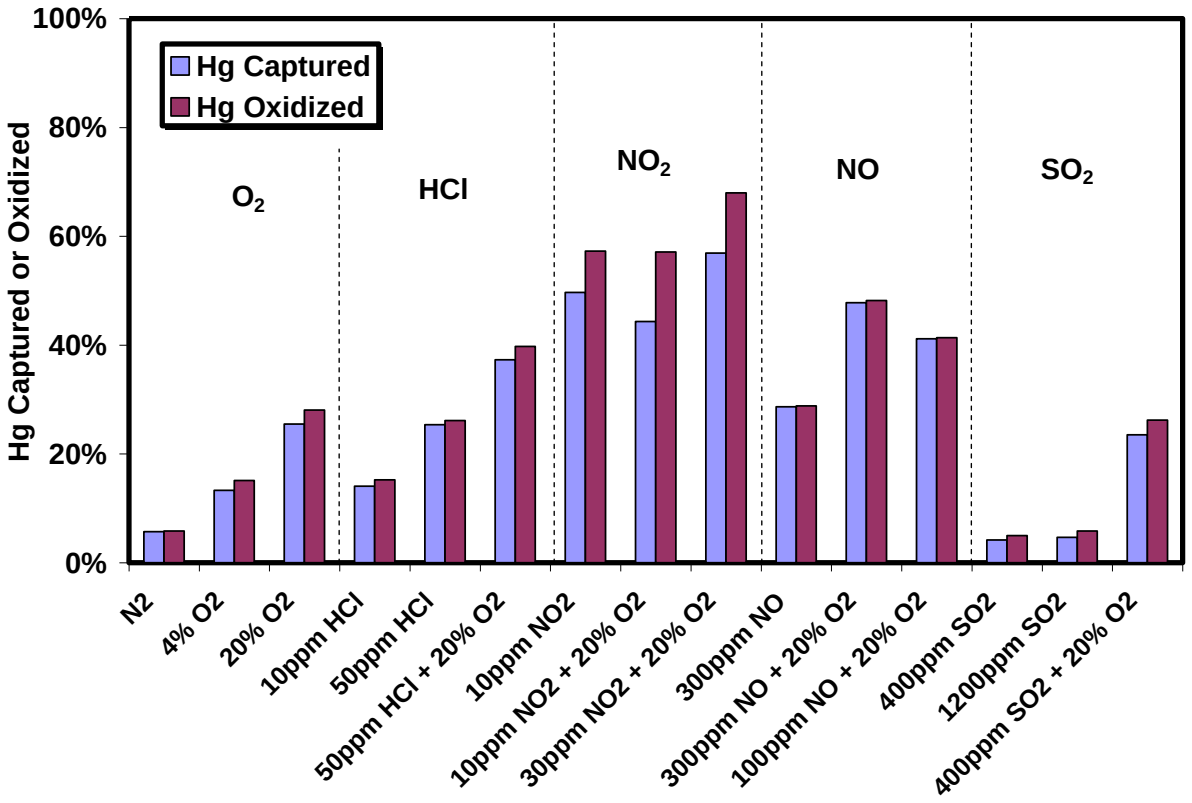

Figure 5-6. The role of flue gas components on Hg removal using 250 mg SV5 powder under dry conditions.

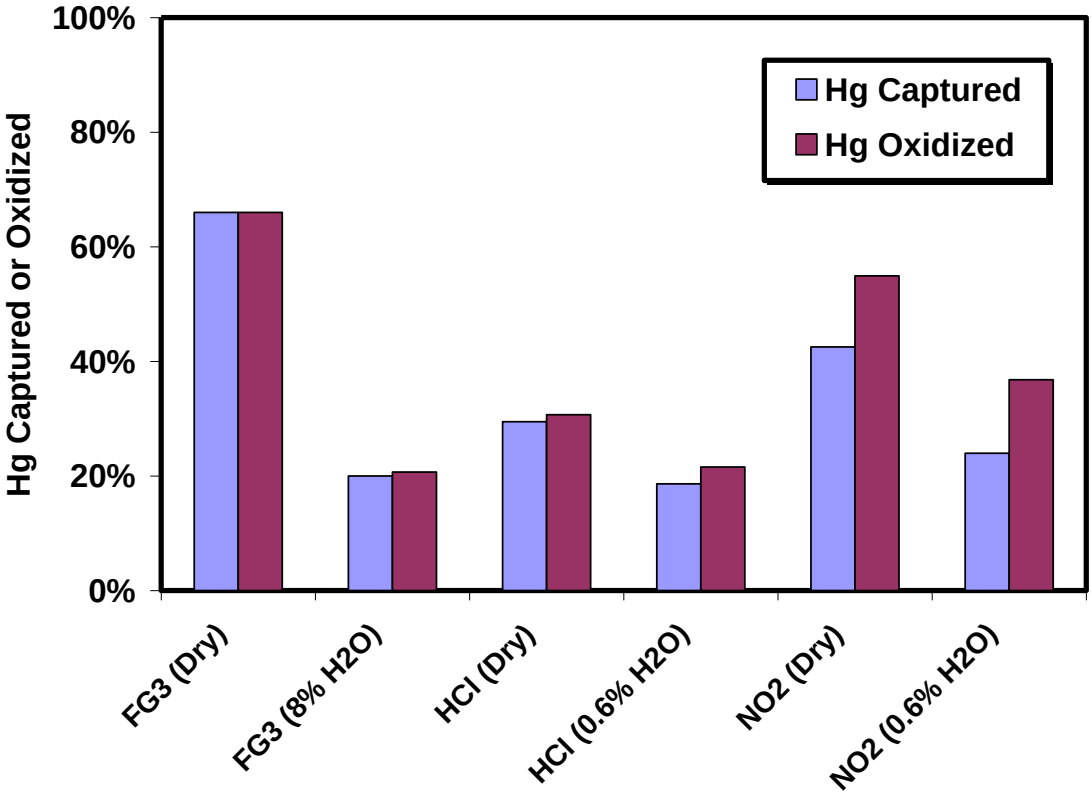

Figure 5-7. The role of water vapor on Hg removal using 250 mg SV5 powder .

CHAPTER 6
UV-ABSORPTION-BASED MEASUREMENTS OF OZONE AND MERCURY: AN INVESTIGATION ON THEIR MUTUAL INTERFERENCES*

Background

The regulations on Hg emissions and the development of Hg control technologies require that reliable methods be used for accurate Hg measurement. Currently, the EPA accepted methods for Hg measurement in the United States are manual procedures based on wet-chemistry such as EPA Methods 29 and 101A (for total mercury) and the Ontario Hydro Method (for speciated mercury) (Laudal et al., 2004). However, continuous mercury monitors (CMMs) have distinct advantages over these manual methods in that CMMs are able to provide a real-time or near-real-time response for Hg measurements and to perform long-term emission measurement to truly characterize a process' temporal emissions. On the other hand, a significant disadvantage of CMMs lies in their measurement interferences, which may vary depending on the principle of the Hg detection technique.

Atomic absorption spectrometry (AAS) is one of the major techniques applied to current CMMs. In the case of AAS, the concentration of elemental Hg in a gas sample is determined by measuring the light that is absorbed by Hg atoms at their characteristic wavelengths (usually at the resonance line of 254 nm). Thus, interferences can occur when other components of the sample gas possess strong absorption bands near this wavelength (254 nm). The EPA's Environmental Technology Verification (ETV) program (USEPA, 2001a) identified sulfur dioxide (SO_2), nitrogen oxides (NO_X), hydrogen chloride (HCl) and chlorine (Cl_2) as interference gases by assessing the CMMs' responses to each gas as well as to a mixture of the gases. Although pretreatment or conditioning systems can be used to remove or negate the effects of

* Reprinted with permission from Li, Y., Lee, S.-R., Wu, C.-Y., 2006. UV-Absorption-Based Measurements of Ozone and Mercury: An Investigation of Their Mutual Interferences. Aerosol Air Qual. Res. 6, 418-429.

these interfering gases prior to the sample delivery to the detectors (Laudal et al., 2004), they may increase the complexity and cost of the instrumentation and impair the real-time feature of the CMMs. Consequently, many types of AAS based CMMs do not have pretreatment systems.

Since the 254 nm Hg emission line also falls into the absorption spectra of ozone, which is capable of absorbing UV light below 290 nm, the presence of ozone in the sampling environment may impact the Hg measurement by AAS based CMMs. Granite and Pennline (2002) studied photochemical oxidation of Hg and speculated that photosensitized formation of ozone may interfere with Hg measurement by absorbing UV radiation. However, no quantitative data were reported on the magnitude of ozone interference. Therefore, the first objective of this study was to quantitatively investigate the interference of ozone on Hg measurement. This study may be of particular importance to ambient and indoor Hg measurement because ozone and Hg coexist in these conditions.

Monitoring ground level of ozone, another significant air pollutant, is also required by US EPA. Control of ozone is expensive, with costs estimated in the billions of dollars (USEPA, 2005b). Hence, deployment of accurate ozone measurement is of great importance to demonstrate compliance with the National Ambient Air Quality Standard (NAAQS) for ozone. Many methods have been developed for ozone measurement where UV absorption and gas-phase chemiluminescence are the major techniques used nowadays. The method of UV absorption is based on the principle that upon exposure to UV light ozone will absorb some of the light and the intensity difference is directly proportional to the concentration of ozone. Frequently the UV light source is a 254 nm emission line from a Hg discharge lamp. Known interferences on this type of ozone detection method include gaseous hydrocarbons with strong absorption at 254 nm, such as aromatic hydrocarbons (i.e., benzene and substituted benzene rings) (NARSTO, 1999).

Since 254 nm is exactly one of the Hg absorption lines, it is speculated that even a small amount of Hg in the sample gas may absorb a considerable amount of UV light. The U.S EPA (1999b) reported that at a baseline ozone concentration of approximately 75 ppb, the addition of 0.04 ppb (300 ng m^{-3} at room temperature) Hg caused an increase in measured ozone concentration by 12.8% at low humidity (RH = 20 ~ 30%) and 6.4% at high humidity (RH = 70 ~80%) using a UV photometric ozone monitor. The interferences of Hg using another two types of ozone monitors were above 30% at either low or high humidity. However, the interference data were reported only at one Hg level (0.04 ppb). More data at other levels of Hg are needed to determine the relationship between Hg concentration and its corresponding interference. Therefore, the second objective of this study was to quantitatively investigate Hg interference on ozone measurement. This is of importance in accurate ozone measurement in ambient and indoor conditions.

Methods

Descriptions of Hg and Ozone Instruments

The CMM used in this study is a RA-915+ Hg analyzer (OhioLumex Co.), which is capable of recording Hg concentrations every second. It employs Zeeman AAS using High Frequency Modulated light polarization (ZAAS-HFM) (Sholupov et al., 2004), which combines the approach of AAS with a simultaneous background correction provided by the Zeeman splitting of the Hg resonance line (254 nm). In the RA-915+ Hg analyzer, the emissions from a Hg discharge lamp are subjected to a strong magnetic field, which causes the three-fold splitting of the Hg resonance line (π, σ+ and σ-, respectively). Two of these components (σ+ and σ-) have identical intensity when Hg is absent in the analytical cell. When Hg is present in the cell, the difference between the intensities of the two components is proportional to the Hg concentration. The calibration was conducted by the manufacturer using Dynacal® permeation device (VICI

Metronics Inc.) which is certified traceable to NIST (National Institute of Standards and Technology) standards. Two optical cells are available for different ranges of Hg concentration. A single-path cell is available for measuring higher Hg concentrations from 0.5 to 200 μg m^{-3}. A multi-path cell with an effective length of 9.6 m is used to enhance the sensitivity of analysis, and thus the detection limit can reach as low as 2 ng m^{-3}. The RA-915+ Hg analyzer may not be suitable for ambient Hg measurement since the ambient Hg concentration has been reported to be approximately 1.5 to 1.9 ng m^{-3} in the northern hemisphere (Ebinghaus et al., 2002; Weiss-Penzias et al., 2003), which is lower than the detection limit of this instrument. However, the RA-915+ Hg analyzer has been used for measurement in stationary sources or Hg contaminated sites (including indoor areas) (Kinsey et al., 2004; Pogarev et al., 2002; Sholupov et al., 2004).

A M146 dynamic gas calibration system (Thermo Electron Instrument) served as the ozone generating source using its internal ozonator. The precision of the ozone concentration that can be generated is 1 ppb. A M49 UV photometric ozone analyzer (Thermo Electron Instrument) was used to measure the ozone concentration in the sample gas. The UV light source in the ozone analyzer is a 254 nm emission line from a Hg discharge lamp. The full scale of the ozone analyzer was set to be from 0 to 500 ppb. Its precision is 2 ppb while the noise is within ±1 ppb. This type of ozone monitor is equipped with a standard (manganese-dioxide) scrubber, which was reported to suffer the lowest interference from Hg compared to other two types of ozone monitors (USEPA, 1999b). A M49-PS UV photometric ozone calibrator (Thermo Electron Instrument) was applied to calibrate both the ozone generator and analyzer.

Experimental Setup and Procedures

A schematic diagram of the experimental system is shown in Figure 6-1. All the experiments were carried out at room temperature (25 ± 1°C). To test the ozone interference on Hg measurement (Figure 6-1A), zero air was produced using a zero air supplier (M111, Thermo

Electron Instrument) and then passed through the ozone generator to provide designated ozone concentrations. The total air flow rate at the outlet of the ozone generator was controlled to be 5 L/min. The ozone laden air was then divided into two streams and connected to the RA-915+ Hg analyzer and the ozone analyzer respectively. The reading from the Hg analyzer would indicate potential interference caused by ozone. The interferences from a designated range of ozone concentrations were measured. Each time before changing the ozone concentration, the entire system was purged by ozone-free air until the readings from both Hg and ozone analyzers were zero. This was to minimize the experimental error from residual ozone in the system. Finally, the sample gas was cleaned through an activated carbon trap before exhausted to the vent hood.

Figure 6-1B shows the experimental setup for testing Hg interference on ozone measurement. The incoming zero air with a flow rate of 5 L/min was split into two streams. One stream was passed through the surface of a liquid Hg reservoir, which was placed in an ice-water bath to maintain a constant Hg vapor pressure. By doing this, saturated Hg vapor was introduced into the system. The other stream served as dilution air and was used to adjust the Hg concentration. Both air streams were controlled by mass flow controllers (MFC, Model. FMA 5400/5500, Omega Engineering, Inc.). The RA-915+ Hg analyzer was used to measure the Hg concentration in the sample gas while the ozone analyzer was used to detect the potential interference caused by Hg. Similarly, the interferences from a designated range of Hg concentrations were measured, and each time before changing the Hg concentration, the entire system was cleaned until the readings from both Hg and ozone analyzers were zero.

Results and Discussion

Interference of Ozone on Hg Measurement

The NAAQS for ozone is 80 ppb for an 8-hour average and 120 ppb for a 1-hour average (USEPA, 1997b). Thus, the ozone concentration generated in this work ranged from 0 to 120

ppb. The corresponding interference on the RA-915+ Hg analyzer is shown in Figure 6-2. The blank test showed that no interference was detected when no ozone was fed into the gas stream. As the ozone concentration increased, the reading on the Hg analyzer was almost linearly elevated. At each ozone concentration level, tests were repeated for three times. For ozone concentrations at 80 and 120 ppb, the interferences on Hg measurement reached approximately 46 and 63 ng m^{-3}, respectively. The relationship between ozone concentration and its corresponding interference can be approximated as:

$$C_{Hg,e} = 0.5559 \times C_{O_3} \quad (6\text{-}1)$$

where $C_{Hg,e}$ is the equivalent Hg concentration, i.e., the interference on Hg analyzer (in unit of ng m^{-3}) and C_{O_3} is the ozone concentration (in unit of ppb). 1 ng m^{-3} of Hg is equivalent to 1.22 × 10^{-4} ppb at room temperature. For a convenient understanding of the significance of the interference magnitudes, units used in Equation 6-1 and Equation 6-2 are in line with the EPA standards (USEPA, 1997b, 1999a).

This observed ozone interference may have an important effect on Hg measurement. For example, Ferrara (1999) used the RA-915+ Hg analyzer to measure the Hg distribution over the area of Idria, where one of the largest European Hg mines was located. The Hg concentration was reported to range from 50 to 170 ng m^{-3} in the central part of Idria near the Hg mines and dumps. Suppose that 40 ppb ozone existed in that local atmosphere, an overestimate of Hg concentration at about 22 ng m^{-3} would have been involved according to the results from this work. Indoor Hg measurement can also be affected by ozone interference. Although the indoor ozone levels are typically less than those outdoors (Weschler, 2000), they can be much greater when strong ozone generating sources are present such as photocopiers, electrostatic filters, and ozone generators (Godish, 2001). In addition, the use of ozone for the removal of indoor air

contaminants has been widely promoted in the United States (Li et al., 2002). In those areas with elevated ozone concentrations, the interference of ozone on Hg measurement may result in a significant overestimate of Hg concentrations when using RA-915+ or other similar Hg analyzers. It has been indicated by Singhvi et al. (2001) that water vapor can have positive interference on UV Hg analyzers. The magnitude of this interference was not reported, and it could vary for different UV Hg analyzers. If this positive interference of water vapor were applied to the RA-915+ Hg analyzer used in this study, the total interference on Hg measurement (caused by both ozone and water vapor) could be even larger.

The interference of ozone on Hg measurement can also impact the risk assessment of human exposure to Hg. The Reference Concentration (RfC) for elemental Hg specified by the EPA is 300 ng m^{-3} based on central nervous system (CNS) effects in humans (USEPA, 1999a). Hg concentrations above this level may result in a further investigation of hazardous exposure. According to the findings in this work, an ozone concentration in the range of 0-120 ppb can exert a positive bias in Hg measurement up to 21% (63 ng m^{-3}) of the EPA RfC (300 ng m^{-3}). The interference may be especially critical for conditions where the measured Hg concentration is slightly above the RfC level, because after subtracting the bias caused by ozone interference, the actual Hg concentration may not exceed the RfC any more. Therefore, eliminating ozone from sample gas is essential to obtain accurate Hg concentration and thus is important for risk assessment of human exposure to Hg. Helmig (1997) reviewed ozone removal techniques in sampling of atmospheric volatile organic trace gases. These techniques may be applicable to ozone removal in Hg sampling as long as they do not tamper with Hg concentrations.

Interference of Hg on Ozone Measurement

A designated range of Hg concentrations were fed into the gas stream to investigate the possible Hg interference on ozone measurement. Due to the limitation of the Hg vapor generating unit used in this work (the dilution ratio was relatively small compared with the saturated Hg vapor concentration), the minimum Hg concentration introduced was about 2300 ng m^{-3}. In addition, Hg levels were controlled so that the interferences on ozone readings were within the measurement range of the ozone analyzer (0-500 ppb). A blank test showed no interference when no Hg was present. As the Hg concentration in the sample gas increases, the corresponding reading on the ozone analyzer also increases (as shown in Figure 6-3). An approximately linear relationship can be obtained as expressed in the following equation:

$$C_{O_3,e} = 0.1165 \times C_{Hg} \qquad (6\text{-}2)$$

where $C_{O_3,e}$ is the equivalent ozone concentration, i.e., the interference on ozone analyzer (in unit of ppb) and C_{Hg} is the Hg concentration (in unit of ng m^{-3}).

Equation 6-2 implies that Hg can exert a significant interference on ozone measurement, which is very likely due to the UV absorption by Hg when passing through the ozone analyzer (USEPA, 1999b). Although the Hg level in the ambient and indoor environment is typically lower than the minimum Hg concentration (2300 ng m^{-3}) tested in this work, the results obtained can be used as a reference to predict the practical conditions. It should be noted that extrapolation beyond the tested concentration range might involve errors that could impact the accuracy of the prediction. However, given the high value of R^2 (0.9957) of the regression analysis which has incorporated the origin point, it is suggested that the error associated with the extrapolation to the range of 0 to 2300 ng m^{-3} may not be significant. Carpi and Chen (2001) reported that the highest Hg concentration measured at 12 indoor sites in New York City was

523 ng m^{-3}. This Hg level would result in 61 ppb interference on ozone measurement using a UV-absorption-based ozone analyzer, provided that Equation 6-2 is valid at lower Hg concentration levels. The interference, 61 ppb, added to the normal ambient ozone concentration (0-50 ppb) (Lim and Turpin, 2002), may have many chances to exceed the NAQQS for ozone (80 ppb). In the case when Hg concentration is equal to the EPA RfC (300 ng m^{-3}), an interference of 35 ppb would be involved, which is comparable to the average ambient ozone concentration. Since indoor ozone concentration is typically lower than that outdoors (Weschler, 2000) and indoor Hg concentrations generally higher than that outdoors due to various indoor Hg contamination sources (such as accidental spills of Hg from natural gas meters, Hg thermometers, fluorescent light bulbs, etc.) (Carpi and Chen, 2001), the impact of Hg interference on indoor ozone measurement may be much greater. These results indicate that it is essential to eliminate the Hg interference to obtain correct ozone concentration at Hg contaminated places.

Now that the linear relationship between Hg concentration and corresponding interference on ozone measurement was successfully established, it is necessary to compare the results with those by the EPA (1999b) where the same type of ozone monitor was used. At a Hg concentration of 0.04 ppb (328 ng m^{-3} at 25°C), Equation 6-2 predicts an ozone interference of 38 ppb, whereas the EPA (1999b) reported approximately 10 ppb at low humidity (RH = 20 to 30%) and 5 ppb at high humidity (RH = 70 to 80%). Since in this work the experiments were conducted using dry zero air, comparison of the above results suggests that higher humidity may diminish the interference caused by Hg. A possible reason is the deposition of water vapor in the optical cell attenuates the incident UV light, causing a negative interference by water vapor itself. The finding also suggests that the reported interference may not be so significant in

ambient and indoor air as in the dry air used in this work. Further research is needed to verify this hypothesis.

Summary

Mutual interferences of UV-absorption-based measurements of ozone and Hg were investigated in this study. It was found that ozone in the range of 0 to 120 ppb can exert an interference of up to 63 ng m^{-3} on an AAS based Hg analyzer. A linear relationship was established between the ozone concentration and corresponding interference on Hg measurement. On the other hand, it was found that Hg can also result in significant interferences on an ozone analyzer based on UV absorption. Results showed that Hg at a concentration of 300 ng m^{-3} can potentially cause a bias in ozone measurement of approximately 35 ppb. These mutual interferences may consequently affect the risk assessment of human exposure to both Hg and ozone. It should be noted that the results were obtained from a relatively small set of equipment (only one Hg and one ozone analyzer). There are many different types of Hg or ozone analyzers based on principle of UV absorption. It is possible that certain types of analyzers are not compromised by the interferences found in this work. Thus, the findings in this work should be considered as analyzer-specific. Further investigation is needed to determine whether the trends observed in this work can be extended to other types of analyzers.

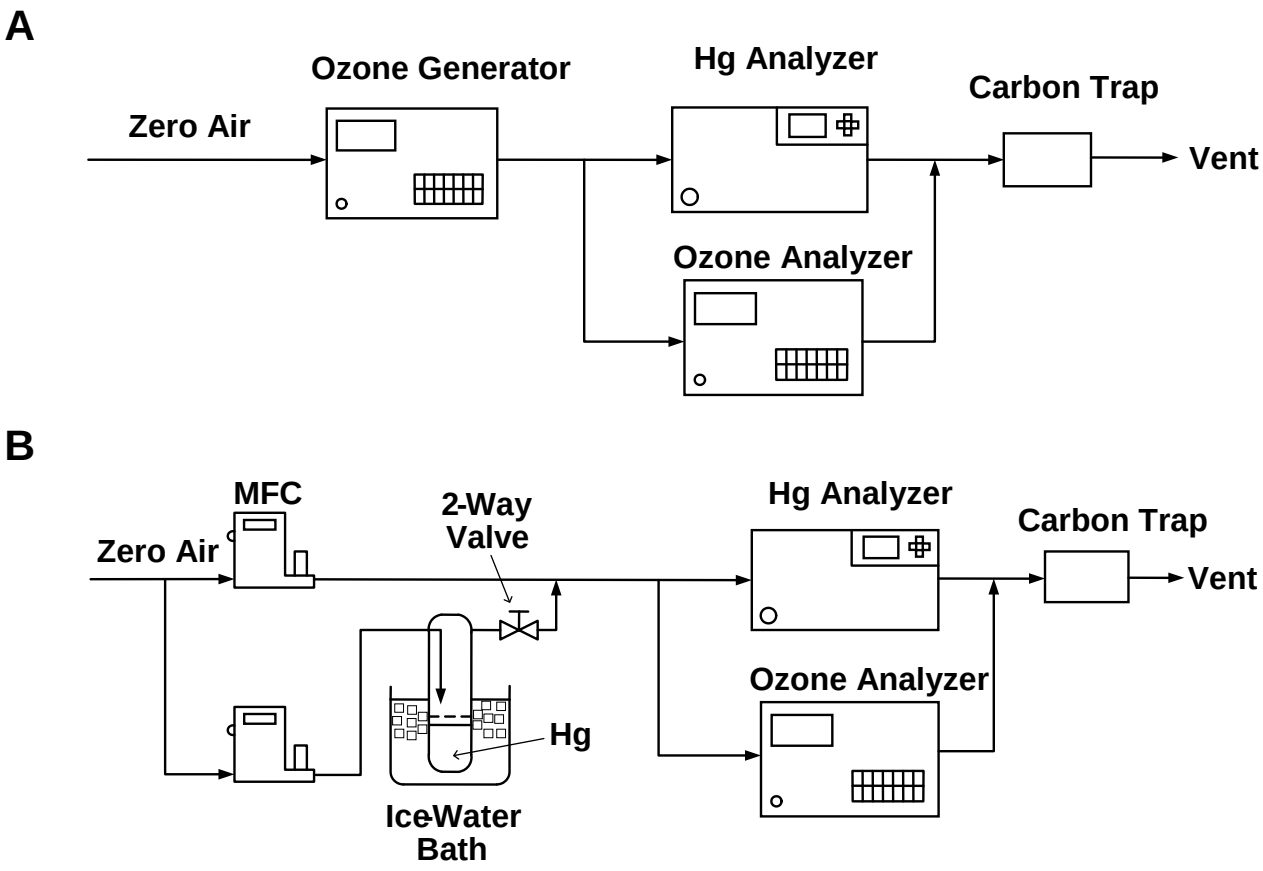

Figure 6-1. Experimental setup. A) Ozone interference on Hg measurement. B) Hg interference on ozone measurement.

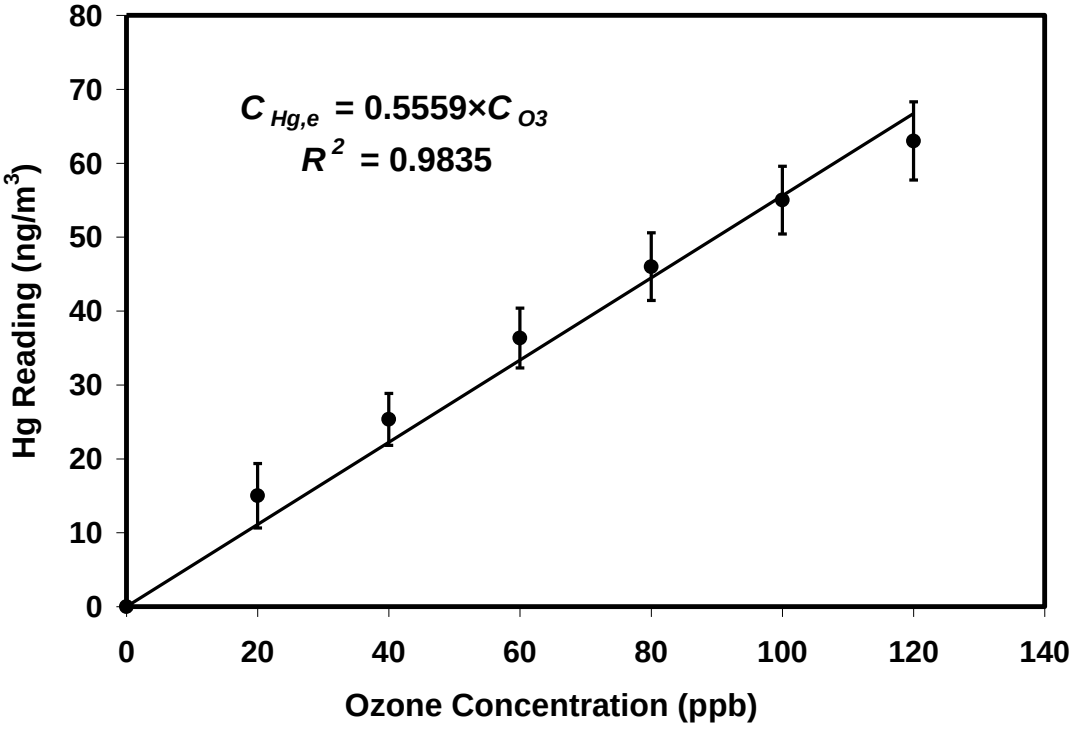

Figure 6-2. Measurement interference of ozone on the RA-915+ Hg analyzer as a function of ozone concentration (The error bars represent one standard deviation).

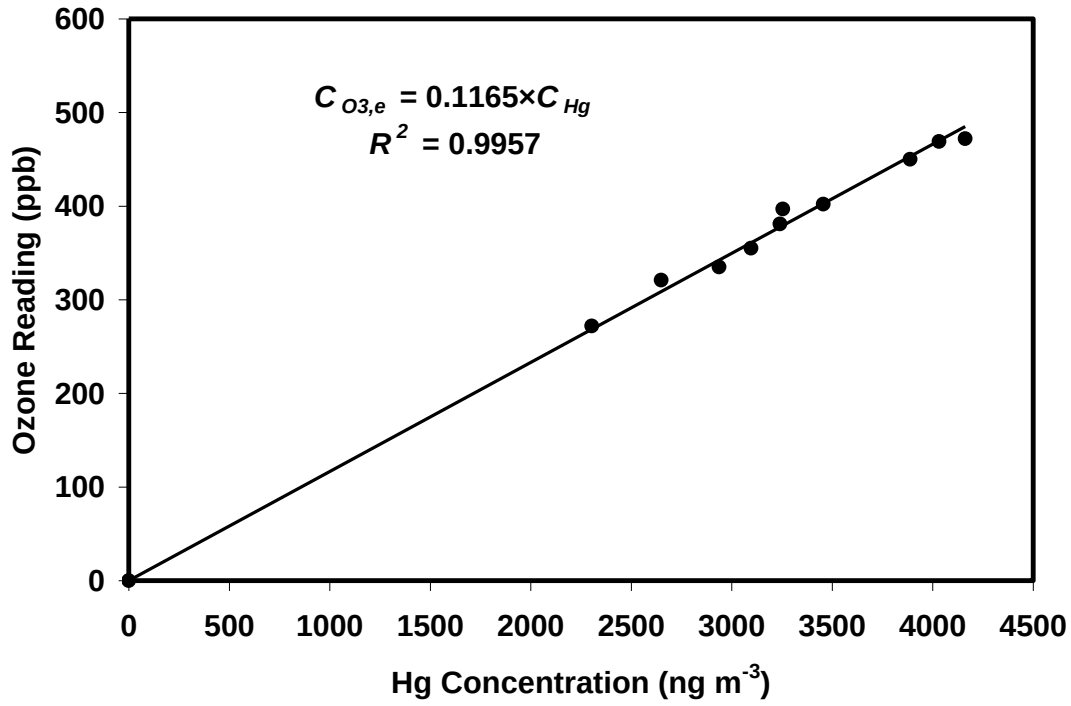

Figure 6-3. Measurement interference of Hg on the ozone analyzer as a function of Hg concentration.

CHAPTER 7
CONCLUSIONS AND RECOMMENDATIONS

This doctoral research has focused on the fixed-bed studies of Hg^0 removal using nanostructured $SiO_2/TiO_2/V_2O_5$ composites. Three types of composites were tested for their catalytic activities in both pellet and powder forms: (1) TiO_2 nanoparticles doped on high surface area SiO_2 gel (SiO_2-TiO_2), (2) V_2O_5 doped on SiO_2 gel (SiO_2-V_2O_5), and (3) V_2O_5 doped on the SiO_2-TiO_2 support (SiO_2-TiO_2-V_2O_5). Experiments were conducted under both room conditions and flue gas conditions. The kinetics of the Hg oxidation was studied, and the interactions between Hg and the flue gas components on the catalyst surfaces were investigated. The catalytic activities of the three catalysts were also compared. The following conclusions have been obtained from this research.

- **Conclusion 1:** A Langmuir-Hinshelwood (L-H) model can be used to express the kinetics of photocatalytic oxidation of Hg^0 on the SiO_2-TiO_2 nanocomposite under room conditions. Good agreement between the experimental data and the L-H model was demonstrated. The model predicted a great potential of the SiO_2-TiO_2 nanocomposite for Hg^0 removal even at very high Hg^0 concentrations. The rate of photocatalytic Hg^0 oxidation increased when the inlet Hg^0 concentration increased and it reached a maximum value in the absence of water vapor. The addition of water vapor was found to inhibit Hg^0 photocatalytic oxidation, which may be explained by the competitive adsorption of water vapor with Hg^0 on the TiO_2 surface.
- **Conclusion 2:** The mechanisms of Hg^0 removal and reemission from used catalysts were investigated in a fixed-bed reactor at 65 °C using air as the carrier gas. Without UV irradiation, Hg^0 adsorption was found to be insignificant, but it could be enhanced by the photocatalytic oxidation product, HgO, possibly due to the high affinity between HgO and Hg^0. Under dry conditions 95% of Hg^0 can be removed; however, increased humidity levels

remarkably suppress both Hg^0 adsorption and photocatalytic oxidation. Introducing water vapor can also result in significant reemission of captured Hg^0 from the nanocomposite, which may be ascribed to the repellant effect of water vapor adsorbed on the superhydrophilic TiO_2 surface. Exposure to UV light was found either to prohibit Hg^0 reemission when photocatalytic oxidation of reemitted Hg^0 prevailed or to promote Hg^0 reemission when photocatalytic reduction of HgO to Hg^0 dominated later on. It is concluded that Hg^0 capture on the SiO_2–TiO_2 nanocomposite in a humid environment under UV irradiation is controlled by four mechanisms: adsorption, photocatalytic oxidation, desorption, and photocatalytic reduction. The observed inhibitory effect of water vapor is contributed by its competitive occupancy of the available adsorption sites, displacement of adsorbed Hg^0, and participation in the photocatalytic reduction of HgO to Hg^0.

- **Conclusion 3:** Hg^0 removal using the SiO_2–TiO_2 nanocomposite has been investigated in simulated flue gas of coal-fired power plants. The flue gas components were found to have significant effects on Hg removal efficiency. H_2O inhibited Hg oxidation and capture and the inhibitory effect was proportional to the H_2O concentration. HCl enhanced Hg^0 oxidation probably following an Eley-Redeal mechanism where adsorbed Cl species reacts with gas-phase Hg^0. SO_2 promoted Hg oxidation, possibly forming mercury sulfate species. NO significantly inhibited Hg removal by scavenging OH radicals that are necessary for Hg^0 oxidation. The effect of NO_2 was found to be insignificant. Experiments in simulated flue gases also showed that high rank coals are preferable to low rank coals because of the lower moisture and higher HCl and SO_2 concentrations in the flue gas.
- **Conclusion 4:** A method has been developed to dope V_2O_5 on the SiO_2 and SiO_2-TiO_2 supports. Improvements in Hg removal from flue gas were observed in fixed-bed studies

using both pellet and powder forms of the SiO_2-V_2O_5 and SiO_2-TiO_2-V_2O_5 catalysts. No UV light activation is needed for the V_2O_5 doped catalysts. For SiO_2-V_2O_5 catalysts, the Hg removal efficiency increased as the V_2O_5 loading increased from 2 to 8% but decreased as the V_2O_5 loading further increased to 10%. The results suggested that the optimal V_2O_5 loading for a maximum catalytic activity is somewhere between 5 and 8%. The SiO_2-TiO_2-V_2O_5 catalysts have an even greater ability of oxidizing Hg compared to SiO_2-V_2O_5, which can be advantageous to power plants equipped with wet-scrubbers where oxidized Hg can be easily captured. It was found that the Hg oxidation on the V_2O_5 doped catalysts may follow an Eley-Rideal mechanism where HCl, NO, and NO_2 are first adsorbed on the catalyst and then react with gas-phase Hg. On the contrary, water vapor dramatically inhibits Hg oxidation while SO_2 has an insignificant effect.

- **Conclusion 5:** Mutual interferences of UV-absorption-based measurements of ozone and Hg were also investigated in this research. It was found that ozone in the range of 0 to 120 ppb can exert an interference of up to 63 ng m^{-3} on an AAS based Hg analyzer and the interference is linearly related to the ozone concentration. On the other hand, it was found that Hg can have significant interferences on ozone analyzers that are based on UV absorption. Hg at a concentration of 300 ng m^{-3} can potentially cause a bias in ozone measurement of approximately 35 ppb, an average ozone concentration in the air under normal conditions. These mutual interferences may consequently affect the risk assessment of human exposure to both Hg and ozone.

Based on the findings of this doctoral research, future research is recommended on the following topics:

1. It has been verified in this research that V_2O_5 is the active center for the Hg oxidation, but the SiO_2-TiO_2-V_2O_5 composites exhibit much higher oxidation abilities than the SiO_2-V_2O_5 composites. This warrants further studies to understand the enhancement of Hg oxidation on the superior TiO_2 support and to explore the optimal V_2O_5/TiO_2 ratio. Finding the optimal V_2O_5/TiO_2 loading is of great importance to the advancement of a most cost-effective catalyst. Surface analysis techniques such as X-ray photoelectron spectroscopy (XPS) are recommended to be used to examine the surface structure of the catalysts before and after the Hg oxidation experiments. XPS may provide information on the oxidation states of the vanadium and the dispersion of the vanadia on the surface by providing the V/Ti ratio on the surface. This information would be helpful for a better understanding of the catalyst characteristics as well as the reaction mechanisms.
2. A long term test on the performance of the SiO_2-TiO_2-V_2O_5 composites on Hg removal is recommended. Although this research demonstrated a stabilized activity of the catalyst in a 20-hr test, a longer testing time, probably a few hundred hours, would be considered sufficient to verify its long-term performance. However, some modifications of the current system may be needed for the long-term test.
3. Exploring the potential of the SiO_2-TiO_2-V_2O_5 composites as a multipollutant control strategy, i.e. a low temperature SCR catalyst for control of both Hg and NOx. It is promising because the catalyst contains the same active phases as the commercial SCR catalysts. However, the effect of the injected ammonia (NH_3) on Hg removal is yet to be investigated.
4. A pilot-scale study using the SiO_2-TiO_2-V_2O_5 composites is recommended as a scale-up of the current bench-scale system. Kinetic studies may be necessary to determine the amount (or total surface area) of the catalyst that is needed for treating a higher flow rate of flue gas. A

good configuration of the packed-bed reactor may also be critical to achieve a high efficiency of Hg removal in the pilot-scale study.

LIST OF REFERENCES

Argyle, M. D., Chen, K. D., Resini, C., Krebs, C., Bell, A. T., Iglesia, E., 2004. Extent of reduction of vanadium oxides during catalytic oxidation of alkanes measured by in-situ UV-visible spectroscopy. J. Phy. Chem. B. 108, 2345-2353.

Augugliaro, V., Coluccia, S., Loddo, V., Marchese, L., Martra, G., Palmisano, L., Schiavello, M., 1999. Photocatalytic oxidation of gaseous toluene on anatase TiO_2 catalyst: mechanistic aspects and FT-IR investigation. Appl. Catal. B-Environ. 20, 15-27.

Bai, M., Zhang, Z., Bai, M., Yi, C., Bai, X., 2006. Removal of SO_2 from Gas Streams by Oxidation using Plasma-Generated Hydroxyl Radicals. Plasma Chem. Plasma Process. 26, 177-186.

Benson, S. A., Laumb, J. D., Crocker, C. R., Pavlish, J. H., 2005. SCR catalyst performance in flue gases derived from subbituminous and lignite coals. Fuel Process. Technol. 86, 577-613.

Berglund, F., Bertin, M., 1969. Chemical Fallout. Tomas Publisher, Springfield.

Bidstrup, P. C., 1964. Toxicity of Mercury and its Compounds. Elsevier, Amsterdam.

Borderieux, S., Wu, C.-Y., Bonzongo, J.-C., Powers, K., 2004. Control of Elemental Mercury Vapor in Combustion Systems Using Fe_2O_3 Nanoparticles. Aerosol Air Qual. Res. 4, 74-90.

Bosch, H., Janssen, F., 1988. Formation and control of nitrogen oxides. Catal. Today. 2, 369-379.

Brown, T. D., Smith, D. N., Hargis, R. A., O'Dowd, W. J., 1999. Mercury measurement and its control: What we know, have learned, and need to further investigate. J. Air. Waste Manage. 49, 628-640.

Busca, G., Lietti, L., Ramis, G., Berti, F., 1998. Chemical and mechanistic aspects of the selective catalytic reduction of NOx by ammonia over oxide catalysts: A review. Appl. Catal. B-Environ. 18, 1-36.

Calvert, J. G., Lindberg, S. E., 2005. Mechanisms of mercury removal by O_3 and OH in the atmosphere. Atmospheric Environment. 39, 3355-3367.

Canela, M. C., Alberici, R. M., Jardim, W. F., 1998. Gas-phase destruction of H_2S using TiO_2/UV-VIS. J. Photochem. Photobio. A-Chem. 112, 73-80.

Carey, T. R., Hargrove, C. W., Richardson, C. F., Chang, R., 1998. Factors affecting mercury control in utility flue gas using activated carbon. J. Air Waste Manage. Assoc. 48, 1166-1174.

Carpi, A., Chen, Y. F., 2001. Gaseous elemental mercury as an indoor air pollutant. Environ. Sci. Technol. 35, 4170-4173.

Chen, S., Rostam-Abadi, M., Chang, R., 1996. Mercury removal from combustion flue gas by activated carbon injection: mass transfer effects. Prepr. Pap.-Am. Chem. Soc., Div. Fuel Chem. 41, 442-446.

Ebinghaus, R., Kock, H. H., Coggins, A. M., Spain, T. G., Jennings, S. G., Temme, C., 2002. Long-term measurements of atmospheric mercury at Mace Head, Irish west coast, between 1995 and 2001. Atmos. Environ. 36, 5267-5276.

Edwards, J. R., Srivastava, R. K., Kilgroe, J. D., 2001. A study of gas-phase mercury speciation using detailed chemical kinetics. J. Air Waste Manage. Assoc. 51, 869-877.

Eswaran, S., Stenger, H. G., 2005. Understanding Mercury Conversion in Selective Catalytic Reduction (SCR) Catalysts. Energy Fuels. 19, 2328-2334.

Ferrara, R., 1999. Mercury Contaminated Sites. Springer, Berlin.

Flora, J. R. V., Vidic, R. D., Liu, W., Thurnau, R. C., 1998. Modeling powdered activated carbon injection for the uptake of elemental mercury vapors. J. Air Waste Manage. Assoc. 48, 1051-1059.

Fujishima, A., Rao, T. N., Tryk, D. A., 2000. Titanium dioxide photocatalysis. J. Photochem. Photobio. C: Photochem. Reviews. 1, 1-21.

Galbreath, K. C., Zygarlicke, C. J., Tibbetts, J. E., Schulz, R. L., Dunham, G. E., 2005. Effects of NOx, α-Fe_2O_3, γ-Fe_2O_3, and HCl on mercury transformations in a 7-kW coal combustion system. Fuel Process. Technol. 86, 429-448.

Godish, T., 2001. Indoor Environmental Quality. Lewis Publishers, Boca Raton, Florida.

Goodsite, M. E., Plane, J. M. C., Skov, H., 2004. A theoretical study of the oxidation of Hg^0 to $HgBr_2$ in the troposphere. Environ. Sci. Technol. 38, 1772-1776.

Grabowski, R., Pietrzyk, S., Sloczynski, J., Genser, F., Wcislo, K., Grzybowska-Swierkosz, B., 2002. Kinetics of the propane oxidative dehydrogenation on vanadia/titania catalysts from steady-state and transient experiments. Appl. Catalysis A-Gen. 232, 277-288.

Granite, E. J., Pennline, H. W., 2002. Photochemical removal of mercury from flue gas. Ind. Eng. Chem. Res. 41, 5470-5476.

Granite, E. J., Pennline, H. W., Hargis, R. A., 2000. Novel sorbents for mercury removal from flue gas. Ind. Eng. Chem. Res. 39, 1020-1029.

Guan, K. H., 2005. Relationship between photocatalytic activity, hydrophilicity and self-cleaning effect of TiO_2/SiO_2 films. Surface & Coatings Technology. 191, 155-160.

Helmig, D., 1997. Ozone removal techniques in the sampling of atmospheric volatile organic trace gases. Atmos. Environ. 31, 3635-3651.

Kantcheva, M., Bushev, V., Klissurski, D., 1994. Study Of The NO_2-NH_3 Interaction On A Titania (Anatase) Supported Vanadia Catalyst. J. Catalysis. 145, 96-106.

Kim, S. B., Hong, S. C., 2002. Kinetic study for photocatalytic degradation of volatile organic compounds in air using thin film TiO2 photocatalyst. Appl. Catal. B-Environ. 35, 305-315.

Kinsey, J. S., Anscombe, F. R., Lindberg, S. E., Southworth, G. R., 2004. Characterization of the fugitive mercury emissions at a chlor-alkali plant: overall study design. Atmos. Environ. 38, 633-641.

Kobayashi, M., Kuma, R., Masaki, S., Sugishima, N., 2005. TiO_2-SiO_2 and V_2O_5/TiO_2-SiO_2 catalyst: Physico-chemical characteristics and catalytic behavior in selective catalytic reduction of NO by NH_3. Appl. Catal. B-Environ. 60, 173-179.

Kobayashi, M., Kuma, R., Morita, A., 2006. Low temperature selective catalytic reduction of NO by NH_3 over V_2O_5 supported on TiO_2-SiO_2-MoO_3. Catal. Letters. 112, 37-44.

Laudal, D. L., Brown, T. D., Nott, B. R., 2000. Effects of flue gas constituents on mercury speciation. Fuel Process. Technol. 65, 157-165.

Laudal, D. L., Thompson, J. S., Pavlish, J. H., Brickett, L. A., Chu, P., 2004. Use of continuous mercury monitors at coal-fired utilities. Fuel Process. Technol. 85, 501-511.

Laumb, J. D., Benson, S. A., Olson, E. A., 2004. X-ray photoelectron spectroscopy analysis of mercury sorbent surface chemistry. Fuel Process. Technol. 85, 577-585.

Lee, C. W., Srivastava, R. K., Ghorishi, S. B., Hastings, T. W., Stevens, F. M., 2004. Investigation of selective catalytic reduction impact on mercury speciation under simulated NOx emission control conditions. J. Air Waste Manage. Assoc. 54, 1560-1566.

Lee, C. W., Srivastava, R. K., Ghorishi, S. B., Karwowski, J., Hastings, T. W., Hirschi, J. C., 2006. Pilot-scale study of the effect of selective catalytic reduction catalyst on mercury speciation in Illinois and powder river basin coal combustion flue gases. J. Air Waste Manage. Assoc. 56, 643-649.

Lee, T. G., Biswas, P., Hedrick, E., 2001. Comparison of Hg^0 capture efficiencies of three in situ generated sorbents. AICHE J. 47, 954-961.

Lee, T. G., Biswas, P., Hedrick, E., 2004. Overall kinetics of heterogeneous elemental mercury reactions on TiO_2 sorbent particles with UV irradiation. Ind. Eng. Chem. Res. 43, 1411-1417.

Li, T. H., Turpin, B. J., Shields, H. C., Weschler, C. J., 2002. Indoor hydrogen peroxide derived from ozone/d-limonene reactions. Environ. Sci. Technol. 36, 3295-3302.

Li, Y., Wu, C.-Y., 2006. Role of Moisture in Adsorption, Photocatalytic Oxidation, and Reemission of Elemental Mercury on a SiO_2-TiO_2 Nanocomposite. Environ. Sci. Technol. 40, 6444-6448.

Li, Y., Wu, C.-Y., 2007. Kinetic Study for Photocatalytic Oxidation of Elemental Mercury on a SiO_2–TiO_2 Nanocomposite. Environ. Eng. Sci. 24, 3-12.

Lim, H. J., Turpin, B. J., 2002. Origins of primary and secondary organic aerosol in Atlanta: Results' of time-resolved measurements during the Atlanta supersite experiment. Environ. Sci. Technol. 36, 4489-4496.

Maroto-Valer, M. M., Zhang, Y. Z., Granite, E. J., Tang, Z., Pennline, H. W., 2005. Effect of porous structure and surface functionality on the mercury capacity of a fly ash carbon and its activated sample. Fuel. 84, 105-108.

Martra, G., Arena, F., Coluccia, S., Frusteri, F., Parmaliana, A., 2000. Factors controlling the selectivity of V_2O_5 supported catalysts in the oxidative dehydrogenation of propane. Catal. Today. 63, 197-207.

McLarnon, C. R., Granite, E. J., Pennline, H. W., 2005. The PCO process for photochemical removal of mercury from flue gas. Fuel Process. Technol. 87, 85-89.

Meites, L., Ed. 1963. Handbook of Analytical Chemistry. New York, McGraw Hill.

Meserole, F. B., Richardson, C. F., Miller, S. D., Searcy, K., Chang, R. 2000, Estimated the costs of electric utility mercury control using sorbent injection. Proceedings of the Air and Waste Management Association 93rd Annual Meeting, Salt Lake City, UT.

Miller, S. J., Dunham, G. E., Olson, E. S., Brown, T. D., 2000. Flue gas effects on a carbon-based mercury sorbent. Fuel Process. Technol. 65, 343-363.

Mishima, A., 1992. Bitter Sea: The Human Cost of Minamata Disease. Kosei Pub. Co., Tokyo, Japan.

North American Research Strategy for Tropospheric Ozone (NARSTO), 1999. Measurement Methods Compendium - Ozone Method. Oak Ridge National Laboratory, Oak Ridge, TN. http://narsto.ornl.gov/Compendium/methods/o3.shtml. Date last accessed: June 2007.

Niksa, S., Fujiwara, N., 2005a. Predicting extents of mercury oxidation in coal-derived flue gases. J. Air Waste Manage. Assoc. 55, 930-939.

Niksa, S., Fujiwara, N., 2005b. A predictive mechanism for mercury oxidation on selective catalytic reduction catalysts under coal-derived flue gas. J. Air Waste Manage. Assoc. 55, 1866-1875.

Niksa, S., Helble, J. J., Fujiwara, N., 2001. Kinetic modeling of homogeneous mercury oxidation: The importance of NO and H_2O in predicting oxidation in coal-derived systems. Environ. Sci. Technol. 35, 3701-3706.

Norton, G. A., Yang, H. Q., Brown, R. C., Laudal, D. L., Dunham, G. E., Erjavec, J., 2003. Heterogeneous oxidation of mercury in simulated post combustion conditions. Fuel. 82, 107-116.

Obee, T. N., 1996. Photooxidation of sub-parts-per-million toluene and formaldehyde levels an titania using a glass-plate reactor. Environ. Sci. Technol. 30, 3578-3584.

Obee, T. N., Hay, S. O., 1997. Effects of moisture and temperature on the photooxidation of ethylene on Titania. Environ. Sci. Technol. 31, 2034-2038.

Olson, E. S., Sharma, R. K., Pavlish, J. H., 2002. On the analysis of mercuric nitrate in flue gas by GC–MS. Anal. Bioanal. Chem. 374, 1045–1049.

Pal, B., Ariya, P. A., 2004. Gas-phase HO-Initiated reactions of elemental mercury: Kinetics, product studies, and atmospheric implications. Environ. Sci. Technol. 38, 5555-5566.

Pan, H. Y., Minet, R. G., Benson, S. W., Tsotsis, T. T., 1994. Process for Converting Hydrogen-Chloride to Chlorine. Ind. Eng. Chem. Res. 33, 2996-3003.

Parfitt, G. D., Ramsboth.J, Rocheste.Ch, 1971. Infra-Red Study of Hydrogen Chloride Adsorption on Rutile Surfaces. Trans. Faraday Society. 67, 3100-&.

Parvulescu, V. I., Grange, P., Delmon, B., 1998. Catalytic removal of NO. Catal. Today. 46, 233-316.

Pavlish, J. H., Sondreal, E. A., Mann, M. D., Olson, E. S., Galbreath, K. C., Laudal, D. L., Benson, S. A., 2003. Status review of mercury control options for coal-fired power plants. Fuel Process. Technol. 82, 89-165.

Pitoniak, E., Wu, C. Y., Londeree, D., Mazyck, D., Bonzongo, J. C., Powers, K., Sigmund, W., 2003. Nanostructured silica-gel doped with TiO2 for mercury vapor control. J. Nanopart. Res. 5, 281-292.

Pitoniak, E., Wu, C. Y., Mazyck, D. W., Powers, K. W., Sigmund, W., 2005. Adsorption enhancement mechanisms of silica-titania nanocomposites for elemental mercury vapor removal. Environ. Sci. Technol. 39, 1269-1274.

Pogarev, S. E., Ryzhov, V., Mashyanov, N., Sholupov, S., Zharskaya, V., 2002. Direct measurement of the mercury content of exhaled air: a new approach for determination of the mercury dose received. Anal. Bioanal. Chem. 374, 1039-1044.

Presto, A. A., Granite, E. J., 2006. Survey of Catalysts for Oxidation of Mercury in Flue Gas. Environ. Sci. Technol. 40, 5601-5609.

Raillard, C., Hequet, V., Le Cloirec, P., Legrand, J., 2004. Kinetic study of ketones photocatalytic oxidation in gas phase using TiO_2-containing paper: effect of water vapor. J. Photochem. Photobio. A-Chem. 163, 425-431.

Ravichandran, M., 2004. Interactions between mercury and dissolved organic matter - a review. Chemosphere. 55, 319-331.

Rodella, C. B., Nascente, P. A. P., Franco, R. W. A., Magon, C. J., Mastelaro, V. R., Florentino, A. O., 2001. Surface characterisation of V_2O_5/TiO_2 catalytic system. Phy. Stat. Solidi A-Appl. Res. 187, 161-169.

Rodriguez, S., Almquist, C., Lee, T. G., Furuuchi, M., Hedrick, E., Biswas, P., 2004. A mechanistic model for mercury capture with in situ-generated titania particles: Role of water vapor. J. Air Waste Manage. Assoc. 54, 149-156.

Romero, C. E., Li, Y., Bilirgen, H., Sarunac, N., Levy, E. K., 2006. Modification of boiler operating conditions for mercury emissions reductions in coal-fired utility boilers. Fuel. 85, 204-212.

Rostam-Abadi, M., Chen, S. G., Hsi, H.-C., Rood, M., Chang, R., Carey, T. R., Hargrove, B., Richardson, C., Rosenhoover, W., Meserole, F. 1997, Novel vapor phase mercury sorbents. Proceedings of the EPRI-DOE-EPA Combined Utility Air Pollutant Control, Washington, DC.

Schroeder, W. H., Munthe, J., 1998. Atmospheric mercury - An overview. Atmospheric Environment. 32, 809-822.

Senior, C. L., 2006. Oxidation of mercury across selective catalytic reduction catalysts in coal-fired power plants. J. Air Waste Manage. Assoc. 56, 23-31.

Senior, C. L., Sarofim, A. F., Zeng, T. F., Helble, J. J., Mamani-Paco, R., 2000. Gas-phase transformations of mercury in coal-fired power plants. Fuel Process. Technol. 63, 197-213.

Shang, J., Du, Y. G., Xu, Z. L., 2002. Photocatalytic oxidation of heptane in the gas-phase over TiO2. Chemosphere. 46, 93-99.

Shikada, T., Fujimoto, K., Kunugi, T., Tominaga, H., Kaneko, S., Kubo, Y., 1981. Reduction of Nitric-Oxide with Ammonia on Vanadium-Oxide Catalysts Supported on Homogeneously Precipitated Silica-Titania. Ind. Eng. Chem. Prod. Res. Dev. 20, 91-95.

Sholupov, S., Pogarev, S., Ryzhov, V., Mashyanov, N., Stroganov, A., 2004. Zeeman atomic absorption spectrometer RA-915+for direct determination of mercury in air and complex matrix samples. Fuel Process. Technol. 85, 473-485.

Singhvi, R., Turpin, R., Kalnicky, D. J., Patel, J., 2001. Comparison of field and laboratory methods for monitoring metallic mercury vapor in indoor air. Journal of Hazardous Materials. 83, 1-10.

Sloczynski, J., 1996. Kinetics and mechanism of reduction and reoxidation of the alkali metal promoted vanadia-titania catalysts. Appl. Catalysis A-Gen. 146, 401-423.

Sommar, J., Gardfeldt, K., Stromberg, D., Feng, X. B., 2001. A kinetic study of the gas-phase reaction between the hydroxyl radical and atomic mercury. Atmospheric Environment. 35, 3049-3054.

Son, H. S., Lee, S. J., Cho, I. H., Zoh, K. D., 2004. Kinetics and mechanism of TNT degradation in TiO2 photocatalysis. Chemosphere. 57, 309-317.

Tesser, R., Maradei, V., Di Serio, M., Santacesaria, E., 2004. Kinetics of the oxidative dehydrogenation of ethanol to acetaldehyde on V2O5/TiO2-SiO2 catalysts prepared by grafting. Ind. Eng. Chem. Res. 43, 1623-1633.

Tseng, H.-H., Wey, M.-Y., Liang, Y.-S., Chen, K.-H., 2003. Catalytic removal of SO_2, NO and HCl from incineration flue gas over activated carbon-supported metal oxides. Carbon. 41, 1079.

US EPA, 1997a. Mercury Study Report to Congress. EPA-452/R-97-003.

US EPA, 1997b. National ambient air quality standards for ozone, final rule. Federal Register 62 (138).

US EPA, 1997c. Standards of Performance for New Stationary Sources and Emission Guidelines for Existing Sources: Hospital/Medical/Infectious Waste Incinerators; Final Rule. Fed. Regist., *62*, 48347-448391.

US EPA, 1999a. Integrated Risk Information System (IRIS) on Elemental Mercury. National Center for Environmental Assessment, Office of Research and Development, Washington, DC.

US EPA, 1999b. Laboratory Study to Explore Potential Interferences to Air Quality Monitors. EPA-454/C-00-002.

US EPA, 2000. Regulatory Finding on the Emissions of Hazardous Air Pollutants from Electric Utility Steam Generating Units. Federal Register 65 (245), 79825–79831.

US EPA, 2001a. Environmental Technology Verification Program, Verification Reports and Statements for each tested Mercury CEM. Research Triangle Park, NC. http://www.epa.gov/etv/verifications/vcenter1-11.html. Date last accessed: June 2007.

US EPA, 2001b. Standards of Performance for Large Municipal Waste Combustors; Final Rule and Proposed Rule. Fed. Regist., *66*, 57823-57828.

US EPA, 2003. National Emission Standards for Hazardous Air Pollutants: Mercury Emissions from Mercury Cell Chlor-Alkali Plants; Final Rule. Fed. Regist., *68*, 70903-70946.

US EPA, 2005a. Clean Air Mercury Rule; Standards of Performance for New and Existing Stationary Sources: Electric Utility Steam Generating Units. 40 CFR Parts 60, 63, 72, and 75.

US EPA, 2005b. Regulatory Impact Analyses for the Particulate Matter and Ozone NAAQS and Proposed Regional Haze Rule. Research Triangle Park, NC. http://www.epa.gov/ttn/oarpg/naaqsfin/ria.html. Date last accessed: June 2007.

Wang, R., Hashimoto, K., Fujishima, A., Chikuni, M., Kojima, E., Kitamura, A., Shimohigoshi, M., Watanabe, T., 1997. Light-induced amphiphilic surfaces. Nature. 388, 431-432.

Weast, R. C., Astle, M. J., Beyer, W. H., Eds. 1983. CRC Handbook of Chemistry and Physics. Boca Raton, FL, CRC Press.

Weckhuysen, B. M., Keller, D. E., 2003. Chemistry, spectroscopy and the role of supported vanadium oxides in heterogeneous catalysis. Catal. Today. 78, 25-46.

Weiss-Penzias, P., Jaffe, D. A., McClintick, A., Prestbo, E. M., Landis, M. S., 2003. Gaseous elemental mercury in the marine boundary layer: Evidence for rapid removal in anthropogenic pollution. Environ. Sci. Technol. 37, 3755-3763.

Weschler, C. J., 2000. Ozone in indoor environments: Concentration and chemistry. Indoor Air. 10, 269-288.

Wu, C. Y., Lee, T. G., Tyree, G., Arar, E., Biswas, P., 1998. Capture of mercury in combustion systems by in-situ generated titania particles with UV irradiation. Environ. Eng. Sci. 15, 137-148.

Yang, C. S., Chen, C. J., 2005. Synthesis and characterization of silica-capped titania nanorods: An enhanced photocatalyst. Applied Catalysis a-General. 294, 40-48.

Zhang, F.-S., Nriagu, J. O., Itoh, H., 2004. Photocatalytic removal and recovery of mercury from water using TiO_2-modified sewage sludge carbon. J. Photochem. Photobio. A: Chemistry. 167, 223-228.

BIOGRAPHICAL SKETCH

Ying Li was born in 1977 in Luzhou, Sichuan Province, China. He earned his B.S. degree in thermal engineering in June 1999 at Zhejiang University, China. He continued his master studies in thermal engineering at Zhejiang University and received his M.S. degree in March 2002. Ying Li came to the United States in August 2002. He studied in mechanical engineering at Lehigh University, Pennsylvania, and worked as a research assistant at the Energy Research Center. He earned his second M.S. degree at Lehigh University in 2004. He joined the research group of Dr. Chang-Yu Wu at the University of Florida in August 2004 and started pursuing his Ph.D. degree in the Department of Environmental Engineering Sciences. His doctoral research focused on mercury removal from power plant flue gas using novel catalysts.

Ying Li was the president of the student chapter of Air & Waste Management Association (A&WMA) at the University of Florida in 2006-2007. He was awarded the Milton Feldstein Memorial Scholarship from A&WMA in 2006. He was awarded the Axel Hendrickson Scholarship and the Clair Fancy Scholarship from Florida Section A&WMA in 2005 and 2006, respectively. He won 1st place in the student paper poster competition (doctoral level) in the 2006 A&WMA Annual Conference. He won 1st place in the student poster competition (graduate level) in the 2006 Florida A&WMA Annual Conference.